KU LEUVEN

FACULTY OF
ENGINEERING SCIENCE

The role of hybrid space heating systems in reaching the CO_2 emission targets of Flemish school buildings

Jorrit Loos

Thesis voorgedragen tot het behalen
van de graad van Master of Science
in de ingenieurswetenschappen:
energie

Promotor:
Prof. dr. ir. Lieve Helsen

Evaluatoren:
Prof. dr. ir.-arch. Dirk Saelens
Ir. Tars Verschelde

Begeleider:
Ir. Jelger Jansen

Academiejaar 2023 – 2024

Preface

This thesis represents the concluding chapter of my engineering studies at KU Leuven. I reflect on the past five years with great pleasure and even already a little nostalgia. Despite the many hours I spent behind my books, I enjoyed myself immensely.

The completion of this thesis was made possible with the assistance of numerous individuals. Firstly, I would like to express my gratitude to my mentor, Jelger Jansen, who was consistently willing to provide useful feedback, and with whom the weekly meetings always yielded new insights. Secondly, I would like to thank my promotor, prof. Helsen, for her invaluable feedback during the meetings that took place throughout the academic year and for sparking my interest during the *Thermal Systems* course. I would also like to express my gratitude to dr. Marco Wirtz for his swift and informative replies to the questions I had regarding the *nPro* tool, and to Tom Neven from UCLL for providing me with the data of a real-life school building that I could utilise in my analysis. Last but not least, I would like to thank my parents for their continuous support during my entire school career.

Jorrit Loos

Contents

Preface i

Abstract iv

Samenvatting v

List of Figures vii

List of Tables ix

List of Abbreviations and Symbols xi

1 Introduction 1
- 1.1 Problem statement . . . 3
- 1.2 Research questions . . . 4
- 1.3 Thesis outline . . . 6

2 Literature research 7
- 2.1 Hybrid heat pumps . . . 7
- 2.2 Heat demand of buildings . . . 12
- 2.3 Used software tools . . . 15
- 2.4 Conclusion . . . 18

3 Testing the *nPro* tool 19
- 3.1 Building data . . . 19
- 3.2 Load profile generation . . . 20
- 3.3 Energy system design optimisation and simulation . . . 21
- 3.4 *nPro* limitations and (implicit) assumptions . . . 26
- 3.5 Conclusion . . . 26

4 The school building model 29
- 4.1 Building architecture . . . 29
- 4.2 Building envelope . . . 30
- 4.3 Occupancy data . . . 33
- 4.4 Meteorological data . . . 34
- 4.5 Heating system . . . 35
- 4.6 Conclusion . . . 39

5 The impact of the *nPro* optimisation settings 41
- 5.1 Important parameters . . . 41
- 5.2 Comparison of *nPro* and *Modelica* load profiles . . . 43

5.3 Baseline scenarios . . . 44
5.4 System configuration . . . 45
5.5 Minimal CO_2 emission reduction . . . 47
5.6 Conclusion . . . 48

6 The impact of the relevant building parameters 49
6.1 Building envelope U-value . . . 50
6.2 Window-to-wall ratio . . . 51
6.3 Building airtightness . . . 53
6.4 Building orientation . . . 54
6.5 Conclusion . . . 55

7 The impact of optimal control 57
7.1 Optimisation model and settings . . . 57
7.2 Optimal control of gas-fired heating system . . . 59
7.3 Optimal control of hybrid heating system . . . 61
7.4 Conclusion . . . 63

8 Recommendations for schools 65

9 Conclusion 69

A *nPro* 75
A.1 Screenshots . . . 75
A.2 Input parameters . . . 79

B The school building model 81
B.1 Model validation . . . 81
B.2 Building architecture . . . 83
B.3 *Modelica* representation of building model . . . 84
B.4 Building envelope . . . 85
B.5 Occupancy data . . . 86
B.6 Nominal pressure rise of pumps . . . 91

C The impact of optimal control 93
C.1 Heating system models . . . 93
C.2 Heat pump model equations . . . 95
C.3 Optimal control of hybrid heating system . . . 96

Bibliography 99

Abstract

Achieving (inter)national climate goals will require commitment from a range of sectors. For buildings, the majority of emissions originates from space heating. Non-residential buildings, and school buildings in particular, present challenges in reducing CO_2 emissions due to the specific characteristics of these buildings and the limited availability of budgets. Hybrid heating systems offer a solution, as they permit the integration of heat pumps into the current heating system, resulting in a reduced initial investment cost and no necessity for other energy-saving measures.

This thesis investigates how heat pumps can be integrated into the fossil-fuel based heating system of typical Flemish school buildings to achieve a cost-effective CO_2 emission reduction, while maintaining thermal comfort.

Air-source heat pumps in particular are interesting for schools, as they have a lower investment cost and less stringent locational requirements than ground-source heat pumps. The sizing of the heat pump in a hybrid heating system is important, as it determines investment cost, annual energy cost and achieved emission reduction. Different parameters affect the optimal heat pump size in a hybrid heating system: the remaining lifetime of the currently installed heating system, the required CO_2 emission reduction, but also building parameters of which insulation levels, window-to-wall ratio, airtightness and building orientation are the most important ones.

The larger the heat demand of a school building, the lower the cost per tonne of CO_2 emission reduction relative to the baseline scenario. For the average Flemish school building, achieving the 2030 emission target will always come at a certain cost. This 25% emission reduction is achievable with an air-source heat pump between 10% and 20% of the peak heat demand. If the school building has a well-insulated building envelope, or if it has average insulation levels but high infiltration rates, or if due to building orientation the amount of solar gains is limited, it is advisable to select the capacity of the heat pump in the upper half of this range.

Optimising the control strategy of the heating system, for example by implementing model predictive control, significantly improves the performance of hybrid heating systems, leading to higher coverage ratios, lower CO_2 emissions and lower annual energy costs. It can also significantly improve the performance of the currently present gas-fired heating system, and it allows to install a slightly smaller capacity of heat pump to achieve the same CO_2 emission reduction.

The installation of an air-source heat pump thus is a cost-effective way for schools to reach the 2030 emission targets. This allows schools to spread energy-saving measures in time, paving the way for carbon neutrality of heating by 2050.

Samenvatting

Om de (inter)nationale klimaatdoelstellingen te halen, is de inzet van verschillende sectoren nodig. Voor de gebouwensector is het grootste deel van de emissies afkomstig van ruimteverwarming. Voor niet-residentiële gebouwen, en schoolgebouwen in het bijzonder, kan het verlagen van hun CO_2-emissies een uitdaging vormen vanwege de specifieke kenmerken van deze gebouwen en de eerder beperkte beschikbare budgetten. Hybride verwarmingssystemen bieden een oplossing, omdat ze de integratie van warmtepompen in het huidige verwarmingssysteem mogelijk maken zonder zeer hoge investeringskosten en zonder de directe noodzaak van energiebesparende maatregelen.

Deze thesis onderzoekt hoe warmtepompen geïntegreerd kunnen worden in het op fossiele brandstoffen gebaseerde verwarmingssysteem van typische Vlaamse schoolgebouwen, om op die manier een kosteneffectieve CO_2-emissiereductie te bereiken, met behoud van thermisch comfort.

Vooral lucht-water warmtepompen zijn interessant voor scholen, omdat ze een lagere investeringskost hebben en minder strenge locatievereisten dan grond-water warmtepompen. De dimensionering van de warmtepomp in een hybride verwarmingssysteem is belangrijk, omdat dit de investeringskost, de jaarlijkse energiekost en de emissiereductie bepaalt. Verschillende parameters zijn van invloed op de optimale grootte van de warmtepomp in een hybride verwarmingssysteem: de resterende levensduur van het huidige verwarmingssysteem, de vereiste CO_2-emissiereductie, maar ook gebouwparameters waarvan de kwaliteit van isolatie, de raam-wandverhouding, de luchtdichtheid en de oriëntatie van het gebouw de belangrijkste zijn.

Hoe groter de warmtevraag van een schoolgebouw, hoe lager de kosten per ton CO_2-emissiereductie in vergelijking met het basisscenario. Voor het gemiddelde Vlaamse schoolgebouw zal het bereiken van de emissiedoelstelling van 2030 altijd een bepaalde kostprijs hebben. Deze 25% emissiereductie is haalbaar met een lucht-water warmtepomp met een capaciteit tussen de 10% en 20% van de piekwarmtevraag. Als het schoolgebouw een goed geïsoleerde gebouwschil heeft, of als het een gemiddeld isolatieniveau heeft maar een hoge infiltratiegraad, of als door de oriëntatie van het gebouw de hoeveelheid zonnewinsten beperkt is, is het aan te raden om het vermogen van de warmtepomp aan de bovenkant van dit bereik te kiezen.

Optimale regeling, bijvoorbeeld door het implementeren van *model predictive control*, verbetert de prestaties van een hybride verwarmingssysteem aanzienlijk, wat leidt tot een hogere dekkingsgraad van de warmtepomp, minder CO_2-emissies en lagere jaarlijkse energiekosten. Het kan ook de prestaties van het huidige gasgestookte verwarmingssysteem aanzienlijk verbeteren en maakt het mogelijk om een iets kleinere

capaciteit warmtepomp te installeren om dezelfde CO_2-emissiereductie te bereiken.

De installatie van een lucht-water warmtepomp is dus een kosteneffectieve manier voor scholen om de emissiedoelstellingen van 2030 te halen. Hierdoor kunnen scholen energiebesparende maatregelen spreiden in de tijd, om op die manier het pad te effenen voor koolstofneutraliteit op vlak van verwarming tegen 2050.

List of Figures

1.1 Graphical overview of the structure of this thesis. 6

2.1 General working principle of a heat pump. 8
2.2 Parallel and series system configuration. 9
2.3 Example of a simplified cost - CO_2 abatement graph. 11
2.4 Example of a HLDC. 13
2.5 HLDC of a Polish school building with a hybrid heating system. 15
2.6 The working principle of *nPro*. 16

3.1 Heat demand profile and HLDC for building D of UCLL Campus Proximus generated by *nPro*. 20
3.2 Heat demand profile and HLDC for building D of UCLL Campus Proximus generated by *nPro*, with adapted normalised day profiles. . . . 21

4.1 Floor plan of the representational Flemish school building model. 30
4.2 Graphical *Modelica* representation of the heating system model. 35
4.3 Heating curve used in model. 36
4.4 Supply temperature and outdoor temperature for simulated year. 37
4.5 Typical temperature profile in winter (zone 9). 39

5.1 Heat demand comparison between dynamic simulation using the *Modelica* representative school building model and load profile generation by *nPro*. 44

6.1 HLDCs for different values of $\bar{U}_{env}$. 50
6.2 HLDCs for different values of WWR. 52
6.3 HLDCs for different values of $n50$. 53
6.4 HLDCs for different values of γ_{front}. 54
6.5 HLDCs for different values of γ_{front}, relative to the average HLDC of the eight cases. 55

7.1 HLDCs for two different control strategies of a gas-fired heating system. 59
7.2 Comparison of the total heat demand, for an eight-day period, using RBC and OC. 60
7.3 Comparison of the temperature of zone 13 and the delivered heat in zone 13, for an eight-day period, using RBC and OC. 60

7.4 Results for optimal control of a series hybrid heating system consisting of a natural gas boiler of 160 kW and a heat pump of 20 kW. 62
7.5 Heat demand profile, for an eight-day period, of optimal control of gas-fired heating system and optimal control of series hybrid heating system. 62

A.1 Adapting standard daily load profiles. 75
A.2 Example of space heating load generation. 76
A.3 All possible technologies. 76
A.4 Example of multi-objective optimisation. 77
A.5 Original (default) normalised day profile of heat demand in school buildings. 78
A.6 Newly defined normalised day profile of heat demand in school buildings. 78
A.7 All enabled technologies for the case of building D of UCLL Campus Proximus. 79
A.8 COP curves for 'Carrier 30 AW (ASHP)' as defined in *nPro*. 79
A.9 COP curves for 'Carrier 30 WG (water/brine)' as defined in *nPro*. . . . 80

B.1 Typical heat demand during a week in winter. 82
B.2 Average daily heat demand and occupancy schedule. 82
B.3 Temperature profile of zone 12 and global horizontal irradiance. 83
B.4 Graphical *Modelica* representation of the school building model. 84
B.5 Year, week and day occupancy schedule of zone 1 (canteen). 86
B.6 Year, week and day occupancy schedule of zone 2 (kitchen). 86
B.7 Year, week and day occupancy schedule of zone 4 (classroom). 87
B.8 Year, week and day occupancy schedule of zone 9 (teachers' room). . . . 87
B.9 Year, week and day occupancy schedule of zone 10 (office). 88
B.10 Year, week and day occupancy schedule of zones 19 and 20 (hallways). . 88
B.11 Year, week and day setpoint schedule of zone 10 (office). 89
B.12 Year, week and day setpoint schedule of zone 12 (gym). 89
B.13 Year, week and day setpoint schedule of all other zones. 90

C.1 *Modelica* heating system model in the case of optimal control of a gas-fired heating system. 93
C.2 *Modelica* heating system model in the case of optimal control of a series hybrid heating system. 94
C.3 *Modelica* heating system model in the case of optimal control of a parallel hybrid heating system with two two-way valves. 94
C.4 *Modelica* heating system model in the case of optimal control of a parallel hybrid heating system with a three-way valve. 95
C.5 Results for optimal control of a parallel hybrid heating system (with two two-way valves) consisting of a natural gas boiler of 160 kW and a heat pump of 20 kW. 96

C.6 Heat demand profile, for an eight-day period, of optimal control of gas-fired heating system and optimal control of parallel hybrid heating system (with two two-way valves). 97
C.7 Results for optimal control of a parallel hybrid heating system (with one three-way valve) consisting of a natural gas boiler of 160 kW and a heat pump of 20 kW. 97
C.8 Heat demand profile, for an eight-day period, of optimal control of gas-fired heating system and optimal control of parallel hybrid heating system (with one three-way valve). 98

List of Tables

1.1 Historical GHG emissions and GHG emission targets for the Flemish buildings sector. . . . 1

2.1 Comparison of different heat pump types. . . . 9

3.1 Relevant data of building D of UCLL Campus Proximus. . . . 19
3.2 Costs of different technologies. . . . 22
3.3 Results system optimisation with all relevant technologies enabled. . . . 24
3.4 Results system optimisation with only GSHP enabled. . . . 25
3.5 Results system optimisation with only ASHP enabled. . . . 25

4.1 U-values found in literature and default U-values. . . . 32
4.2 Occupancy data per zone. . . . 33
4.3 Internal heat gains. . . . 34

5.1 Relevant parameters in the analysis of the impact of the *nPro* optimisation settings and building parameters on heat demand and optimal hybrid heating system size. . . . 42
5.2 Building parameter values for the baseline scenario. . . . 43
5.3 Values for baseline scenarios. . . . 45
5.4 Results for parallel and series configuration. . . . 46
5.5 Results for various minimal emission reductions. . . . 47

6.1 Investigated values of building parameters. . . . 49
6.2 Results for various building envelope U-values. . . . 51
6.3 Results for various window-to-wall ratios. . . . 52
6.4 Results for various airtightness values. . . . 53
6.5 Results for various building orientations. . . . 56

B.1 Architectural properties of the modelled school building. . . . 83
B.2 Constructions used in school building model. . . . 85
B.3 Thermodynamic properties of used materials. . . . 85
B.4 Calculation of nominal pressure rise of each pump. . . . 91

List of Abbreviations and Symbols

Abbreviations

ASHP	Air source heat pump
CAPEX	Capital expenditures
COP	Coefficient of performance
DHW	Domestic hot water
EPC	Energy performance certificate
ETS	Emission trading system
GHG	Greenhouse gas
GSHP	Ground source heat pump
HC	Heating curve
HDD	Heating degree-day
(H)LDC	(Heat) load duration curve
HLT	Heating limit temperature
HPT TCP	Technology Collaboration Programme on Heat Pumping Technologies
IEA	International Energy Agency
IPCC	Intergovernmental Panel on Climate Change
MPC	Model predictive control
Mt CO_2-eq	Million tonnes of carbon dioxide equivalents
OC	Optimal control
PUR	Polyurethane
RBC	Rule-based control
SPF	Seasonal performance factor
SQ	Sub-question
TACO	Toolchain for Automated Control and Optimization
TMY	Typical meteorological year
TRV	Thermostatic radiator valve
UCLL	University Colleges Leuven-Limburg
WSHP	Water source heat pump
WWR	Window-to-wall ratio

Symbols

γ	Azimuth [$^\circ$]
ΔCE_{min}	Minimal CO_2 emission reduction [%]
ρ	Density [$\frac{\text{kg}}{\text{m}^3}$]
A	Area [m^2]
c	Specific heat capacity [$\frac{\text{J}}{\text{kg K}}$]
$C_{\Delta CE}$	Cost of CO_2 emission reduction [$\frac{€}{\text{tCO}_2}$]
C_{CO_2}	CO_2 price [$\frac{€}{\text{tCO}_2}$]
$C_{an,tot}$	Total annual cost (excl. CO_2 cost) [$\frac{€}{\text{year}}$]
$C_{inv,ini}$	Initial investment cost [€]
CE	CO_2 emissions [$\frac{\text{tCO}_2}{\text{year}}$]
COP	Coefficient of performance [/]
d	Thickness [cm]
E_{heat}	Heating energy [$\frac{\text{MWh}}{\text{year}}$]
f	Fraction [%]
h	Height [m]
k	Thermal conductivity [$\frac{\text{W}}{\text{m K}}$]
L_{boi}	Remaining lifetime of current gas boiler [years]
$\dot{m}$	Mass flow rate [$\frac{\text{kg}}{\text{s}}$]
$n50$	Air exchange rate occurring at a pressure difference of 50 Pa [h^{-1}]
$P_{boi,cur}$	Capacity of current gas boiler [kW]
$P_{boi,new}$	Capacity of new gas boiler [kW]
P_{hp}	Capacity of heat pump [kW]
$\dot{Q}$	Heat flow rate [kW]
$\dot{Q}_{peak}$	Peak heat demand [kW]
R	Thermal resistance [$\frac{\text{m}^2\ \text{K}}{\text{W}}$]
T	Temperature [K]
TD	Thermal discomfort [$\frac{\text{degree h}}{\text{year}}$]
U	U-value or thermal transmittance [$\frac{\text{W}}{\text{m}^2\ \text{K}}$]
V	Volume [m^3]
WWR	Window-to-wall ratio [%]

Chapter 1

Introduction

Article 2 of the Paris Agreement states that the participating countries will aim to "hold the increase in the global average temperature to well below 2°C above pre-industrial levels and pursue efforts to limit the temperature increase to 1.5°C above pre-industrial levels" [1]. According to a 2023 report issued by the Intergovernmental Panel on Climate Change (IPCC), it is necessary to reach global net zero CO_2 emissions and a substantial reduction in the emissions of other greenhouse gases by 2050, to reach this goal of limiting global warming to 1.5°C [2].

In 2021, 73.4 million tonnes (Mt) of CO_2 equivalent (CO_2-eq) greenhouse gases were emitted in Flanders [3]. The buildings sector was accountable for 17% of these emissions (12.6 Mt CO_2-eq). About a quarter of these emissions (3.4 Mt CO_2-eq) originated from non-residential buildings. Since 2005, there has been a 20% greenhouse gas (GHG) emission reduction in the Flemish buildings sector, but it is worth noting that most of this reduction can be attributed to the *residential* buildings sector. The target for 2030 is to achieve a 42% reduction in emissions compared to the 2005 levels [4]. For the existing non-residential buildings, the goal is to reach carbon neutrality for heating, domestic hot water, cooling and lighting by 2050 [5]. An overview of the historical GHG emissions and maximum allowed future GHG emissions for 2025, 2030 and 2050 is given in Table 1.1.

	2005	2021	2025	2030	2050
Non-residential buildings	3.5	3.4	3.2	2.6	n/a
Residential buildings	12.2	9.1	8.3	6.5	n/a
Total buildings sector	15.7	12.6	11.5	9.2	2.3

TABLE 1.1: Historical GHG emissions (2005 and 2021) and GHG emission targets (2025, 2030 and 2050) for the Flemish buildings sector (in Mt CO_2-eq) [4, 5].

These numbers show that most GHG emission reductions will need to take place in the residential buildings sector, but that non-residential buildings cannot be overlooked. The majority of GHG emissions of Flemish buildings comes from heating [4], either directly through the use of fossil fuels in heating systems (e.g. gas boilers) or indirectly through the generation of electricity and heat that is

subsequently used in these buildings for heating purposes [6]. There are two main approaches in which emission reductions can happen. On the one hand, the energy demand must be minimised, for example by increasing the energy efficiency of the building envelope. On the other hand, the heating and cooling installations must be made more sustainable, for example via electrification. The Flemish Energy and Climate Plan [4] suggests that achieving significant decreases in energy consumption, as anticipated for residential buildings, is improbable within the non-residential buildings sector due to the typologies and usage of these kinds of buildings. Thus, the primary objective is to aim for carbon neutrality by increasing the share of renewables in their final energy use for heating and cooling. In terms of this share, the Belgian buildings sector is one of the worst performers in the European Union, with a share of only 9.2%, well below the EU average of 22.9% [7]. Therefore, a transition towards district heating (often combined with (centralised) heat pumps) is necessary in areas with high heat demand density, while heat pumps are required in areas with low heat demand density.

School buildings make up a significant proportion of the total number of non-residential buildings. Estimations from 2018 by the Flemish Agency for School infrastructure show that there are 17 995 distinct school buildings in Flanders with an average gross floor area of 1 063 m^2 [8]. In 2008, heating oil was used in 43% of the heating installations of these school buildings. Ten years later, this number decreased to 22% and the usage of gas for heating increased from 74% to 84%. In 2018, 9% of school buildings had a heat pump installed and 5% of them used additional solar collectors [8]. These data show a positive trend, but it also becomes clear that there is still a lot of room for improvement in the Flemish school building stock. In Flanders, half of the school buildings are at least 50 years old [8], which often means a lack of proper insulation and consequently higher peak demands. Completely replacing current (gas) boilers with heat pumps would therefore require very high investment costs and could possibly endanger thermal comfort. A hybrid heating system, which uses both a heat pump and the existing gas boiler to provide heat, offers a solution. As the existing heating installation will continue to be utilised, fewer capital investments will be required, which is beneficial since schools often have only limited budgets available.

Another positive outcome of partially electrifying the heating system is that part of the CO_2 emissions is shifted to the power generation sector, which falls under the European Emission Trading System (ETS). The combustion of fuels in buildings for heating purposes will become a component of this 'cap and trade' mechanism only starting in 2027, with the launch of ETS 2. This will result in an increase of the price of natural gas for heating [9].

Hybrid heat pumps, sometimes also called bivalent heat pumps, are the combination of an electric heat pump and a fossil-fuelled boiler or furnace [10]. This combination allows the base heat load of a building to be covered by the energy-efficient heat pump, while meeting peak demands using the non-renewable boiler. In the final report on hybrid heat pumps made in 2019 by the Technology Collaboration Programme on Heat Pumping Technologies (HPT TCP) by the International Energy Agency (IEA) [11], two of the presented key findings are the following:

1. "Hybrid heat pumps may enable quick and successful application of heat pump technology in existing buildings without the immediate need for renovation."
2. "Hybrid heat pumps may serve as a gateway towards low-carbon heating."

These two findings make hybrid heat pumps ideal for the case of the Flemish school building stock that was described above.

1.1 Problem statement

It is thus clear that there is significant potential for increasing the share of renewable energy in Flemish school buildings. While schools are committed to reducing their carbon footprint, they face challenges due to budget constraints and aging infrastructure. The implementation of a hybrid heating system can serve as an effective initial step towards achieving the 2050 climate targets.

This thesis focuses on the *heating* demand of Flemish school buildings. The majority of existing school buildings does not have a cooling installation, as during the summer holidays, typically the warmest time of the year, school buildings are not used. Also, according to ir. arch. Friedl Decock, schools should prioritise passive cooling techniques such as efficient solar shading or night cooling [12].

The heating demand of buildings typically consists of two components: space heating and domestic hot water (DHW). The focus of this thesis is on space heating, as schools often only have limited use of DHW. The DHW demand that they do have is sometimes provided in a decentralised manner, e.g. by using small electric boilers.

When a school considers introducing a heat pump into its heating system, the primary concerns are determining the appropriate type and size of the heat pump.

In the literature review by Beccali et al. on electrical hybrid heat pumps assisted by natural gas boilers [10], the authors highlight the need for additional investigation into the design and sizing rules of system and components based on final use and climate conditions. Furthermore, the review underscores the importance of further researching environmental considerations, such as CO_2 emissions, throughout the operation and entire life cycle of hybrid heat pumps.

Although there are general numbers available in literature, there has not been much research into finding a quantitative way to do this sizing, taking into account the most important factors, mainly being the total (annualised) cost. Often, heat load duration curves (HLDCs) are used for the sizing of hybrid heating systems [13]. However, another typical feature of this specific problem is the fact that the data school buildings can offer may be limited. The installation of digital natural gas meters is only a recent development, so most schools only have a monthly or annual record of their natural gas consumption. It can thus be assumed that annual heating load profiles are not available, so that it is not possible to calculate a HLDC for a given building. It is therefore necessary to consider how different parameters affect heat demand and how these parameters should be taken into account in the sizing of the hybrid heating system.

Another aspect that requires further research is optimal control. By applying an optimal control strategy, the heat pump may be sized smaller due to a lower peak demand. Also, optimal control might lead to higher average coefficient of performance (COP) values. Sun et al. [14] concluded that with smart control of hybrid heat pumps, higher average COPs can be reached in residential buildings. Berthou et al. [15] investigated the optimal control of the heating system of an elementary school building in France and showed that one of the strategies could save 5% of energy during cold weeks while guaranteeing a comfortable indoor temperature. However, the investigated heating system consisted of electrical heaters and air handling units, which is not representative for the Flemish school building stock. It should thus be investigated whether significant gains can be achieved by using an optimal control strategy in a heating system either consisting of a gas boiler or consisting of a gas boiler and a heat pump.

1.2 Research questions

The main research question of this thesis is the following.

> *How can heat pumps be integrated into the fossil fuel-based heating system of typical Flemish school buildings to achieve a cost-effective CO_2-reduction while maintaining thermal comfort?*

To answer this question, several sub-questions (SQ) are addressed. These are briefly presented in the current section.

> SQ1 - *Which parameters have an influence on the heat demand of typical Flemish school buildings?*

Identifying these parameters is important because they will need to be considered when studying the heat demand of typical Flemish school buildings, and their impact on the optimal hybrid heating system size. A comprehensive literature review is conducted, where patterns and characteristics of the heat demand of school buildings are also identified.

> SQ2 - *Can the nPro tool be used to determine the optimal size of a hybrid heating system for an existing school building?*

nPro [16] is a web-based planning tool for designing district energy systems and thermal networks, offered by *nPro Energy GmbH* and developed by Dr. Marco Wirtz of RWTH Aachen University. *nPro* is capable of optimising energy system configurations and sizes.

Data of a real school building is used as input for the tool. Applying the tool on this case will provide insights into the functionality, working principles and limitations of the tool. If *nPro* requires input data that is not available, an assumption is made or a default value from the tool is used. Furthermore, the (underlying) assumptions

made by *nPro* are identified. These assumptions (made by the user and the tool) are further investigated in SQ3. The proposed hybrid heating system is critically reviewed and different technologies and configurations are compared and investigated.

> SQ3 - *What is the impact of changing the influential parameters that were determined in SQ1 and the assumptions discovered in SQ2 on both the heat demand of a typical school building and the optimal size of the hybrid heating system that nPro calculates?*

This investigation focuses on hybrid heating systems consisting of a gas boiler and an air-source heat pump. The capacity of the air-source heat pump is optimised. A model of a school building (representing the 'average' Flemish school building) is developed using *Modelica*. This allows for the generation of annual heat demand profiles.

As a first step, the particular assumptions or limitations of *nPro*, which were revealed in SQ2, are examined. Annual heat demand profiles are generated by performing simulations of the representative school building *Modelica* model, assuming typical values for different building parameters. Next, these annual heat demand profiles are imported in *nPro*. Then, the optimal hybrid heating system size is compared for different values of the parameters involving the specific assumptions or limitations of *nPro*.

Then, more dynamic simulations are performed using the *Modelica* model, but for different values of the parameters identified in SQ1. The heat demands are compared, and used as input in *nPro*, after which the system optimisations can also be compared. This allows the sensitivity of these factors on both the heat demand and optimal hybrid heating system size to be analysed.

The results are always compared to each other and to the relevant baseline scenario. This will indicate to what extent the *nPro* tool can take into account the factors identified in SQ1 and SQ2, and how much the heat demand (annual heat demand profile and HLDC) and optimal hybrid heating system size are affected.

> SQ4 - *What is the impact of implementing an optimal control strategy on the heat demand and the optimal size of the hybrid heating system?*

Next, the focus shifts to exploring optimal control. For this, *TACO* (Toolchain for Automated Control and Optimisation) [17] is used, which is a *Modelica*-based automated toolchain for model predictive control (MPC) of building systems.

> SQ5 - *What recommendations can be given to schools that want to reduce their carbon footprint by implementing a hybrid heating system?*

This sub-question concludes the thesis. An answer to this question is formulated based on the results of previous sub-questions.

1.3 Thesis outline

Chapter 2 presents the results of the comprehensive literature study that was conducted. Key concepts are explained and the methodology is further specified. Additionally, the parameters that influence the heat demand of typical Flemish school buildings, which is the subject of SQ1, are identified. Chapter 3 covers the answer to SQ2. The *nPro* tool is applied to a real-life school building that wants to implement a hybrid heating system. In Chapter 4, the representative school building model that is used in the remainder of this thesis is presented in detail. Chapters 5 and 6 concern SQ3 and present the results of the analysis regarding aspects such as system configuration and the desired emission reduction, as well as building parameters like window-to-wall ratio (WWR) and building orientation. This will provide insights into the extent to which the *nPro* tool can take into account the factors identified in the first two sub-questions, and the extent to which heat demand (annual heat demand profile and HLDC) and optimal system sizing are affected. The impact of optimal control is investigated in Chapter 7, which is the subject of SQ4. The initial step is to test an optimal control strategy for the current heating system. Subsequently, an optimal control strategy is tested for a hybrid heating system. Finally, the results of previous chapters are combined and recommendations for schools considering the implementation of a hybrid heating system are listed in Chapter 8, thus addressing SQ5. Chapter 9 contains the overall conclusion of this thesis and suggestions for future research.

Figure 1.1 provides a graphical overview of how the chapters of this thesis are related, indicating which sub-question is addressed in each chapter.

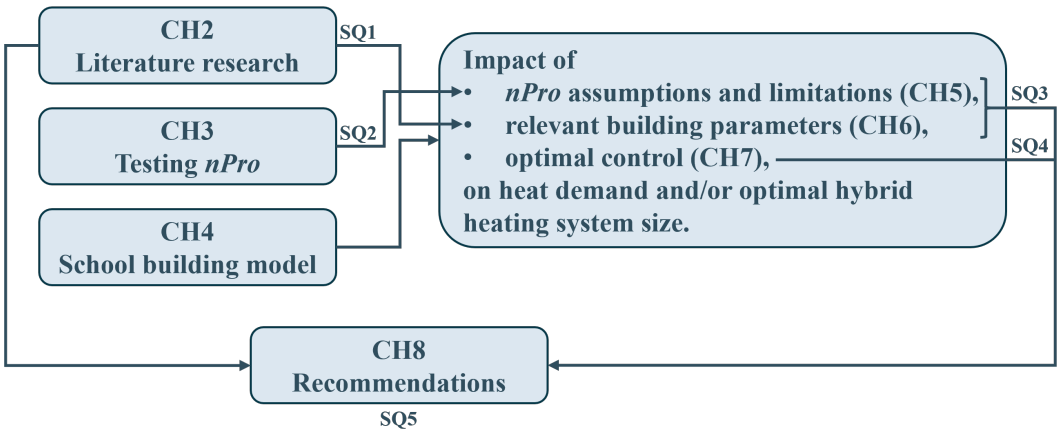

Figure 1.1: Graphical overview of the structure of this thesis.

Chapter 2

Literature research

This chapter presents the results of a comprehensive literature study that was conducted. Sections 2.1 and 2.2 introduce the key concepts of this thesis: hybrid heat pumps and (school) building heating demand, respectively. In Section 2.3, the used software tools are presented.

2.1 Hybrid heat pumps

Hybrid heating systems use two or more heating technologies to provide space heating and domestic hot water in buildings. A hybrid heat pump is the most common example of a hybrid heating system. The 2019 final report on hybrid heat pumps by the IEA HPT TCP defines a hybrid heat pump as "the combination of an electric heat pump and a fossil-fueled boiler or furnace under a single (optimised) control strategy" [11]. This is the definition that will be used throughout this thesis.

2.1.1 Classification

Although the definition of a hybrid heat pump is now established, there are still many possible variations to the concept. The following paragraphs discuss these aspects and their relevance in the specific context of this thesis.

Integrated or non-integrated

With integrated hybrid heat pumps, the boiler, heat pump and system controller are sold as a single unit [11]. This configuration is less relevant to this thesis as the main focus is on non-integrated systems where heat pump and system controller are installed alongside an existing boiler, so retrofit cases. Gas boiler and heat pump remain discrete units. According to [18], integrated and non-integrated hybrid heat pumps can have similar performances.

Fossil-fueled boiler type

According to [11], it does not matter much which fossil heating system is used to support a heat pump in a hybrid system. However, the majority of Flemish schools use gas as their energy source for space heating (84% in 2018 [8]). Most of the other schools use either heating oil or electricity for heating. In 2018, the use of heating oil had already largely decreased. The focus of this thesis is therefore on gas boilers.

Electric heat pump type

In this thesis, the term 'heat pump' will exclusively refer to electric heat pumps. The general working principle of an electric heat pump is shown in Figure 2.1. The coefficient of performance (COP) of a heat pump is defined as the ratio between the delivered thermal power and the consumed electrical power. Heat pumps are classified according to their heat source and working fluids. The three most common types of heat pumps are air source heat pumps (ASHPs), water source heat pumps (WSHPs), and ground source heat pumps (GSHPs).

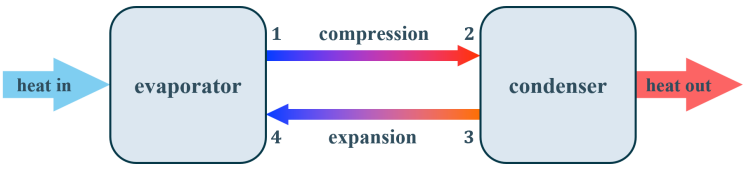

(a) Schematic overview.

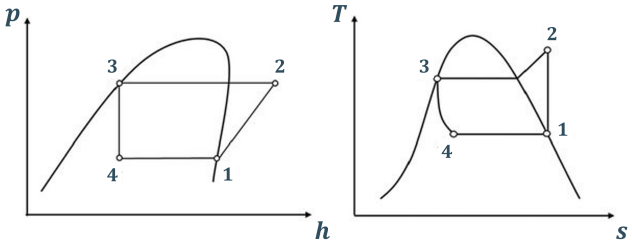

(b) $p-h$ and $T-s$ diagram [19].

Figure 2.1: General working principle of a heat pump.

ASHPs are the most prevalent type due to the straightforward installation and relatively low capital expenditures (CAPEX) or installation cost. They are also easy to install in existing buildings [20]. They exist in both air-to-air and air-to-water forms. This text will not cover air-to-air heat pumps as Flemish schools almost exclusively use water-based central heating. An unfavourable characteristic of ASHPs is that their capacity and COP are reduced in the coldest period of the year (due to the low temperature of the heat source, being the environment), when the building heat demand is high [21].

WSHPs use water as low-temperature heat source, usually surface water (e.g. a river) or ground water (e.g. an aquifer), which must be available near the building. Advantages of WSHPs are the fact that water has a more stable temperature than

outside air, which results in higher average COP values, and the possibility of passive cooling. However, WSHPs have high installation costs.

GSHPs for large buildings use a borefield consisting of multiple vertical boreholes as a low-temperature heat source. This results in a more stable source temperature and allows for passive cooling. However, GSHPs have a very high installation cost, and the feasibility of a borefield must be assessed beforehand.

Table 2.1 provides an overview of the most significant benefits and drawbacks of these three technologies in the context of this thesis. The most crucial factors are CAPEX and location requirements, which make the ASHP the best option. The main focus will thus be on this heat pump type, although a brief investigation of the GSHP is also conducted in Chapter 3.

	CAPEX	Location requirements	Impact of ambient conditions	Typical COP [22]
ASHP	+	+	−	3
WSHP	−	−	+	4.5
GSHP	−	−	+	3.5-4

TABLE 2.1: Comparison of different heat pump types (benefit: +, drawback: −).

System configuration

In literature, both parallel and series hybrid heating systems are discussed. These two configurations are shown in Figure 2.2. In the parallel configuration, heat pump and gas boiler operate in parallel. They thus have the same supply temperature, unless a mixing valve is used. In the series configuration, the heat pump heats the water, and the gas boiler can provide additional heating if needed. In both cases, thermal energy storage (TES) is possible in the form of a hot water tank.

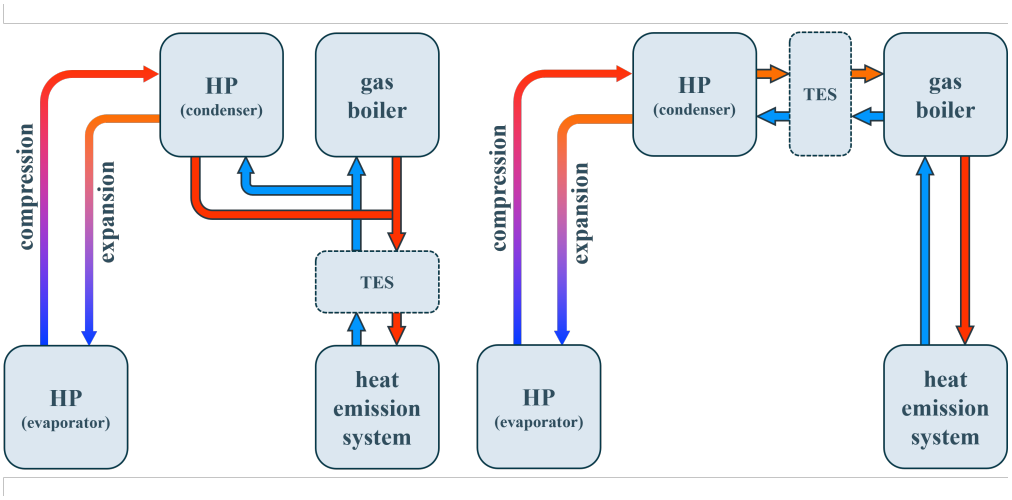

FIGURE 2.2: Parallel (left) and series (right) system configuration.

According to Klein et al. [23], the advantage of the series configuration is that the heat pump can benefit from lower supply temperatures. The fact that gas boiler and heat pump can operate at different temperature levels is also mentioned by Roccatello et al. [24]. According to Bagarella et al. [21], the parallel configuration is the most common in existing hybrid heating applications in residential buildings. The authors compared this configuration with what they called the 'bivalent alternative plant', where the heat pump and gas boiler are also in parallel but never operate simultaneously. They concluded that this 'bivalent alternative plant' is less advantageous, especially when the heat pump has a relatively low capacity. Lee et al. [25] concluded that for hybrid GSHPs, the parallel configuration is preferable as it offers a better heating performance and higher exergy efficiency. A similar conclusion was drawn by Park et al. [26]. A comparison between parallel and series hybrid heating systems (with an ASHP) for large buildings has not yet been made. Furthermore, it is not possible to draw any general conclusions about the preference for one of the two configurations based on the current literature. Therefore, both configurations will be investigated in this thesis, but focus will be on the parallel configuration for reasons discussed in Section 2.3.1.

Control strategy

The possible control strategies of a hybrid heating system can be classified in rule-based control methods (RBC) and model predictive control methods (MPC) [10]. RBC uses predefined rules to regulate the operation of the heating system based on various factors such as temperature, time of day and weather conditions.

An example of an RBC strategy is the 'alternative-parallel bivalent' operating scheme as described by Klein et al. [23]. In this operating scheme, two temperature thresholds are defined: the cut-off point $T_{\text{cut-off}}$ and the bivalence point T_{biv}. When the ambient temperature is below $T_{\text{cut-off}}$, only the gas boiler is used. When the ambient temperature is between $T_{\text{cut-off}}$ and T_{biv}, both heating technologies are used. Above T_{biv}, only the heat pump is used.

MPC on the other hand is an optimal control method. Over a certain prediction horizon, the heating system's control inputs are optimised using a model of the system and predictions of the system's disturbances to minimise a cost function. The optimised control actions of the first control interval are applied after which the prediction horizon is shifted, and the process is repeated using the latest measurements [27]. According to [10], RBC methods are most prevalent because they can be very simple and cost-effective. Currently, MPC is not commonly used yet [10], but this kind of control has the potential to significantly decrease energy costs while maintaining or even increasing thermal comfort [28].

An RBC strategy will be assumed for the dynamic simulations performed with the representative school building model, which is described in Section 4.5.5. In *nPro*, the design calculation is based on an ideal system operation, which assumes, a perfect foresight of future demands for example. Chapter 7 will further examine the impact of optimal control, i.e. a control strategy that has a perfect foresight of

future demands and minimises a certain objective by calculating the optimal values for every control variable at every time instance.

2.1.2 Sizing of the heat pump

According to the report of the IEA HPT TCP [11], the size of the heat pump component in a hybrid heating system has an important impact on the coverage ratio, which is the ratio of the heat provided by the heat pump to the total heat demand [29]. For relatively small heat pumps (and thus small coverage ratios), coverage ratio rapidly increases as heat pump capacity increases. However, when coverage ratio is already high, an extra increase in heat pump capacity will only lead to a small increase in coverage ratio. In [11], it is also mentioned that for the 'average' European climate zone, a heat pump capacity between 30% and 50% of the peak heat demand gives an optimal compromise between the investment cost of the heat pump and the heat pump coverage ratio. According to Klein et al. [23], medium-sized heat pumps achieve the highest seasonal performance factor (SPF) values. The SPF is the efficiency of the system evaluated over one year. A similar conclusion is presented by Dongellini et al. [30]. According to that paper, the SPF benefits from a smaller heat pump capacity for two reasons: the smaller number of defrost cycles and the reduced period of low COP heat pump operation.

A logical approach to heat pump sizing is sizing based on minimum total cost. This allows for the consideration of CO_2 costs. However, this could result in no heat pump being proposed at all because, for example, the decrease in operational costs might not outweigh the required high capital investments. It is therefore important to consider that schools wish to achieve a certain emission reduction and that there are emission targets that must be met. An approach to visualising this is plotting cost against CO_2 emission reduction, as demonstrated in the Master's thesis of Arno Meessens [31] and shown in Figure 2.3.

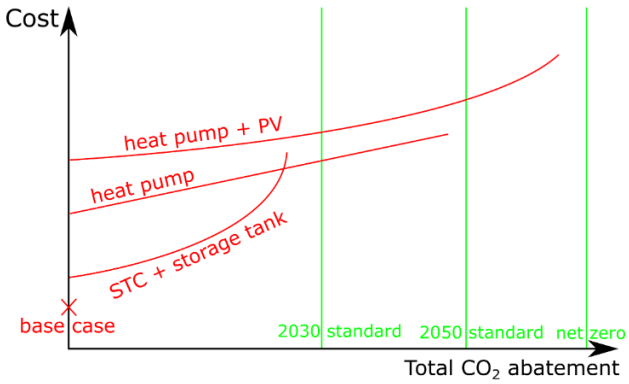

FIGURE 2.3: Example of a simplified cost - CO_2 abatement graph [31].

Heat load duration curves (HLDCs) can also be used to visualise the impact of choosing a certain capacity of heat pump on the heat demand that can be covered with that heat pump. This was for example done in case studies like [32] and [33]. In

the PhD of Damien Picard, optimal HVAC design is done using HLDCs of buildings [34]. However, in his work, the generation of these load duration curves based on a small amount of parameters is not implemented yet. HLDCs are explained in more detail in Section 2.2.1.

2.2 Heat demand of buildings

2.2.1 General aspects

Heat losses and heat gains

A building has a heating demand due to the requirement for each zone to be maintained at a certain temperature, because occupants desire thermal comfort.

However, heat losses occur in buildings, which can be categorised into three types: transmission, infiltration and ventilation losses. Transmission losses are heat losses due to the transmission of heat through all elements of the building envelope, being floors, external walls and roofs. These losses can be described by the equation $\dot{Q}_{transmission} = U \cdot A \cdot \Delta T$, where U is the heat transfer coefficient or U-value (in $\frac{\mathrm{W}}{\mathrm{m^2\ K}}$), A is the loss area (in $\mathrm{m^2}$) and ΔT is the temperature difference (in K). The U-value of a building element is the heat loss (in W) through 1 $\mathrm{m^2}$ of that building element, when there is a temperature difference of 1 K across it. The total transmission losses thus depend on the area of the building envelope (loss area), the quality of insulation, the ambient air temperature and the setpoint temperature inside the building.

Infiltration losses are losses due to the leakage of indoor (warm) air into the environment and outside (cold) air into the building. This air infiltration occurs continuously due to cracks and crevices (adventitious openings) in the building envelope and can lead to significant heat losses [35]. The amount of infiltration losses thus also depends mainly on characteristics of the building envelope. The air infiltration rate of a particular zone is typically expressed by a $n50$ value, which is the air exchange rate (per hour) occurring at a pressure difference of 50 Pa [36].

Ventilation losses take place when a ventilation system is present. It is inevitable that ventilation will result in a certain amount of heat losses, as with ventilation (colder) outside air is forced into the building. However, installing a heat recovery system can greatly reduce ventilation losses. In this thesis, ventilation losses will not be considered, as the assumption is made that no ventilation is present. This is further elaborated upon in Section 4.2.6.

One other aspect contributing to the heat demand of buildings is intermittent heating. If the temperature during non-occupied periods has a certain setback value, additional heating will be needed in the morning to get back to the setpoint temperature of the occupied periods.

Next to heat losses, buildings are also subject to heat gains. Two types can be distinguished: solar and internal gains. Solar gains result from absorbed solar radiation and are often a significant part of the total heat gains of a zone [35]. The amount of solar gains depends on glazing type, window-to-wall ratio (WWR) and

the presence of solar shading. Internal gains occur because of occupants, electrical equipment and lighting.

In summary, based on the reasoning described above, the following parameters have most impact on the heat demand of buildings and should therefore be considered when studying it:

- the indoor temperature setpoint,
- the overall building geometry (floor and loss area, conditioned volume, zone heights),
- the building's orientation,
- the (U-values of the) building envelope (glazing type, quality of wall and roof insulation),
- the building's airtightness,
- the window-to-wall ratio,
- the amount of solar shading,
- the amount of internal gains due to people (occupational schedule, occupant density and occupant activity level),
- the amount of internal gains due to equipment and lighting,
- the weather conditions (mainly temperature and solar irradiation),
- the presence and quality of ventilation.

This list is not in any particular order. These parameters affect the heat demand of buildings in general, including Flemish school buildings. In Section 2.2.2, this list is condensed to the parameters that are most relevant in the context of this thesis.

Heat load duration curve

HLDCs express the relationship between time and heat demand. They show the duration during which heat demand is greater than or equal to a certain level (i.e. in W) [13]. The area under the HLDC is equal to the total heat demand (i.e. in Wh).

An annual HLDC is created by ordering the heat demand data of an annual heat demand profile in descending order. Figure 2.4 provides an example of a HLDC. From this curve, it can be easily observed that the peak heat demand is equal to 185 kW, that the heat demand is at least 32 kW during 1 000 hours of the year, and that there is a heat demand for approximately 3 000 hours of the year.

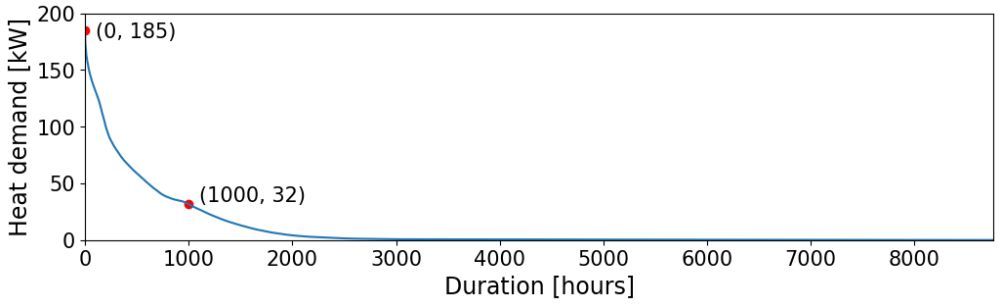

FIGURE 2.4: Example of a HLDC.

2.2.2 School buildings

Parameters affecting heat demand

According to Wauman et al. [37], who investigated boundary conditions for Flemish schools for use in energy assessment methods, some of the most influential parameters affecting the energy demand of Flemish schools are occupational schedule, setpoint temperature and the use of equipment and lighting. In their study, the sensitivity of building-specific parameters was not analysed. Building activity is also mentioned by Hawkins et al. [38] as a strong determinant for energy use. Alghamdi et al. [39] also concluded that heating setpoint temperature strongly influences energy consumption and occupancy density moderately influences energy consumption. However, Wauman et al. provide deterministic and representative values for occupational schedule, setpoint temperature as well as equipment and lighting use. These values will be used in this thesis. It can be assumed that there is little variation in occupational schedule and setpoint temperature between different Flemish school buildings. The same is true for internal heat gains because of people, equipment and lighting, partly due to the fact that these are linked to the occupational schedule.

Hawkins et al. [38], Alghamdi et al. [39] and Mohamed et al. [40] did look into the effect of building-specific parameters on the heating demand of educational buildings. Hawkins et al. mention environment, primary material, glazing type and ratio, height and aspect ratio as strong determinants for energy use. Alghamdi et al. concluded that external wall construction, infiltration and WWR moderately influence energy consumption. According to Albatayneh et al. [41], building orientation can be a low-cost option to improve thermal comfort and decrease the heating and cooling demand of buildings, and it can be easy to control during the conceptual design phase.

Within the scope of this thesis, solar shading is not considered. This is a reasonable assumption, given that schools often lack external solar shading, either due to a focus in the design phase on maintaining a comfortable temperature in winter, or due to a lack of budget [42]. A specific building geometry will also be assumed, based on the representative school building model of Wauman et al. [37]. Expressing the heating demand in $\frac{\mathrm{W}}{\mathrm{m}^2}$ rather than W and in $\frac{\mathrm{kWh}}{\mathrm{m}^2}$ rather than kWh allows for a more consistent comparison across different buildings. As this thesis focuses on Flemish school buildings in particular, there is little or no variation in climate and average weather conditions. These boundary conditions are therefore also assumed to be constant.

Thus, the parameters of which the sensitivity on the heat demand and on the optimal heat pump sizing will be investigated in Chapter 6 are:

- the U-values of the building envelope,
- the window-to-wall ratio,
- the building's airtightness,
- the building's orientation.

Heat demand profile and heat load duration curve

Limited information can be found regarding typical heat demand profiles and HLDCs of school buildings. However, some conclusions can be drawn from the few sources that are available. Ivanko et al. [43] analysed daily heat demand profiles of Norwegian educational buildings before and during the COVID-lockdown of 2020. They observed that the heat demand profile before and during lockdown had a very similar shape: a peak in heat demand around 09:00, a declining heat demand between 10:00 and 17:00 and a significant heat demand reduction between 20:00 and 06:00. Lindberg et al. [44] predicted heat load profiles of school and office buildings for a cold winter week and also obtained similar daily heat demand profiles. Moreover, Guan et al. [45] acquired an averaged daily heat demand with a similar shape, although the peak heat demand of their profiles was less outspoken. They however studied an entire university campus building complex, which could lead to a more spread-out daily heat demand profile because of the different buildings with different purposes. The characteristic features of the daily heat demand profile of school buildings thus are: a morning peak situated around the school's opening hour, a declining demand from noon until the school's closing hour and a low and steady heat demand during nighttime, weekends and holidays. Only one HLDC of a school building was found in literature, which is shown in Figure 2.5. The HLDC was constructed by Zimny et al. [32] for a school building in Poland with a hybrid heating system. The HLDC shows a peak heat demand of 100 kW and a heating season (duration of non-zero heat demand) of approximately 5 000 hours. The heat pump in the hybrid heating system has a capacity of around 32 kW, with a relatively high share in the total provision of heat (coverage ratio).

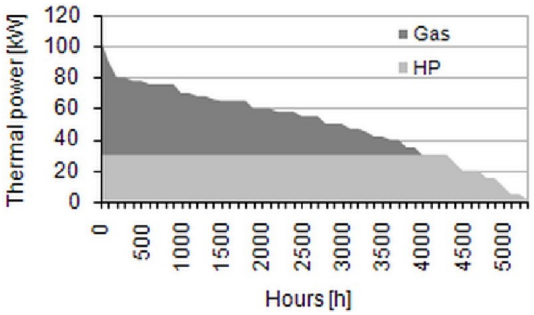

FIGURE 2.5: HLDC of a Polish school with a hybrid heating system [32].

2.3 Used software tools

2.3.1 *nPro*

This section is mainly based on the documentation found on the *nPro* website [16] and a paper about the tool written by Wirtz [46].

nPro is a web-based planning tool for designing district energy systems and thermal networks, offered by *nPro Energy GmbH* and developed by Dr. Marco

Wirtz of RWTH Aachen University. *nPro* can be used to quickly and easily design energy systems for buildings and districts and evaluate them from a techno-economic perspective. For the purposes of this thesis, the focus will be on the project type 'building' within the tool.

nPro covers the three main steps in the planning of (district) energy systems: load profile generation, thermal network calculation, and energy system design optimisation. As the second one is not relevant in the context of this thesis, only the first and the last step will be explained in detail in the following paragraphs. A graphical overview of the software's overall working principle is shown in Figure 2.6. Clarifying screenshots are included in Section A.1.1 of Appendix A and referred to throughout the text.

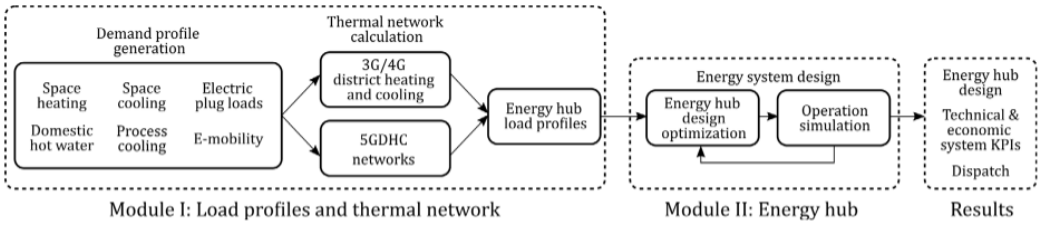

Figure 2.6: The working principle of *nPro* [46].

Load profile generation

The first calculation step of the *nPro* software is the generation of energy demand profiles. These profiles have an hourly resolution. Five types of energy demand are distinguished: space heating, domestic hot water (DHW), space cooling, process cooling and electricity (plug loads and e-mobility). Different types of energy demand require different profiles. As previously stated, this thesis focuses on the space heating demand.

The load profile generation for space heating is based upon normalised day profiles and the degree-day method. On the coldest day, 50% of the heat demand is distributed according to the normalised day profiles and the other 50% is distributed based on the degree-day method. On the other days, this profile is scaled down based on the degree-day method. Normalised day profiles are available in *nPro* for each day of the week (weekday, Saturday or Sunday) and depend on the chosen building type (e.g. school, office, residential building). The user can also define their own normalised day profiles (Figure A.1). The degree-day method is commonly used to determine the energy consumption required for space heating of buildings (e.g. [47] and [48]). It assumes a linear relationship between the heating demand and the difference between outdoor temperature and indoor setpoint temperature. The amount of heating degree-days (HDD [K day]) is calculated by *nPro* as shown in Equation 2.1.

$$HDD = \sum_{i=1}^{365} (T_{in,h} - T_{out,i}) \quad \text{if } T_{out,i} < T_{HLT} \tag{2.1}$$

$$\text{with} \begin{cases} T_{out,i} & \text{the mean outdoor temperature of day } i \\ T_{in,h} & \text{the indoor temperature for all days } i \text{ where } T_{out,i} < T_{HLT} \\ T_{HLT} & \text{the heating limit temperature (HLT)} \end{cases}$$

In this equation, there is an indoor setpoint temperature ($T_{in,h}$) and a base temperature (T_{HLT}). These are the key parameters of the degree-day method. The HLT of a building is the minimum T_{out} at which the building does not require heating energy to maintain a certain T_{in}. *nPro* uses a database with heating limit temperatures for each building type. This heating limit temperature can also be provided by the user. *nPro* chooses the indoor setpoint temperature to ensure that the user's specified boundary conditions are met. A fast-converging bisection optimisation algorithm is used to automatically select an appropriate base temperature and indoor setpoint temperature when both annual energy demand and peak demand are provided by the user. Annual energy demand can be expressed in $\frac{\text{kWh}}{\text{m}^2 \text{ year}}$ or in $\frac{\text{MWh}}{\text{year}}$, peak demand can be expressed as a specific peak demand, a total peak demand, an amount of full load hours or a heating limit temperature. Furthermore, a heating season can be defined. An example of a space heating demand profile generated by *nPro* is shown in Figure A.2.

Energy system design optimisation

The next step in the calculation is the optimal sizing of all technologies. A large amount of different technologies can be selected including for example ground source heat pumps, solar thermal collectors and electric heaters. A screenshot of *nPro* showing all possible technologies (both energy conversion and energy storage) is provided in Figure A.3. All technologies have settings that can be adjusted such as capital and operation costs, lifetimes, efficiencies and operation temperature ranges. The optimisation is done using an hourly resolution, which leads to both a sufficient accuracy and an acceptable computation time [46].

nPro includes four different optimisation objectives. The first three are minimising total annualised costs, minimising CO_2 emissions and maximising self-sufficiency. The last option is doing a multi-objective optimisation where both total annualised costs and CO_2 emissions are considered. A Pareto frontier consisting of four points (or another specified amount) is calculated where the optimal system designs can be compared for different CO_2 costs. An example is shown in Figure A.4.

The costs that are included when calculating the total annualised cost are: annualised investment costs, operational costs, electricity import costs, natural gas import costs and CO_2 costs. The constraints being considered during the optimisation include energy balances, efficiency equations, capacity constraints, storage constraints and user-defined operating restrictions.

2.3.2 *Dymola*, *Modelica* and *IDEAS*

The modelling and simulation of the school building is done using the commercial tool *Dymola* [49], which is an integrated environment for developing and simulating models in the object-oriented, multi-domain modelling language *Modelica*. The school building model, described in Chapter 4, is created using *IDEAS*[†] (Integrated District Energy Assessment Simulations), which is a library that was originally developed by KU Leuven and *3E* and is currently developed and maintained by the *Thermal Systems Simulation* research group of KU Leuven. The free open-source *Modelica* Buildings library[‡] [50, 51] is also used as it contains models for water- and air-based HVAC systems.

2.3.3 *TACO*

TACO (Toolchain for Automated Control and Optimisation) is a *Modelica*-based automated toolchain for model predictive control (MPC) of building systems [17]. *TACO* is capable of translating an optimal control problem (the combination of a *Modelica* building model, an objective function and constraints) into an optimisation problem, which it then solves.

2.4 Conclusion

This chapter provided a comprehensive overview of hybrid heat pumps and the relevance of (school) building heat demand in this context. It highlighted the predominance of gas boilers in Flemish schools and the suitability of ASHPs due to their lower installation cost. Furthermore, the chapter discussed the various configurations of hybrid heating systems. Additionally, it addressed the importance of control strategies and the sizing of the heat pump in a hybrid heating system to optimise the coverage ratio and system efficiency. Also, the parameters that affect the heat demand of buildings most were summed up, which was the subject of SQ1 (see Section 1.2). The list was condensed to the parameters that are most relevant and will thus be investigated in this thesis: the U-values of the building envelope, the window-to-wall ratio, the building's airtightness and the building's orientation. The chapter concluded with an overview of the software tools used in this thesis. Also, the stage was set for further investigation into the sizing and control of hybrid heating systems in school buildings.

[†]For more information, see: https://github.com/open-ideas/IDEAS.
[‡]More information can be found here: https://simulationresearch.lbl.gov/modelica/.

Chapter 3

Testing the *nPro* tool

In this chapter, the *nPro* tool is applied to a real-life case: building D of the Campus Proximus site of University Colleges Leuven-Limburg (UCLL), situated in Heverlee. This provides insights into the functionality and working principles of the tool. First, the relevant data available of this building are presented in Section 3.1. The following two sections are structured according to the calculation steps of *nPro*, as outlined in Section 2.3.1. Section 3.2 demonstrates the generation of the annual heat demand profile, while Section 3.3 demonstrates the energy system design optimisation and the simulation of system operation. When necessary, clarifying screenshots of the *nPro* tool, which can be found in Section A.1.2 of Appendix A, are referred to throughout the text. Finally, the discovered assumptions and limitations of *nPro* are presented in Section 3.4.

3.1 Building data

The data presented in Table 3.1 were provided by Tom Neven, who is responsible for the technical installations of the UCLL campuses. The absence of a digital natural gas meter in the building is expected, given that the installation of these digital meters is only a recent development. The natural gas consumption is recorded approximately every two weeks, which limits the resolution of the heat demand profile or HLDC to a maximum of two weeks. Furthermore, no information is available regarding the peak heat demand, but for the fact that it cannot be higher than the installed gas boiler capacity.

Total heated area	$\pm\,18\,500$ m^2
Natural gas consumption in 2022	89 238 m^3
Installed gas boiler capacity	1 700 kW
DHW	Covered decentrally
Supply temperature	Heating curve

TABLE 3.1: Relevant data of building D of UCLL Campus Proximus.

3.2 Load profile generation

The total annual heat demand is estimated using the natural gas consumption of 2022. The building utilises high-calorific gas [52]. The calculation is conducted with the lower heating value of natural gas, as the building does not use a condensing boiler. The lower heating value is approximately 10% less than the higher heating value [53]. In 2022, the higher heating value of high-calorific gas in Leuven was approximately 11.5 $\frac{\text{kWh}}{\text{m}^3}$ [54]. Therefore, the lower heating value is assumed to have been 10.3 $\frac{\text{kWh}}{\text{m}^3}$. Furthermore, it is assumed that the boiler has a constant efficiency of 90%. The total heat demand in 2022 can thus be estimated as follows: $89\,238\ \frac{\text{m}^3}{\text{year}} \times 10.3\ \frac{\text{kWh}}{\text{m}^3} \times 90\% = 827.2$ MWh.

The *nPro* tool can now be employed to generate the annual heat demand profile. The only value used as input for the tool is the total annual demand of 827.2 MWh. The results of the demand profile generation are shown in Figure 3.1.

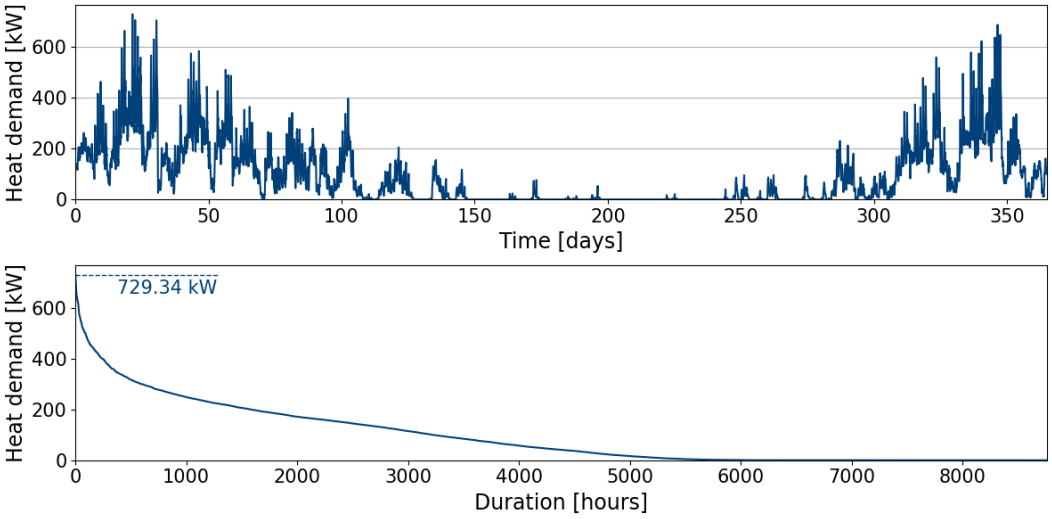

Figure 3.1: Heat demand profile and HLDC for building D of UCLL Campus Proximus generated by *nPro*.

It is clear that *nPro* attributes a considerable proportion of the heat demand to the 'base' heat demand. During approximately 2 000 hours of the year, the heat demand exceeds 200 kW. The peak heat demand is 729.3 kW, which is relatively low in comparison to the actual installed heating capacity of 1 700 kW. Given that *nPro* might overestimate the 'base' heat demand, the load generation is repeated using new normalised day profiles with a lower heat demand during unoccupied periods. These profiles are based on the findings of Section 2.2.2. The original (default) and new normalised day profiles of the heat demand are shown in Figures A.5 and A.6 respectively. The new heat demand profile and HLDC are presented in Figure 3.2. The peak heat demand now equals 1 119.9 kW, which is a more realistic value, but still relatively low, given that the installed heating capacity is 1 700 kW. However, it should be recalled that *nPro* uses an hourly resolution in its calculations, meaning a

peak heat demand of 1 119.9 kW corresponds to a maximum heat demand within one hour of 1 119.9 kWh.

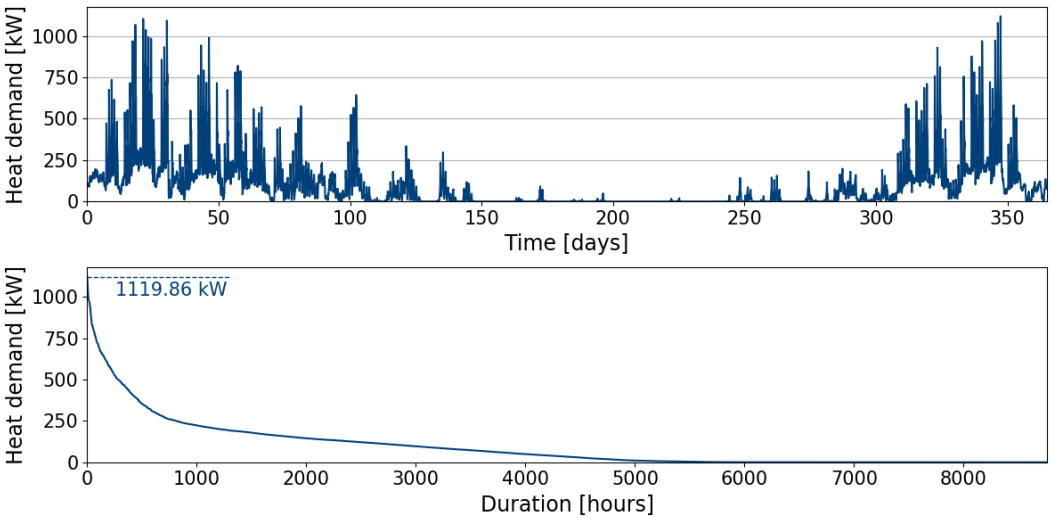

FIGURE 3.2: Heat demand profile and HLDC for building D of UCLL Campus Proximus generated by *nPro*, with adapted normalised day profiles.

3.3 Energy system design optimisation and simulation

The generated heat demand profile is now utilised as an input for different energy system design optimisations in *nPro*. The required input parameters are elaborated upon in Section 3.3.1. Subsequently, the baseline scenario is explained in Section 3.3.2. Sections 3.3.3 and 3.3.4 present the optimisation of three different system configurations.

3.3.1 Input parameters

In order to perform an energy system design optimisation in *nPro*, a number of input parameters must be defined. The values for these parameters, as outlined in this section, also apply to the analysis conducted in Chapters 5 and 6, unless otherwise stated.

The assumed costs and lifetimes of different technologies are presented in Table 3.2, which is based on the overview found in the Master's thesis of Arno Meessens [31]. These values include all relevant investment costs, and thus no other lump sum costs are defined in the project settings of *nPro*.

An observation period of 15 years is chosen, as this is the shortest lifetime of any of the different components. This could be, for example, the period 2025-2040, during which the 2030 emission targets will thus have to be met. A new design decision will then have to be made in 2040, bearing the 2050 emission targets in mind. The focus is on the design decision to be made now. An imputed interest

	Specific investment costs	Fixed investment costs	Annual maintenance costs	Lifetime
Gas boiler	150 €/kW	€2 000	0.5% of inv. cost	15 years
ASHP	533 €/kW	€8 400	3.0% of inv. cost	15 years
GSHP & borefield	1 444 €/kW	€33 667	3.0% of inv. cost	35 years
Storage tank	1 000 €/m^3	€800	0.5% of inv. cost	30 years
Solar thermal collector	600 €/m^2	€2 500	0.5% of inv. cost	30 years
Solar panels	1 370 €/kW_p	€4 500	2.0% of inv. cost	20 years

Table 3.2: Costs of different technologies [31].

rate of 5% is assumed. Observation period and imputed interest rate are used to annualise investments and to calculate net present value (NPV).

In *nPro* it is not possible to upload time series of energy prices for the entire observed period. Instead, annual time series can be uploaded and a yearly price increase or decrease can be assumed. In this thesis, energy prices are assumed to remain constant throughout the observed period.

The electricity tariff is assumed to be 0.20 $\frac{€}{kWh}$. This value is estimated by assuming an average energy price of 0.08 $\frac{€}{kWh}$ for the observed period [55] and assuming that the energy cost is approximately 38% of the total electricity tariff [56]. The feed-in tariff is assumed to be 0.03 $\frac{€}{kWh}$, but this is only relevant when considering solar panels. The CO_2 emissions of imported electricity are assumed to be 150 $\frac{gCO_2}{kWh}$. This parameter depends on the electricity mix of the grid, and it is thus chosen based on forecasts for the observed period [57, 58].

Similarly, the natural gas tariff is assumed to be 0.07 $\frac{€}{kWh}$. It is assumed that the average energy price is 0.04 $\frac{€}{kWh}$ for the observed period [59] and that the energy cost represents approximately 58% of the total natural gas tariff [56]. The CO_2 emissions of natural gas import are set to 250 $\frac{gCO_2}{kWh}$, a reasonable estimation according to *nPro*.

As *nPro* calculates the COP of a heat pump at each timestep, it is also necessary to specify the supply temperature for the heat demand. It is not possible to model a mixing valve in *nPro*. Therefore, if the system is configured as a heat pump and a gas boiler in parallel, the supply temperature must be the same for both. Conducting the analysis with high supply temperatures will disadvantage the heat pump, as it operates more efficiently at lower supply temperatures. Natural gas boilers however can easily achieve supply temperatures above 90°C. In order to conduct a fair analysis, the supply temperature in *nPro* is limited to 65°C. Thus, for the UCLL case, a heating curve is assumed where the supply temperature is 65°C for an outdoor temperature of -8°C, 50°C for an outdoor temperature of 10°C, and 20°C for an outdoor temperature of 20°C. A similar curve is shown in Figure 4.3.

The inputs of *nPro* regarding the different technologies (e.g. efficiencies) are mainly based on the default values available in the tool. An overview of these settings is provided in Section A.2 of Appendix A.

3.3.2 Baseline scenario

nPro does not permit the assignment of a specific remaining lifetime for the currently installed natural gas boiler. It is therefore assumed that the boiler can be used throughout the entire observed period of 15 years. The simulation of the system operation yields the following results over the observed period: 919 MWh of natural gas consumption, 230 tonnes of CO_2 emitted and an annual cost of 81 269 $\frac{€}{\text{year}}$, consisting of an energy cost of 79 984 $\frac{€}{\text{year}}$ and a maintenance cost of 1 285 $\frac{€}{\text{year}}$.

3.3.3 Enabling all relevant technologies

As explained in Section 2.3.1, a variety of technologies can be selected when conducting an energy system design optimisation in *nPro*. In the context of this thesis, the relevant technologies are solar panels, solar thermal collectors, GSHP, ASHP and heat storage. Consequently, these technologies are enabled in the energy system that will be optimised (Figure A.7).

The results of the system optimisation are presented in Table 3.3. The conducted system optimisation is a multi-objective optimisation, which means that *nPro* calculates the system configuration with the minimum total annualised cost, assuming four different CO_2 prices. Hence, for the optimisation with the highest CO_2 price, the share of renewable technologies is highest as this leads to fewer CO_2 emissions. It should be noted that the total annual cost shown in the tables does not include the CO_2 cost, in order to allow for a fair comparison between the system designs. The components of the total annual cost are the initial investment cost (annuity), the annual energy cost, the annual maintenance cost, and, if relevant, the annuity of the negative investment cost at the end of the observed period because of the residual value of assets that have not reached their technical lifetime yet. The *nPro* tool assumes linear depreciation for the latter.

The results show that, for this specific case and with the assumptions explained above and in Section A.2, the installation of a GSHP with heat storage can significantly reduce the annual CO_2 emissions, while also slightly reducing total annual costs compared to the baseline scenario. The installation of a GSHP with heat storage reduces the operational costs of the system to such an extent that even the initial investment will be 'paid back' before the end of the observed period. The middle two columns of the table reveal the existence of a system design comprising a GSHP between 96 kW and 109 kW and heat storage with a volume between 9.3 m^3 and 14.8 m^3, which has a total annual cost identical to that of the baseline scenario. This system design achieves a CO_2 reduction between 52.6% and 57.4%.

The selection of a GSHP over an ASHP can be attributed to the superior performance of the GSHP in terms of COP, as the ground temperature is more stable than the air temperature (and in the optimisation even assumed constant). The higher initial investment cost of the GSHP is offset by the significant gains in efficiency, making it a more cost-effective choice. Also, the long lifetime of the borefield results in a high residual value (and thus negative investment cost) at the end of the observed period.

CO_2 price	0 $\frac{€}{tCO_2}$	50 $\frac{€}{tCO_2}$	100 $\frac{€}{tCO_2}$	200 $\frac{€}{tCO_2}$
ASHP	0 kW	0 kW	0 kW	0 kW
GSHP	69 kW	96 kW	109 kW	149 kW
Heat storage	5.5 m^3	9.3 m^3	14.8 m^3	31.4 m^3
Solar thermal collector	0 m^2	0 m^2	0 m^2	0 m^2
Solar panels	0 m^2	0 m^2	0 m^2	0 m^2
Initial investment	€139 615	€182 435	€206 633	€281 015
Total annual cost	80 400 $\frac{€}{year}$	80 934 $\frac{€}{year}$	81 566 $\frac{€}{year}$	84 863 $\frac{€}{year}$
Rel. to baseline scenario	−1.1%	−0.4%	+0.4%	+4.4%
CO_2 emissions	135 $\frac{tCO_2}{year}$	109 $\frac{tCO_2}{year}$	98 $\frac{tCO_2}{year}$	74 $\frac{tCO_2}{year}$
Rel. to baseline scenario	−41.3%	−52.6%	−57.4%	−67.8%
Cost of CO_2 reduction	−9.1 $\frac{€}{tCO_2}$	−2.8 $\frac{€}{tCO_2}$	+2.3 $\frac{€}{tCO_2}$	+23.0 $\frac{€}{tCO_2}$

Table 3.3: Results system optimisation with all relevant technologies enabled.

Finally, it is worth noting that, for this specific case, the system optimisation never leads to the installation of solar panels or solar thermal collectors, given the assumptions explained above and in Section A.2.

3.3.4 Comparing the installation of a GSHP with the installation of an ASHP

As previously explained in Section 2.1.1, the choice of an ASHP over a GSHP in a (retrofit) hybrid heating system may be more advantageous for the case of Flemish school buildings, as the ASHP has no locational requirements and a lower initial investment cost. A comparison is therefore conducted between the *nPro* system optimisation with both of these technologies, for the case of building D of UCLL Campus Proximus. Tables 3.4 and 3.5 show the results for the *nPro* system optimisation with only the GSHP technology enabled and the system optimisation with only the ASHP technology enabled respectively.

Again, it is clear that the installation of a GSHP can be very beneficial in this particular case, as CO_2 emission reduction has a negative cost (relative to the baseline scenario) up to a certain point. The installation of a GSHP with a thermal capacity of 69 kW requires an initial investment of €133 303. However, the total annual cost is expected to decrease by 0.9% compared to the baseline scenario due to the reduction in annual energy costs. This system configuration leads to a CO_2 emission reduction of 40.4% compared to the baseline scenario. Further reductions in CO_2 emissions can be achieved with a GSHP of 97 kW, while still reducing total annual cost compared to the baseline scenario. The long lifetime of the borefield is able to compensate for the necessary high capital investments.

The installation of an ASHP on the other hand will, in this particular case, lead to an increase of total annual cost compared to the baseline scenario. An ASHP

CO_2 price	0 $\frac{€}{tCO_2}$	50 $\frac{€}{tCO_2}$	100 $\frac{€}{tCO_2}$	200 $\frac{€}{tCO_2}$
GSHP	69 kW	97 kW	112 kW	138 kW
Capacity ratio	4.1%	5.7%	6.6%	8.1%
Coverage ratio	47.0%	59.6%	64.7%	71.4%
Initial investment cost	€133 303	€173 735	€195 395	€231 495
Total annual cost	80 545 $\frac{€}{year}$	81 042 $\frac{€}{year}$	81 799 $\frac{€}{year}$	83 791 $\frac{€}{year}$
Rel. to baseline scenario	−0.9%	−0.3%	+0.7%	+3.1%
CO_2 emissions	137 $\frac{tCO_2}{year}$	112 $\frac{tCO_2}{year}$	102 $\frac{tCO_2}{year}$	89 $\frac{tCO_2}{year}$
Rel. to baseline scenario	−40.4%	−51.3%	−55.7%	−61.3%
Cost of CO_2 reduction	−7.8 $\frac{€}{tCO_2}$	−1.9 $\frac{€}{tCO_2}$	4.1 $\frac{€}{tCO_2}$	17.9 $\frac{€}{tCO_2}$

TABLE 3.4: Results system optimisation with only GSHP enabled.

CO_2 price	0 $\frac{€}{tCO_2}$	50 $\frac{€}{tCO_2}$	100 $\frac{€}{tCO_2}$	200 $\frac{€}{tCO_2}$
ASHP	0 kW	0 kW	64 kW	148 kW
Capacity ratio			3.8%	8.7%
Coverage ratio			16.4%	28.2%
Initial investment cost			€42 512	€87 284
Total annual cost			83 945 $\frac{€}{year}$	88 467 $\frac{€}{year}$
Rel. to baseline scenario			+3.3%	+8.9%
CO_2 emissions			199 $\frac{tCO_2}{year}$	177 $\frac{tCO_2}{year}$
Rel. to baseline scenario			−13.5%	−23.0%
Cost of CO_2 reduction			86.3 $\frac{€}{tCO_2}$	135.8 $\frac{€}{tCO_2}$

TABLE 3.5: Results system optimisation with only ASHP enabled.

of a certain capacity leads to a lower CO_2 emission reduction, as the average COP is lower. The mean COP throughout one year for the GSHP is 5.1 while for the ASHP it is 4.1, and especially in the coldest periods of the year, when heat demand is highest, the GSHP's COP is significantly higher than that of the ASHP.

Finally, it is important to note that this specific building is not representative for the 'average' Flemish school building. Most notably, the floor area of the building is considerably larger than the average floor area in Flemish school buildings. This results in a higher heat demand, which in turn leads to higher annual energy costs. Consequently, higher initial investment costs might be justified. Additionally, UCLL is a university, which implies that the use of the building and thus the heat demand may differ significantly from that of a primary or secondary school.

3.4 *nPro* limitations and (implicit) assumptions

The application of *nPro* to this real-life case has led to several findings regarding limitations and assumptions of the tool, which are listed in this section.

Firstly, it is important to note that the demand profile generation is purely based on the assumption of the linear relationship between ambient temperature and heat demand and on the assumption that the normalised day profile is always quite similar. Therefore, other factors like setpoint temperature, building envelope U-value, WWR, etc. are only taken into account implicitly via the total annual heat demand. However, a certain annual heat demand (e.g. in kWh) provides no information regarding the annual heat demand *profile* (e.g. in kW). Two buildings that have the same total annual heat demand can have very different heat demand profiles.

Secondly, it should be noted that when a system consisting of two heat sources in parallel is modelled in *nPro*, the supply temperatures of these two heat sources are assumed to always be equal. In reality, a three-way (mixing) valve may be installed when e.g. a heat pump and a gas boiler work in parallel, connecting the ends of both and enabling the heat pump's supply temperature to be lower than the gas boiler's. Lower supply temperatures are beneficial for the COP of a heat pump so the heat pump having to reach the same supply temperature as the gas boiler might lead to *nPro* proposing a smaller heat pump.

Thirdly, it is not possible yet to optimally size a hybrid heating system consisting of two heat sources in series. Using a workaround, it is possible to split the total heat demand into a low- and a high-temperature heat demand by defining a threshold temperature T_{th}. The low-temperature heat demand is then assigned to the heat pump and the high-temperature heat demand is assigned to the gas boiler. However, this means that there is no optimal sizing of the heat pump as the latter is only sized to meet the low-temperature heat demand. Nevertheless, this method can still be interesting to compare the parallel configuration with the series configuration for a given heat pump capacity.

Lastly, a comment can be made about the definition of component lifetimes in *nPro*. The tool is primarily designed for the planning phase of energy projects. However, this thesis concerns a retrofit problem. A gas boiler is already present in the school building, and the objective is to add a heat pump to create a hybrid heating system. In *nPro*, it is currently not possible to model the gas boiler having a certain remaining lifetime which is smaller than the total gas boiler lifetime. This would require *nPro* to make multiple design decisions on different moments in the investigated time horizon, which is also not possible yet.

3.5 Conclusion

This chapter demonstrated that while *nPro* has certain assumptions and limitations, it can be utilised for the sizing of a hybrid heating system in a real-life case. For the case of building D of UCLL Campus Proximus, it was clear that, when allowing for a

relatively high initial investment, both the total annual cost and the amount of CO_2 emissions can be reduced when installing a GSHP with heat storage. Furthermore, the installation of an ASHP was compared to the installation of a GSHP, in terms of cost and CO_2 emission reduction. This showed that, in this specific case, achieving a CO_2 emission reduction by installing an ASHP leads to an increase in total annual cost compared to the baseline scenario. Finally, some remarks concerning the generation of heat demand profile in *nPro*, the modelling of different hybrid heating system configurations in *nPro* and the definition of component lifetimes in *nPro* in the context of this thesis were presented, which was the subject of SQ2 (see Section 1.2).

Chapter 4

The school building model

As mentioned in Section 2.3.2, the school building model that will be used in the analysis of Chapters 5, 6 and 7 was developed using *Modelica* and *IDEAS*, in the *Dymola* simulation environment. In this chapter, the modelling of the school building architecture in general is explained in Section 4.1. Section 4.2 addresses the modelling of the building envelope, focusing on all relevant aspects: materials and construction, windows, building orientation, thermal transmittance, airtightness and ventilation. Next, Section 4.3 covers all aspects regarding the occupancy of the building. Section 4.4 briefly discusses the weather boundary conditions imposed in the simulations. Finally, the heating system model is presented in Section 4.5. A brief validation of the *Modelica* model can be found in Appendix B, Section B.1.

4.1 Building architecture

The school building modelled for this thesis is based on the representative school building model defined by Wauman et al. in [37]. Their prototypical building model is based on averaged values of 35 Flemish school buildings, chosen from the database of Flemish school characteristics of the Agency for School Infrastructure (AGION). It is noteworthy that their model is based on buildings constructed after 2005, as the authors sought to incorporate current trends and changes. As of 2018, 70% of Flemish school buildings were constructed before 1990. However, in 50% of the buildings constructed before 1990, a major rebuild or renovation has taken place [8]. Still, it is important to consider that Wauman et al. focused on recently constructed buildings, when selecting parameters such as building envelope U-values. It is possible that the values of these parameters are overly optimistic for buildings constructed prior to 2005, which could be the majority of buildings that would be interested in implementing a hybrid heating system.

The floor plan of the modelled building is shown in Figure 4.1. The zones are numbered from 1 to 20. The rectangular building has two floors. There are eight types of zones: a canteen (zone 1), a kitchen (zone 2), classrooms (zones 4, 5, 13, 16, 17), a teachers room (zone 9), an office (zone 10), a gym (zone 12), hallways (zones 19, 20) and sanitary or storage rooms (zones 3, 6, 7, 8, 11, 14, 15, 18). All zones except

for both hallways are heated. The total floor area of the building is 2 052.06 m^2, of which 1 751.28 m^2 is heated. The gym is the only zone that covers both floors. Other general architectural properties of the building are listed in Table B.1, which can be found in Section B.2 of Appendix B.

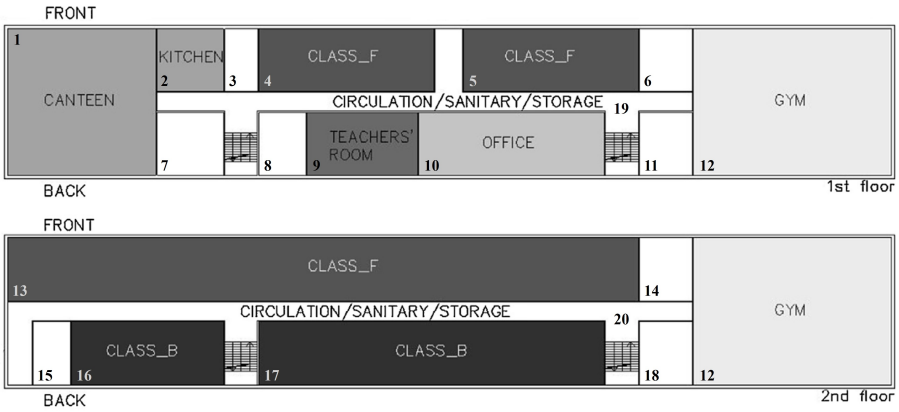

Figure 4.1: Floor plan of the representational Flemish school building model [37].

Figure B.4, which can be found in Section B.3 of Appendix B, shows how the school building was modelled in *Modelica*. Each zone is modelled as a `Zone` component connected to a number of surface components (`InternalWall` for the internal walls and ceilings, `OuterWall` for the external walls and roofs, `SlabOnGround` for the floors and `Window` for the windows). The connections are represented by yellow lines.

Currently, the *IDEAS* library does not support modelling the staircases as vertical passages between the hallways on both floors. Therefore, the school building model just assumes the hallways to not be vertically connected. This implies that convective flows because of a temperature difference between both floors are not possible. However, this will have minimal impact on the results as the hallways are not heated anyway.

4.2 Building envelope

4.2.1 Materials and construction

Construction and material parameters for each of the different surfaces were based on the compositions of structural elements listed in [37]. These constructions are defined in Table B.2. Material properties of all used materials can be found in Table B.3. Both tables can be found in Section B.4 of Appendix B. As mentioned earlier, the authors of [37] focused on buildings constructed after 2005, which means that these constructions might not be representative for older buildings. It is therefore important to investigate the impact of varying the building envelope U-value on the overall heat demand and heat pump sizing. This will be done in Chapter 6 by varying the thickness of the layer of polyurethane (PUR) in the different surfaces of the building envelope (d_{PUR}).

4.2.2 Windows

Except for some storage rooms (zones 3, 8, 15) and the hallway on the first floor (zone 19), all zones have at least one window. Some zones with multiple external walls have more than one window. All windows are assumed to be 1.55m high (h_{window}). Window width is defined as a certain fraction (f_{window}) of the width of the external wall in which the window is located. This fraction and the window height will be used in the analysis of Chapter 6 as a way to vary the window-to-wall ratio (WWR) of the building. The WWR is defined as:

$$WWR = \frac{A_{window}}{A_{wall} + A_{window}}, \tag{4.1}$$

where A_{window} is the total area of all windows and A_{wall} is the total area of all external walls (excluding window area).

The used `Window` components have '`EpcDouble - Uncoated double glazing`' as glazing type and '`Wooden frame`' as frame type. Both are interface types included in the *IDEAS* library. According to [8], 68% of Flemish school buildings had double (or triple) glazing in 2018.

The default value of f_{window} is set to 0.68, resulting in a WWR of 30%. This value falls precisely between the lower and upper limits of 20% and 40% as mentioned in [37]. The Korean school building described by Kang et al. [60] also has a WWR of around 30%.

4.2.3 Building orientation

Every surface component has an input parameter `azi`, which is the azimuth angle of the surface. This angle, for each surface component, is related to the azimuth angle of the front façade of the school building, γ_{front}. For the external wall of zone 17 for example, `azi` is set to $\gamma_{front} + 180°$. The default value γ_{front} is chosen to be 135°, which means that the front façade is faced to the northwest.

4.2.4 Thermal transmittance

The average U-value of the building envelope, $\bar{U}_{env}$, is calculated as the area-weighted average of the U-values of each of the N surfaces of the building envelope (external walls, roofs, windows and floors). This is shown in Equation 4.2.

$$\begin{aligned} \bar{U}_{env} &= \frac{\sum_{i=1}^{N} U_i \cdot A_i}{A_{env}} \\ &= \frac{U_{wall} \cdot A_{wall} + U_{window} \cdot A_{window} + U_{roof} \cdot A_{roof} + U_{floor} \cdot A_{floor}}{A_{env}} \end{aligned} \tag{4.2}$$

In the `OuterWall`, `Window`, and `SlabOnGround` component of the *IDEAS* library, the U-values are calculated as shown in Equations 4.3 to 4.5.

$$U_{OuterWall} = \frac{1}{\frac{1}{8}\frac{\mathrm{m^2\ K}}{\mathrm{W}} + \sum_{i=1}^{m} R_i + \frac{1}{25}\frac{\mathrm{m^2\ K}}{\mathrm{W}}} \tag{4.3}$$

$$U_{Window} = U_{glazing} \cdot (1 - f_{frame}) + U_{frame} \cdot f_{frame} \tag{4.4}$$

$$U_{SlabOnGround} = \frac{1}{\frac{1}{6}\frac{\mathrm{m^2\ K}}{\mathrm{W}} + \sum_{i=1}^{m} R_i} \tag{4.5}$$

In these equations, $\frac{1}{8}\ \frac{\mathrm{m^2\ K}}{\mathrm{W}}$ and $\frac{1}{25}\ \frac{\mathrm{m^2\ K}}{\mathrm{W}}$ are the internal and external (thermal) surface resistance for walls and roofs as defined in the norm *ISO 6946:2007*. Following that same norm, the internal surface resistance for floors is $\frac{1}{6}\ \frac{\mathrm{m^2\ K}}{\mathrm{W}}$, and the external surface resistance is zero because of the lack of an air layer. The term $\sum_{i=1}^{m} R_i$ is the sum of the thermal resistances of each of the m material layers in the construction type. $U_{glazing}$ and U_{frame} are parameters depending on the window type. f_{frame} is the proportion of the window area that is window frame.

Tian and Choudhary [61] found different U-values in previous studies on school buildings in the United Kingdom [62, 63, 64, 65]. Katić, Krstić and Marenjak [66] investigated 47 schools, of which most constructed before 1988, in Bosnia-Herzegovina. It is unclear how they defined $\bar{U}_{env}$. Also, it is likely that school buildings in Bosnia-Herzegovina will exhibit higher U-values in general because of climatological and socio-economic factors. These values thus might not be representative for the Flemish case. Cecconi, Moretti and Tagliabue [67] investigated the data of 1 632 school buildings that were included in the Energy Performance Certificates (EPC) database of the Lombardy region in Italy [68]. Of the aforementioned sources, [61] is arguably the most representative one, given the similarities in climate and economy (both of which affect typical building insulation quality) between the United Kingdom and Flanders.

Table 4.1 presents an overview of the (average) U-values observed in these three sources. Based on this, the default value of d_{PUR} is chosen to be 2 cm, resulting in $\bar{U}_{env}$ being equal to 1.00 $\frac{\mathrm{W}}{\mathrm{m^2\ K}}$.

	U_{wall}	U_{window}	U_{roof}	U_{floor}	$\bar{U}_{env}$
[61]	0.2-1.5	1.5-4.0	0.2-1.5	0.2-1.5	n/a
[66]	0.25-2.73	1.41-4.29	0.34-4.81	0.34-4.18	0.51-3.09
[67]	0.52-1.38	2.28-3.89	0.53-1.26	n/a	n/a
Chosen default values	0.90	2.72	0.79	0.80	1.00

Table 4.1: U-values found in literature and default U-values [$\frac{\mathrm{W}}{\mathrm{m^2\ K}}$].

4.2.5 Airtightness

In each `Zone` component, a $n50$ value can be defined. This is the amount of air changes per hour at a pressure difference of 50 Pa. The parameter `interzonalAirFlow` is set to `n50FixedPressure`, which means that a constant air exchange rate between

zone and environment is assumed. This actual air exchange rate is calculated by dividing the $n50$ value by 20, which is a common rule of thumb [36, 69, 70].

No data was found regarding typical air infiltration rates for Belgian school buildings. In [71], a median $n50$ of 3.70 h^{-1} is mentioned for a sample base of 18 houses, one industrial building and two offices in Belgium. Fernández-Agüera et al. [72] conducted pressurization tests in 42 Spanish school buildings, resulting in a mean $n50$ value of 6.97 h^{-1}. However, due to the Mediterranean climate in Spain, natural ventilation is more prevalent, and buildings are typically less insulated. Based on these findings, the default $n50$ value of each zone is set to 4.5 h^{-1}.

4.2.6 Ventilation

In 2018, only 15% of Flemish school buildings had mechanical ventilation, with the majority of these systems being found in recently constructed buildings [8]. It is therefore assumed that there is no ventilation system in the modelled school building.

4.3 Occupancy data

4.3.1 Occupancy schedules and occupant density

Occupancy schedules are based on the typical school year, week and day in Flemish schools. A graphical representation of these schedules can be found in Section B.5.1 of Appendix B.

The used values for the occupant densities of each zone are listed in Table 4.2. These values are calculated from the deterministic boundary conditions for Flemish schools presented in [37], by dividing the occupant density by the relative absence factor (which is "the proportion of usage time in which no persons are present in the area being assessed" according to the norm *DIN V 18599-10*).

Zones	Zone type	Occupant density [$\frac{m^2}{person}$]
1	Canteen	1.5
2	Kitchen	10
4, 5, 13, 16, 18	Classroom	$3/0.825 = 3.64$
9	Teachers' room	$3/0.50 = 6$
10	Office	$14/0.70 = 20$
12	Gym	20
19, 20	Hallway	10

TABLE 4.2: Occupancy data per zone [37].

4.3.2 Temperature setpoints

The temperature setpoints are also based on the deterministic boundary conditions presented in [37]. The temperature setpoint during occupancy in the gym is 17°C,

for all other zones the setpoint during occupancy is 21°C. On Tuesdays, Thursdays and Fridays, this setpoint is set between 07:00 and 16:00. On Mondays the setpoint is set between 06:00 and 16:00, one hour earlier because the building may have cooled down considerably over the weekend. On Wednesdays, it is set between 07:00 and 12:00 except for the office, where it is also set between 07:00 and 16:00. In all other instances, so when the building is unoccupied, the setpoint is 14°C. A graphical representation of these schedules can be found in Section B.5.2 of Appendix B.

4.3.3 Internal heat gains

There are three sources of internal heat gains: people, equipment and lighting. For people and equipment, the used values are shown in Table 4.3.

	People		Equipment	
	Sensible	Latent	Sensible	Latent
Canteen	80	80	0	0
Kitchen	75	70	300	300
Classrooms, teachers' room, office	70	45	20	0
Gym	210	315	0	0
Hallways	75	70	0	0

Table 4.3: Internal heat gains [$\frac{\text{W}}{\text{person}}$], based on [73].

For lighting, generic LED lighting is assumed. Lights are on when a zone is occupied. LED lighting is included as a record in the *IDEAS* library. It assumes a luminous efficacy of 150 $\frac{\text{lm}}{\text{W}}$ and a radiant fraction of lighting heat exchange of 35%. The illuminance requirement of the classrooms and the office is 500 lm and for the other zones it is 300 lm. These are values found in the `Generic` and `Office RoomType` records of the *IDEAS* library.

4.4 Meteorological data

Weather boundary conditions are often provided by `TMY` (typical meteorological year) files. These files are specifically designed to support building simulations and contain meteorological parameters like dry bulb temperature, dew point temperature, wind velocity and solar irradiance for a period of one year [74]. The weather file used in this thesis is `BEL_VLG_Uccle.064470_TMYx.2007-2021`[†], which contains weather information of the weather station in Uccle, Belgium. The annual profile of the outdoor temperature is shown in Figure 4.4. The minimum, maximum and mean outdoor temperature are -4.9°C, 33.6°C and 11.1°C respectively.

[†]See: https://climate.onebuilding.org/WMO_Region_6_Europe/BEL_Belgium/index.html.

4.5 Heating system

For the heating system, a custom *Modelica* model is created. A graphical representation is shown in Figure 4.2. In the school building, all zones except for the hallways are heated, so 18 zones in total. The heating system is thus modelled as the combination of a central heater, 18 radiators with a thermostatic radiator valve (TRV) and 18 pumps. In the next subsections, these components are explained in more detail. The fluid in the heating system is water, of which the properties are included in the *IDEAS* package `Media.Water`.

The heating system model has 18×2 input nodes (`TSet` and `TSensor`) and 18×2 output nodes (`heatPortCon` and `heatPortRad`). A `CombiTimeTable` block with the setpoint temperatures of each zone over time is connected with the `TSet` input nodes. The `TSensor` output nodes of each zone are connected with the `TSensor` input nodes of the heating system model. The `heatPortCon` and `heatPortRad` output nodes of the heating system model (for the convective and radiative heat gains) are connected with the `gainCon` and `gainRad` input nodes of each zone.

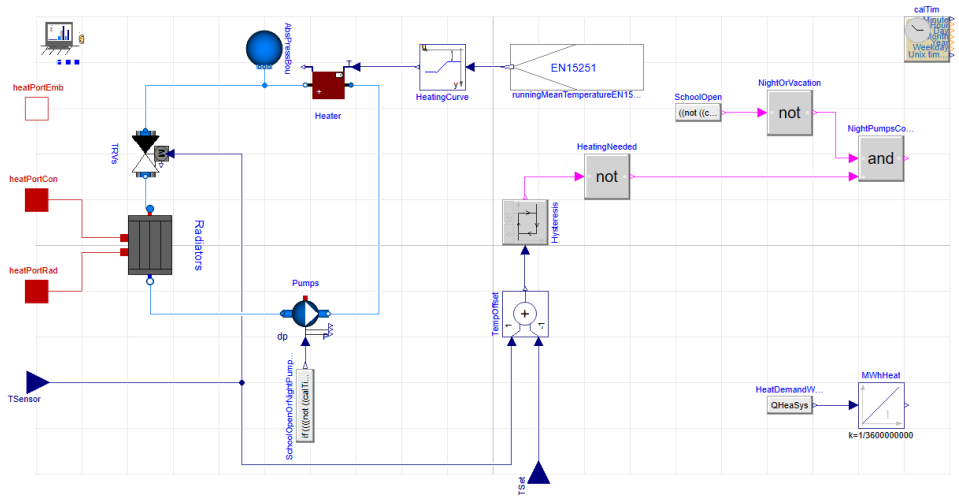

FIGURE 4.2: Graphical *Modelica* representation of the heating system model.

4.5.1 Heater

The heater is modelled by the `Heater_T` component of the *IDEAS* library. The inlet port of the heater is connected to the pumps, while the outlet port is connected to the TRVs. The heater also has one input for the supply temperature setpoint. The nominal mass flow rate of the heater is set to the sum of the nominal mass flow rates of all radiators.

The supply temperature setpoint is determined by means of a heating curve. A heating curve is a type of weather compensation. The supply temperature of the heater is set according to the outdoor temperature. Often, a linear dependency is chosen [75, 76, 77]. As the outdoor temperature decreases, heat losses from the

building to the surroundings increase. To compensate for this effect, the heater's supply temperature is raised, which increases the heat flow rate of the emission system. The heating curve employed in the heating system model is depicted in Figure 4.3. The maximum supply temperature is set to 75°C. This supply temperature is reached when the outdoor temperature goes below -8°C, which is the lowest 'base outdoor temperature' in Flanders. This base outdoor temperature is defined in the norm *EN 12831-1* as the average minimum temperature of the coldest month. For outdoor temperatures exceeding 20°C, it can be assumed that heating is unnecessary. Even for outdoor temperatures between 16°C and 20°C, a need for heating is unlikely. Therefore, the supply temperature is set to 20°C at an outdoor temperature of 20°C. Because a purely linear heating curve might endanger thermal comfort, a bend is added so that the supply temperature is still 60°C when the outside temperature is 10°C. The supply temperature is adjusted on a daily basis, according to the running mean outdoor temperature of seven days as defined in the norms *EN 15251:2007* and *EN 16798-1:2019*.

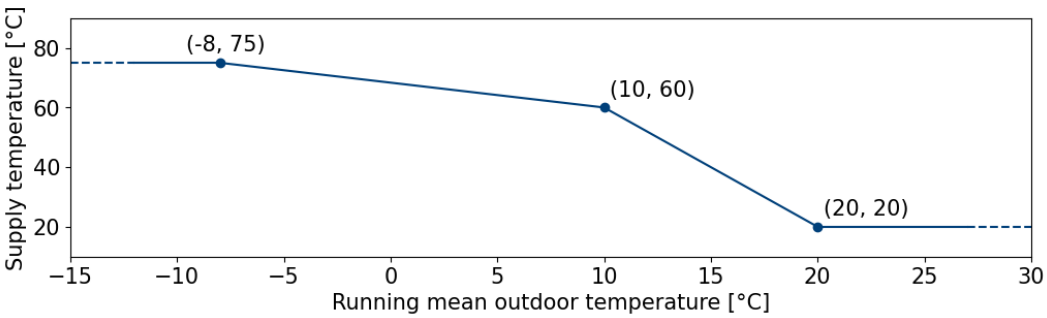

Figure 4.3: Heating curve used in model.

Figure 4.4 illustrates the variation in supply temperature in response to changes in outdoor temperature over the course of a year. The inverse relationship between outside temperature and supply temperature is clearly visible. At some moments during summer, the outdoor temperature temporarily exceeds the supply temperature, which might not be very realistic. This however has no impact on the results because there is no heat demand at these moments.

4.5.2 Radiators

The radiators in each zone are modelled by a `RadiatorEN442_2` component, which is part of the *IDEAS* library. The inlet of each radiator is connected to the outlet of the corresponding TRV. The outlet of each radiator is connected to the inlet of the corresponding pump. In the `RadiatorEN442_2` component, the nominal mass flow rate is calculated as in Equation 4.6.

$$\dot{m}_{nom} = \left| \frac{\dot{Q}_{nom}}{c_p \cdot (T_{a,nom} - T_{b,nom})} \right| \tag{4.6}$$

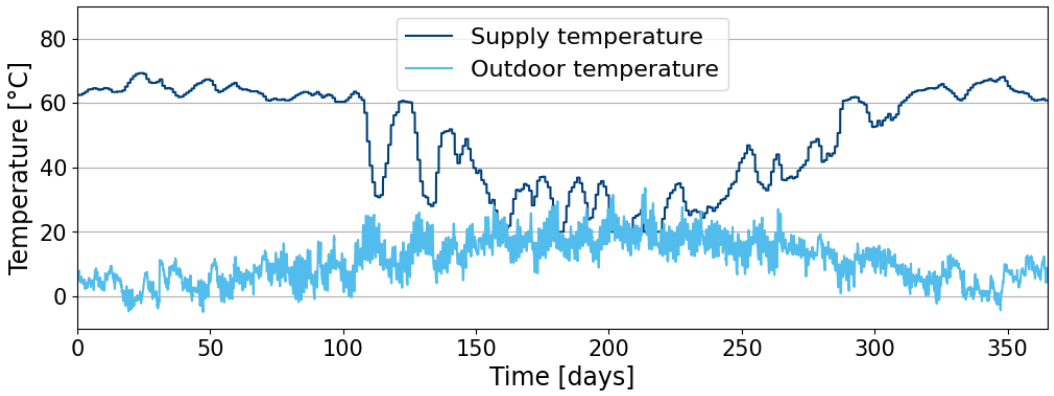

FIGURE 4.4: Supply temperature and outdoor temperature for simulated year.

$T_{a,nom}$ and $T_{b,nom}$ are the nominal inlet and outlet temperature of the radiators. These are set to 65°C and 55°C respectively. As can be seen in Figure 4.4, the supply temperature of the heater is between 60°C and 70°C during the periods when heating is most needed. The parameter $c_{p,nom}$ is the specific heat capacity of water at nominal conditions. Finally, $\dot{Q}_{nom}$ is the nominal heat flow rate of the radiator, so the heat that is injected when the heating system is on. It is a parameter of the `RadiatorEN442_2` component. It is set equal to $\dot{Q}_{design}$, which is the design heat load of each zone based on the heat losses of that zone. This design heat load is calculated automatically in each `Zone` component as in Equation 4.7.

$$\begin{aligned} \dot{Q}_{design} &= \dot{Q}_{inf,design} + \dot{Q}_{tra,design} + \dot{Q}_{rh,design} \\ \text{with} \quad \dot{Q}_{inf,design} &= 1012 \ \frac{\text{J}}{\text{kg K}} \cdot 1.204 \ \frac{\text{kg}}{\text{m}^3} \cdot \frac{V}{3600 \frac{\text{s}}{\text{h}}} \cdot \frac{n50}{20} \cdot (21°\text{C} - T_{design}) \\ \text{and} \quad \dot{Q}_{tra,design} &= \sum_{i=1}^{n} U_i \cdot A_i \cdot (21°\text{C} - T_{design}) \\ \text{and} \quad \dot{Q}_{rh,design} &= A \cdot f_{RH} \end{aligned} \tag{4.7}$$

The term $\dot{Q}_{inf,design}$ represents the design infiltration losses. The $n50$ value in h^{-1} is converted to actual air exchanges per hour by dividing it by 20, as mentioned earlier. This number of air exchanges per hour is multiplied by the zone volume V and divided by 3 600 to get the volume flow rate of air infiltration in $\frac{\text{m}^3}{\text{s}}$. This value is then multiplied by the specific heat capacity and mass density of air to achieve a value describing the relative infiltration losses in $\frac{\text{W}}{\text{K}}$. This value is multiplied by the difference between the assumed setpoint temperature of 21°C and the design temperature of -8°C (see Section 4.5.1) in order to achieve the design infiltration losses.

$\dot{Q}_{tra,design}$ represents the design transmission losses, calculated by multiplying the U-value of each zone surface with the area of the surface and the design temperature difference and adding these values together.

Finally, $\dot{Q}_{rh,design}$ is a term representing the additional heating requirement because of the effects of intermittent heating. It is calculated for each zone by multiplying the zone area with a reheat factor f_{RH}, which is taken equal to 36 $\frac{\mathrm{W}}{\mathrm{m}^2}$, following the norm *EN 12831* and assuming a relatively short reheat time, a relatively large temperature drop during setback and a relatively low building mass.

The heat port for convective heat transfer and heat port for radiative heat transfer of each radiator are connected to the corresponding node of the heating system model.

4.5.3 TRVs

Every radiator has a TRV placed at its inlet port. It is modelled by the `TwoWayTRV` component of the *IDEAS* library. It has the same nominal mass flow rate as the corresponding radiator. Each TRV has an input for the measured temperature in the corresponding zone. The temperature setpoint of each TRV is set 0.5°C above the actual temperature setpoint, to maximise thermal comfort. A proportional band of 1.5K is chosen. Information about the nominal pressure drops defined in this component can be found in Section B.6 of Appendix B.

4.5.4 Pumps

To make the control of the emission system of each zone easier, each zone is modelled to have a separate (circulation) pump. These pumps are modelled by the `FlowControlled_dp` component of the *IDEAS* library. For each pump, the nominal mass flow rate is set equal to the nominal mass flow rate of the corresponding radiator. The nominal pressure rise is set equal to the sum of a share of the nominal pressure rise of the heater and the nominal pressure rise of the corresponding TRV and radiator(s). This is explained in more detail in Section B.6 of Appendix B. Conducting a dynamic simulation for one year shows that the annual electricity usage of the circulation pumps is less then 0.1% of the total annual heat demand, so this energy usage is disregarded in the analysis of Chapters 5 and 6.

4.5.5 Control strategy

During the occupied periods, the control of the heat emission happens through the TRVs. The pumps are continuously on. The TRVs control the mass flow through each radiator based on the difference between measured and setpoint temperature. By doing this, they also control the emitted heat of each radiator ($\dot{Q} = \dot{m} \cdot c_p \cdot \Delta T$).

It is assumed that the TRVs are not motorised, so it is not possible to change the setpoint temperature automatically. Therefore, during unoccupied periods, the pumps are controlled using an on/off-strategy. When the sensor temperature of a zone falls below 14°C, the corresponding pump is switched on. The pump is turned off again when the temperature becomes higher than 14°C + ΔT_{hys}, with ΔT_{hys} equal to 2°C.

Figure 4.5 shows a typical ten-day temperature profile for the teachers' room (zone 9) during winter. In the night of day 27, the building cools down enough to

initiate the on/off-behaviour of the heating system. When the zone temperature falls below 14°C, the pump is activated for about half an hour until the zone temperature reaches 16°C. The zone then continues to heat up by approximately half a degree more due to the hot water still present in the radiator. During the occupied periods, the TRVs control the flow through the radiator and thus the zone temperature.

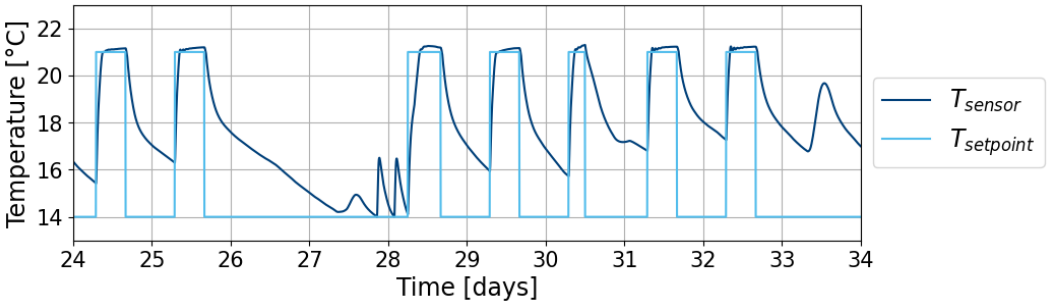

FIGURE 4.5: Typical temperature profile in winter (zone 9).

4.5.6 Thermal discomfort

Finally, thermal discomfort is a parameter that is also considered in the next chapters and thus requires some explanation. As this thesis only covers the aspect of heating, only the thermal discomfort regarding the temperature being too cold is considered. The parameter expresses the amount of time that the sensor temperature of an occupied zone is a certain amount of degrees below the setpoint temperature of that zone. Thermal discomfort is calculated in the *Modelica* model by integrating the difference between setpoint temperature and sensor temperature for each zone, if this difference is positive and the zone is occupied. The resulting values are then summed to achieve the total thermal discomfort of the school building expressed in degree h.

4.6 Conclusion

This chapter gave a comprehensive overview of the modelled school building. Assumptions that have been made were explained and all necessary boundary conditions were established. This school building model is now used for dynamic simulations, of which the results are presented in Chapters 5 and 6. The model is also used in the optimisations conducted in Chapter 7.

Chapter 5

The impact of the *nPro* optimisation settings

This chapter, together with Chapter 6, presents the results of the dynamic simulations that were conducted with the school building model described in Chapter 4. First, an overview of the parameters that are relevant in the analysis of these results is provided in Section 5.1. Next, Section 5.2 presents a brief comparison of the load profiles generated by *nPro* with the results of the dynamic simulations of the *Modelica* model. These load profiles are an important required input for the system optimisation in *nPro*. Section 5.3 covers the baseline scenarios that serve as a benchmark for the rest of the analysis. Section 5.4 then addresses one of the limitations of *nPro*, as identified in Chapter 3, namely the modelling of a hybrid heating system in series configuration. A comparison is made with the results for a hybrid heating system in parallel configuration. Section 5.5 investigates the impact of specifying a certain CO_2 reduction. In these two sections, the aspect of the remaining lifetime of the current gas boiler, also identified in Chapter 3, is investigated as well.

This analysis provides insights into the extent to which the *nPro* optimisation settings corresponding to the limitations of the tool identified in SQ2 affect the results of the optimal hybrid heating system size. From this point onward, the investigation focuses on hybrid heating systems consisting of a gas boiler and an ASHP, as previously outlined in Sections 2.1.1 and 3.3.4.

5.1 Important parameters

Table 5.1 presents the parameters that are important in the further analysis. These parameters are categorised into *Modelica* simulation outputs, *nPro* optimisation inputs, *nPro* optimisation outputs and *nPro* system operation outputs.

The annual heat demand, peak heat demand and thermal discomfort are results of the dynamic simulations conducted using the representative school building model. It should be noted that the values of these parameters remain constant regardless of the system optimisation conducted by *nPro*, as *nPro* merely calculates the optimal

system size capable of perfectly meeting the inputted heat demand. The capacity of the currently installed gas boiler is assumed to be equal to the peak heat demand.

***Modelica* simulation outputs**		
Heating energy	E_{heat}	[MWh/year]
Peak heat demand	$\dot{Q}_{peak}$	[kW]
Capacity of current gas boiler	$P_{boi,cur}$	[kW]
Thermal discomfort	TD	[(degree h)/year]
***nPro* optimisation inputs**		
CO_2 price	C_{CO_2}	[€/tCO_2]
Minimal CO_2 emission reduction	ΔCE_{min}	[%]
Remaining lifetime of current gas boiler	L_{boi}	[years]
***nPro* optimisation outputs**		
New gas boiler capacity	$P_{boi,new}$	[kW]
Heat pump capacity	P_{hp}	[kW]
Capacity ratio	P_{hp}/P_{boi}	[%]
***nPro* system operation outputs**		
Coverage ratio	$E_{heat,hp}/E_{heat}$	[%]
Initial investment cost	$C_{inv,ini}$	[€]
Total annual cost (excl. CO_2 cost)	$C_{an,tot}$	[€/year]
Increase of total annual cost	$\Delta C_{an,tot}$	[%]
CO_2 emissions	CE	[tCO_2/year]
CO_2 emission reduction	ΔCE	[%]
Cost of CO_2 emission reduction	$C_{\Delta CE}$	[€/tCO_2]

Table 5.1: Relevant parameters in the analysis of the impact of the *nPro* optimisation settings and building parameters on heat demand and optimal hybrid heating system size.

Apart from the heat demand profile calculated in the first calculation step (load profile generation, see Section 2.3.1), the second calculation step of *nPro* (energy system design optimisation) requires the input of three variables relevant to this analysis: a CO_2 price, a minimal CO_2 emission reduction and a remaining lifetime of the natural gas boiler that is currently present in the investigated school building. Other *nPro* inputs that need to be defined, like the observed period, technical parameters and cost parameters, are the same as described in Section 3.3.1, unless otherwise stated.

The outputs of the *nPro* system optimisation are the capacity of the new gas boiler (if the remaining lifetime of the current boiler is 0 years) and the capacity of the heat pump. The capacity of the heat pump can be expressed as a percentage of the capacity of the (new) gas boiler in the heating system. This is called the capacity ratio.

Following the system optimisation, *nPro* simulates the system operation for the observed period. The coverage ratio is defined as the ratio of heat provided by the heat pump to the total heat demand [29]. Other important parameters include the initial investment cost of the new heating system and the total annual cost. As previously outlined in Chapter 3, the total annual cost is comprised of several components. These are the initial investment cost (annuity), the annual energy cost, the annual maintenance cost, and, if applicable, an annualised negative investment cost at the end of the observed period due to the residual value of assets that have not reached their technical lifetime yet. It does not include the CO_2 cost, in order to allow for a fair comparison between different system designs. The parameters $\Delta C_{an,tot}$ and ΔCE express the increase or decrease of total annual cost and CO_2 emissions respectively, in comparison to the baseline scenario described in Section 5.3. By dividing ΔCE by $\Delta C_{an,tot}$, the cost per tonne of CO_2 reduction is obtained.

The impact of the U-value of the building envelope ($\bar{U}_{env}$), the window-to-wall ratio (WWR), the building's airtightness ($n50$) and the building's orientation (γ_{front}) on the heat demand and optimal hybrid heating system size is investigated in Chapter 6. Until then, the values shown in Table 5.2 are assumed for these parameters. The reasoning behind these values was explained in Chapter 4.

Parameter	Default values
WWR	30% ($f_{window} = 0.68$, $h_{window} = 1.55$ m)
γ_{front}	135°(northwest)
$\bar{U}_{env}$	1.00 $\frac{\text{W}}{\text{m}^2\,\text{K}}$ ($d_{PUR} = 2$ cm, $U_{window} = 2.72$ $\frac{\text{W}}{\text{m}^2\,\text{K}}$)
$n50$	4.5 h^{-1}

TABLE 5.2: Building parameter values for the baseline scenario.

5.2 Comparison of *nPro* and *Modelica* load profiles

First of all, it should be recalled that *nPro* has an hourly resolution. Therefore, the *Modelica* outputs are also converted to hourly values when they are used as input for *nPro*. This mainly affects the peak heat demand, which is reduced when taking an hourly average. However, as the primary focus is the sizing of the heat pump component in a hybrid heating system, this has a relatively limited impact, as the heat pump is typically sized in such a manner that it does not have to cover these peak demands.

The results of the dynamic simulation conducted with the *Modelica* school building model are presented in Figure 5.1. The annual heat demand E_{heat} is 88.3 MWh, the peak demand $\dot{Q}_{peak}$ is 185.3 kW (171.9 kW when hourly averaged), and the thermal discomfort TD is equal to 135.9 degree h.

The *nPro* load profile generation is now carried out using E_{heat} as input. The result of this is also shown in Figure 5.1. A similar observation as in Chapter 3 can be made: the peak heat demand is underestimated because *nPro* attributes too much of

the heat demand to the non-occupied periods. The degree-day method used by *nPro* is an oversimplification of reality. Two other minor remarks can be made. Firstly, the holiday periods assumed by *nPro* and those defined in the *Modelica* building model slightly differ, which is visible in the middle plot of Figure 5.1. Secondly, *nPro* does not differentiate between Wednesdays and other weekdays. This can also be seen in the middle plot of Figure 5.1. Consequently, Wednesdays are attributed more heat demand than they actually have in reality, which results in a slight reduction of the overall peak heat demand.

So, when using *nPro* for the generation of heat demand profiles, it should be kept in mind that base heat demand might be overestimated and peak heat demand might be underestimated. From now on, the heat demand profiles that are used in *nPro* will be the ones resulting from the dynamic simulations with the *Modelica* school building model.

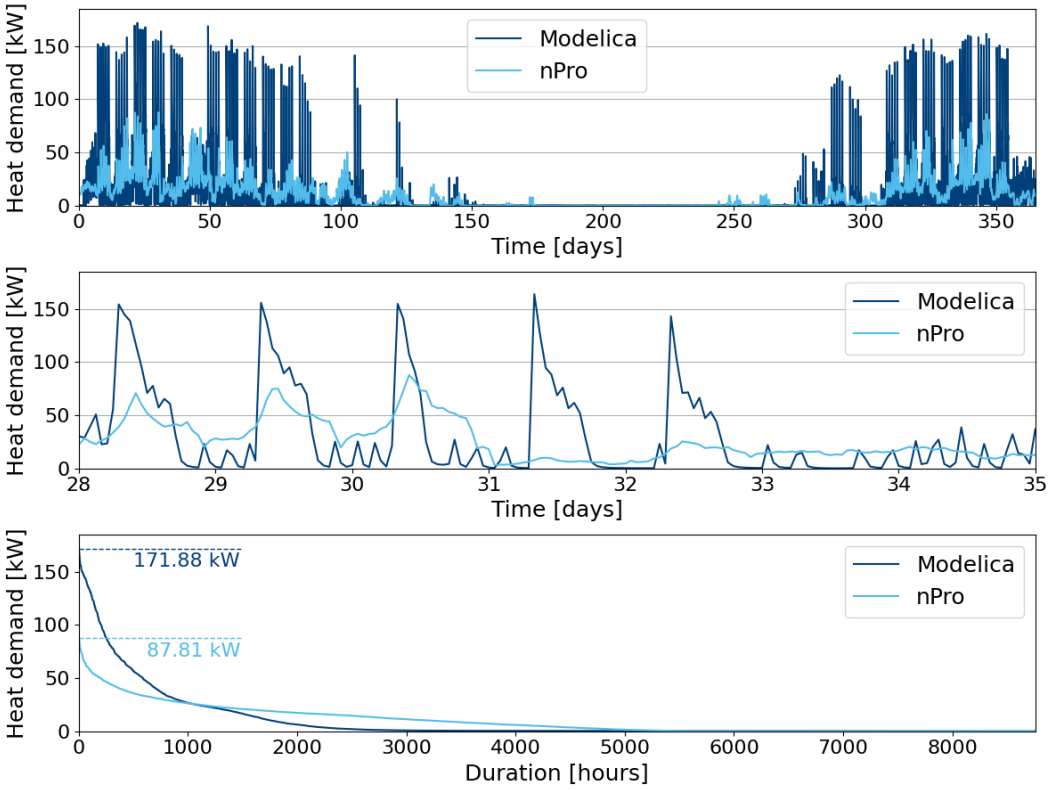

Figure 5.1: Heat demand comparison between dynamic simulation using the *Modelica* representative school building model and load profile generation by *nPro*.

5.3 Baseline scenarios

The parameters $\Delta C_{an,tot}$ and ΔCE require the definition of a baseline scenario. A distinction must be made between the baseline scenario where the current natural

gas boiler can be used for 15 more years, and the baseline scenario where this boiler needs to be replaced now. In the first case, the total annual cost is equal to the sum of the annual energy cost and the annual maintenance cost. In the second case, a new boiler with the same capacity, equal to the peak heat demand, is installed. The total annual cost is thus the sum of the annual energy cost, the annual maintenance cost and the annuity of the investment cost of the new boiler.

Table 5.3 shows the results for these baseline scenarios. 'Current HC, Current radiators' is the baseline scenario of the school building model as described in Chapter 4. This is the baseline scenario assumed in Section 5.4. The choice for this baseline scenario is further elaborated upon in that section.

In the baseline scenario 'New HC, Current radiators', the heating curve of the school building model is lowered. This way, the fact is taken into account that a mixing valve cannot be modelled in a parallel hybrid heating system in *nPro*, which was one of the shortcomings of the tool presented in Section 3.4. This however leads to high values of thermal discomfort, as can be seen in Table 5.3, if the nominal inlet and outlet temperatures of the modelled radiators are not changed. Therefore, the nominal temperatures of the radiators in the school building model are lowered to guarantee thermal discomfort remains within an acceptable range. 'New HC, new radiators' is thus the baseline scenario for Section 5.5, which means that the total annual cost for the baseline scenario with '$L_{boi} = 15$ years' and '$L_{boi} = 0$ years' are equal to 7 006 $\frac{€}{\text{year}}$ and 9 814 $\frac{€}{\text{year}}$, respectively. The former consists of an annual energy cost of €6 860 and an annual maintenance cost of €146. The latter also includes the initial investment of €29 150, which is annualised to an equivalent annual cost of €2 808. The baseline value for the annual CO_2 emissions is 24.4 tCO_2.

	Current HC		New HC			
	Current radiators		Current radiators		New radiators	
E_{heat} [MWh/year]	88.3		85.8		88.0	
$\dot{Q}_{peak}$ [kW]	171.9		138.4		180.8	
$P_{boi,cur}$ [kW]	172		139		181	
TD [(degree h)/year]	135.9		852.6		166.3	
L_{boi} [years]	15	0	15	0	15	0
$P_{boi,new}$ [kW]	/	172	/	139	/	181
$C_{an,tot}$ [€/year]	6 999	9 677	6 764	8 965	7 006	9 814
CE [tCO_2/year]	24.5	24.5	23.8	23.8	24.4	24.4

TABLE 5.3: Values for baseline scenarios.

5.4 System configuration

As explained in Section 3.4, it is currently not possible in *nPro* to conduct the system optimisation with a hybrid heating system consisting of two heat sources in series. Using a workaround, it is only possible to split the total heat demand into

a low- and a high-temperature heat demand by defining a threshold temperature T_{th}. The low-temperature heat demand is then assigned to the heat pump and the high-temperature heat demand is assigned to the gas boiler. The heat pump is thus sized to exactly meet this low-temperature heat demand.

To fairly compare the parallel configuration with the series configuration, the 'Current HC, Current radiators' baseline scenario from Table 5.3 is assumed. The remaining lifetime of the current boiler is set to 15 years, for the same reasons explained in Chapter 3.3.1. Since *nPro* needs a very specific input regarding the supply and return temperatures for the workaround to be able to work, new profiles are defined for these temperatures (which is why the 'Current HC, Current radiators' baseline scenario can be assumed in this case). For the series configuration a heating curve with a maximum value of 75°C at an outdoor temperature of -8°C and a minimum value of 30°C at an outdoor temperature of 20°C is assumed. For the parallel configuration the maximum value is assumed to be 65°C. The temperature difference between supply and return is set to 10°C.

The sizing of the heat pump in the series configuration is conducted for three different threshold temperatures T_{th}. Then, the sizing of the heat pump in the parallel configuration is conducted in such a way that the same CO_2 emission reductions as in the cases of the series configuration are achieved. The outcome is presented in Table 5.4.

	Series			Parallel		
T_{th} [°C]	60	52.5	45	-	-	-
P_{hp} [kW]	308	232	172	196	108	44
$E_{heat,hp}/E_{heat}$ [%]	96.6%	81.8%	53.3%	96.3%	83.0%	55.2%
$C_{an,tot}$ [€/year]	28 726	23 130	18 856	21 025	15 029	10 731
$\Delta C_{an,tot}$ [%]	+310.4%	+230.5%	+169.4%	+200.4%	+114.7%	+53.3%
CE [tCO_2/year]	**5.7**	**8.2**	**13.6**	**5.7**	**8.2**	**13.6**
ΔCE [%]	−76.7%	−66.5%	−44.5%	−76.7%	−66.5%	−44.5%
$C_{\Delta CE}$ [€/tCO_2]	1 156.1	990.2	1 087.5	746.4	492.9	342.3

Table 5.4: Results for parallel and series configuration.

First, it should be noted that, for the $T_{th} = 60$°C and $T_{th} = 52.5$°C case, *nPro* calculates that an ASHP with a nominal thermal capacity exceeding the peak heat demand is required. This can be explained by the fact that, for the nominal thermal capacity of a heat pump, *nPro* assumes a COP of 4. However, at different moments when the heat demand is close to the peak heat demand, this nominal COP is not reached due to the low outside temperature. In *nPro*, the nominal thermal capacity of the proposed heat pump is thus calculated as $P_{hp} = \max\left(COP_{nom} \cdot \frac{\dot{Q}(t)}{COP(t)}\right)^{\dagger}$.

[†]This equation is a reflection of the typical behaviour of a heat pump. As source temperature decreases, electrical power consumption remains relatively constant, while thermal power decreases as well. This can for example be observed in the technical documentation of the Vitocal 300-G heat pump, see https://viessmanndirect.co.uk/files//499b1238-03e0-4b0c-b7d5-adda016de3ff/TechnicalGuide.pdf.

Additionally, in the *nPro* optimisation, the heat demand is precisely split according to the threshold of the supply temperature. In reality, the heat pump in a series configuration would rather be controlled with a varying threshold temperature, which depends on the outdoor temperature as does the COP of the heat pump. This results in a smaller size of the heat pump.

All these reasons account for a lower cost per tonne of CO_2 emission reduction for the parallel configuration, when achieving the exact same emission reduction. The parallel configuration furthermore achieves the same coverage ratio, using a smaller heat pump than the series configuration. Both of these observations can be seen in Table 5.4. The decision to select the parallel configuration over the series configuration is thus, in this case, primarily due to the limitations of the *nPro* tool. Therefore, the parallel configuration and, consequently, the 'New HC, New radiators' case are assumed in the remaining part of this chapter.

5.5 Minimal CO_2 emission reduction

This section examines the impact of the *nPro* optimisation input parameter ΔCE_{min}, the minimal CO_2 emission reduction that needs to be achieved, again considering the remaining lifetime of the currently installed gas boiler. As explained in Section 5.3, the 'New HC, new radiators' baseline scenario is assumed. Table 5.5 presents the outcomes of the *nPro* system optimisation for six different scenarios: three minimal CO_2 emission reductions cases, each with L_{boi} being either 15 or 0 years. As could be seen in Table 1.1, the 2030 target for the non-residential buildings sector is a CO_2 emission reduction of approximately 25% compared to 2021.

ΔCE_{min} [%]	-25%		-50%		-75%	
L_{boi} [years]	15	0	15	0	15	0
$P_{boi,new}$ [kW]	/	172	/	151	/	82
P_{hp} [kW]	20	20	64	64	208	208
P_{hp}/P_{boi} [%]	11.0%	11.6%	35.4%	42.4%	114.9%	253.7%
$E_{heat,hp}/E_{heat}$ [%]	31.7%	31.7%	63.6%	63.6%	96.2%	96.2%
$C_{inv,ini}$ [€]	19 060	46 860	42 512	67 162	119 264	133 564
$C_{an,tot}$ [€/year]	9 384	12 055	12 422	14 774	22 360	23 664
$\Delta C_{an,tot}$ [%]	+25.3%	+18.6%	+43.6%	+33.6%	+68.7%	+58.5%
CE [tCO_2/year]	18.3	18.3	12.2	12.2	6.1	6.1
ΔCE [%]	−25%	−25%	−50%	−50%	−75%	−75%
$C_{\Delta CE}$ [€/tCO_2]	290.6	299.2	250.4	270.3	263.0	313.7

TABLE 5.5: Results for various minimal emission reductions.

These results show that the heat pump is always sized to the extent that the CO_2 emission reduction condition is met, but not exceeded. This means that, for the modelled school building, achieving the CO_2 emission reduction always entails a certain cost $\Delta C_{an,tot}$ compared to the baseline scenario. When the current gas boiler is at the end of its lifetime (and thus requires replacement), the value of $\Delta C_{an,tot}$ is

lower than when the current gas boiler can be used for an additional 15 years. The results also show that a relatively small heat pump (e.g. 20 kW) can already result in a considerable coverage ratio (31.7%). Furthermore, the findings indicate that an initial investment of €19 060 is necessary to achieve the 2030 emission targets if the current gas boiler can continue to be used. Should the current gas boiler be replaced, an investment cost of €46 860 is required: €19 060 for the heat pump and the remainder for the new gas boiler. The values of the cost per tonne of CO_2 emission reduction $C_{\Delta CE}$ prove the existence of a certain emission reduction between 25% and 75%, which leads to the lowest $C_{\Delta CE}$. Looking at the coverage ratio for the $\Delta CE_{min} = -75\%$ case, it is clear that achieving a higher emission reduction will be almost impossible, which is logical because the imported electricity also has a certain CO_2 emission intensity. Achieving zero CO_2 emissions is only feasible when the CO_2 intensity of the imported electricity is zero (i.e. 100% renewable electricity). In that case, a very large heat pump is needed to cover the peak heat demand. Achieving zero CO_2 emissions this way, without considering to adapt the heat demand through measures such as increasing the building insulation or implementing an optimal control strategy, is not recommended.

5.6 Conclusion

This chapter covered the first part of SQ3 (see Section 1.2). It started with a comparison between the load profiles resulting from the dynamic simulations with the *Modelica* school building model and the load profiles generated by *nPro*. This demonstrated that *nPro* attributes too much of the heat demand to non-occupied periods, resulting in an underestimation of the peak heat demand. Subsequently, the impact of system configuration, minimal CO_2 emission reduction and remaining lifetime of the currently installed gas boiler on the optimal hybrid heating system size was investigated. The results showed that achieving a CO_2 emission reduction, for the modelled school building, always entails a certain cost compared to the baseline scenario. The study also showed that modelling two heat sources in series in *nPro* does not yield very realistic results, so in the rest of the chapter the parallel configuration was assumed. Furthermore, it became clear that achieving a 25% emission reduction is feasible with a relatively small heat pump, and that $\Delta C_{an,tot}$ is lower when the current gas boiler needs to be replaced than when it can be used for 15 more years.

For the analysis of Chapter 6, the following assumptions will thus be made: a parallel hybrid heating system configuration, $\Delta CE_{min} = -25\%$, and $L_{boi} = 15$ years.

Chapter 6

The impact of the relevant building parameters

This chapter examines the impact of the influential building parameters, which were identified in Section 2.2.2, on both the heat demand and the optimal hybrid heating system size. As previously explained, a parallel hybrid heating system and the 'New HC, New radiators' case are assumed, of which the baseline scenario was presented in Table 5.3. Table 6.1 shows the different values of the four important building parameters, identified in Section 2.2.2, that are investigated in this chapter: the average U-value of the building envelope $\bar{U}_{env}$, the window-to-wall ratio WWR, the zone airtightness parameter $n50$, and the building orientation parameter γ_{front}. Additionally, the parameters d_{PUR}, U_{window}, f_{window} and h_{window} are shown. As explained in Chapter 4, these were adapted to achieve the different values of $\bar{U}_{env}$ and WWR. The default values of all parameters are in bold.

$\bar{U}_{env}$ $[\frac{\mathrm{W}}{\mathrm{m^2\ K}}]$	d_{PUR} $[cm]$	U_{window} $[\frac{\mathrm{W}}{\mathrm{m^2\ K}}]$	WWR	f_{window} $[/]$	h_{window} $[m]$	$n50$ $[h^{-1}]$	γ_{front} (front façade orientation)
2.00	0.00	3.49	20%	0.48	1.45	2.0	0° (south)
1.50	0.55	2.72	25%	0.57	1.55	3.0	45° (southwest)
1.00	**2.00**	**2.72**	**30%**	**0.68**	**1.55**	**4.5**	90° (west)
0.65	5.30	2.72	35%	0.79	1.55	6.0	**135° (northwest)**
0.30	12.0	1.11	40%	0.79	1.77	7.0	180° (north)
							225° (northeast)
							270° (east)
							315° (southeast)

TABLE 6.1: Investigated values of building parameters.

6.1 Building envelope U-value

The first investigated building parameter is the U-value of the building envelope $\bar{U}_{env}$. This parameter is calculated as shown in Equation 4.2. It is a measure of the quality of the school building's insulation. Based on the findings presented in Table 4.1, five different values of $\bar{U}_{env}$ are chosen. For each of these values, the dynamic simulation of the *Modelica* school building model is repeated. The resulting HLDCs and values of the total annual heat demand are shown in Figure 6.1. The resulting annual heat demand profiles are used as input for the *nPro* tool, which conducts a hybrid heating system optimisation for each case. All relevant results are shown in Table 6.2.

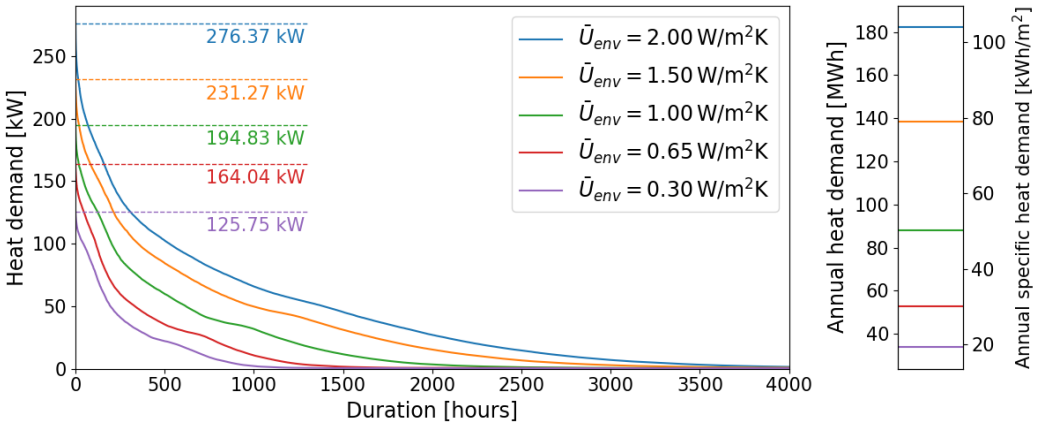

Figure 6.1: HLDCs for different values of $\bar{U}_{env}$.

Figure 6.1 shows that the U-value of the building envelope has a large impact on the heat demand. The U-value is a measure for the heat losses that occur due to a temperature difference between the inside and outside environment. The larger the U-value, the larger these losses, and thus the larger the peak heat demand and the total annual heat demand. It is clear that improving the insulation of a certain building can significantly reduce its heat demand, and thus the amount of CO_2 emissions. The values of TD in Table 6.2 show that thermal discomfort varies between 246.3 degree h and 74.7 degree h. The difference between them thus is quite significant. However, in each case, thermal discomfort remains acceptable, as the maximal annual thermal discomfort for one zone is only 48.0 degree h (zone 4 in the case of $\bar{U}_{env} = 1.50\ \frac{\mathrm{W}}{\mathrm{m^2\ K}}$). Also in the results presented in the following sections, annual thermal discomfort levels consistently remain at acceptable levels. The reason for this is that the nominal output of the heat emission system is calculated according to the design heat losses, as explained in Section 4.5.2.

For every value of $\bar{U}_{env}$, the CO_2 emission reduction is achieved by installing a heat pump that leads to a coverage ratio of approximately 31%. The value of P_{hp}/P_{boi} is approximately 11% for the three cases with highest $\bar{U}_{env}$ and approximately 13% for the two cases with lowest $\bar{U}_{env}$. This can be explained by the fact that a lower $\bar{U}_{env}$ leads to the peak heat demand becoming smaller relative to the average heat demand. This can be seen in Figure 6.1, where the tail of the HLDC is less pronounced for

$\bar{U}_{env}$ [$\frac{\text{W}}{\text{m}^2\,\text{K}}$]	2.00	1.50	1.00	0.65	0.30
E_{heat} [MWh/year]	182.1	138.3	88.0	52.7	33.8
$\dot{Q}_{peak}$ [kW]	243.1	206.4	180.8	153.0	118.1
P_{boi} [kW]	244	207	181	153	119
TD [(degree h)/year]	202.7	246.3	166.3	74.7	92.4
P_{hp} [kW]	28	24	20	20	16
P_{hp}/P_{boi} [%]	11.5%	11.6%	11.0%	13.1%	13.4%
$E_{heat,hp}/E_{heat}$ [%]	30.2%	31.3%	31.7%	31.4%	30.9%
$C_{an,tot}$ [€/year]	17 010	13 503	9 384	6 580	4 811
$\Delta C_{an,tot}$ [%]	+18.7%	+23.4%	+33.9%	+57.2%	+76.6%
CE [tCO_2/year]	38.2	28.8	18.3	11.0	7.1
ΔCE [%]	−25%	−25%	−25%	−25%	−25%
$C_{\Delta CE}$ [€/tCO_2]	212	266	390	656	888

TABLE 6.2: Results for various building envelope U-values.

the lower values of $\bar{U}_{env}$. Thus, a relatively higher heat pump capacity is needed to achieve the same coverage ratio. The ratios of the average heat demand to the peak heat demand are, in order of decreasing $\bar{U}_{env}$: 3.1%, 3.7%, 5.2%, 6.8% and 7.5%.

The results of the *nPro* optimisation again demonstrate that, in all cases, the installation of an ASHP in order to achieve a CO_2 emission reduction will come at a certain cost compared to the baseline scenario. This cost per tonne of CO_2 emission reduction $C_{\Delta CE}$ increases as the U-value of the building envelope decreases. This is due to the fact that the baseline scenario's $C_{an,tot}$ mainly consists of the energy cost, which is low if the heat demand is low. As a result, the investment cost of the heat pump, in relative terms, has a bigger impact on the new $C_{an,tot}$. The same reasoning can be applied if the school building considering a hybrid heating system is larger, as there will also be a larger heat demand. The more floor area a school building has, the lower $C_{\Delta CE}$ will be. This was also observed in the real-life case of Chapter 3, where the heat demand was an order of magnitude larger than that of the modelled 'average' Flemish school building, even resulting in a negative $C_{\Delta CE}$.

6.2 Window-to-wall ratio

The second investigated building parameter is the window-to-wall ratio WWR. The dynamic simulation of the *Modelica* school building model is repeated with five different values of WWR, based on the findings of Section 4.2.2. The resulting HLDCs and values of the total annual heat demand are shown in Figure 6.2. The resulting annual heat demand profiles are used as input for the *nPro* tool, which conducts a hybrid heating system optimisation for each case. All relevant results are shown in Table 6.3.

First, it should be noted that a change in WWR will also result in a change in $\bar{U}_{env}$. The U-value of the windows is higher than the U-value of the external walls, so when the WWR is increased, $\bar{U}_{env}$ also increases, and thus the amount

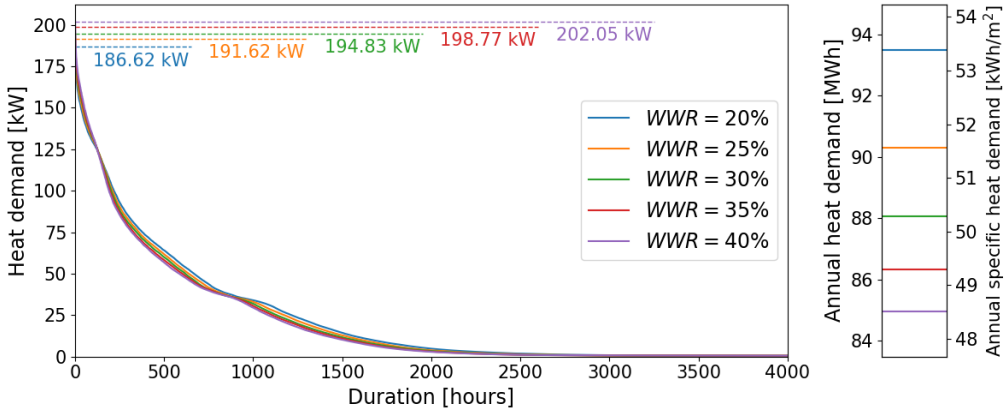

Figure 6.2: HLDCs for different values of WWR.

of transmission losses increases. However, increasing the WWR also increases the solar gains. These two effects counteract each other. Consequently, the impact of modifying the WWR on the heat demand is lower than that of directly modifying $\bar{U}_{env}$. Given that the total annual heat demand is highest for the lowest value of WWR, it can be concluded that, for the assumed U-values, the reduction in solar gains exceeds the decrease in transmission losses. However, the peak heat demand is lowest for the lowest value of WWR, as this peak heat demand typically occurs on a winter morning, when there is little or no sunlight.

WWR [%]	20%	25%	30%	35%	40%
E_{heat} [MWh/year]	93.5	90.3	88.0	86.3	85.0
$\dot{Q}_{peak}$ [kW]	174.1	177.3	180.8	180.1	184.6
P_{boi} [kW]	175	178	181	181	185
TD [(degree h)/year]	243.1	197.5	166.3	143.8	125.4
P_{hp} [kW]	20	20	20	20	20
P_{hp}/P_{boi} [%]	11.4%	11.2%	11.0%	11.0%	10.8%
$E_{heat,hp}/E_{heat}$ [%]	31.6%	31.3%	31.7%	31.5%	31.5%
$C_{an,tot}$ [€/year]	9 739	9 542	9 384	9 254	9 167
$\Delta C_{an,tot}$ [%]	+31.2%	+33.6%	+33.9%	+34.8%	+36.2%
CE [tCO_2/year]	19.4	18.8	18.3	18.0	17.7
ΔCE [%]	−25%	−25%	−25%	−25%	−25%
$C_{\Delta CE}$ [€/tCO_2]	358	382	390	398	413

Table 6.3: Results for various window-to-wall ratios.

Table 6.3 shows that the WWR has little impact on the results of the *nPro* hybrid heating system optimisation. In each case, a heat pump with a nominal thermal capacity of 20 kW is to be installed in order to achieve an emission reduction of 25%. Again, if the total annual heat demand is higher, $C_{\Delta CE}$ is lower.

6.3 Building airtightness

The third investigated building parameter is the airtightness of the building, represented by the $n50$ value. The dynamic simulation of the *Modelica* school building model is repeated with five different values of $n50$, based on the findings of Section 4.2.5. The resulting HLDCs and values of the total annual heat demand are shown in Figure 6.3. Again, the resulting annual heat demand profiles are used as input for the *nPro* tool, which conducts a hybrid heating system optimisation for each case. All relevant results are shown in Table 6.4.

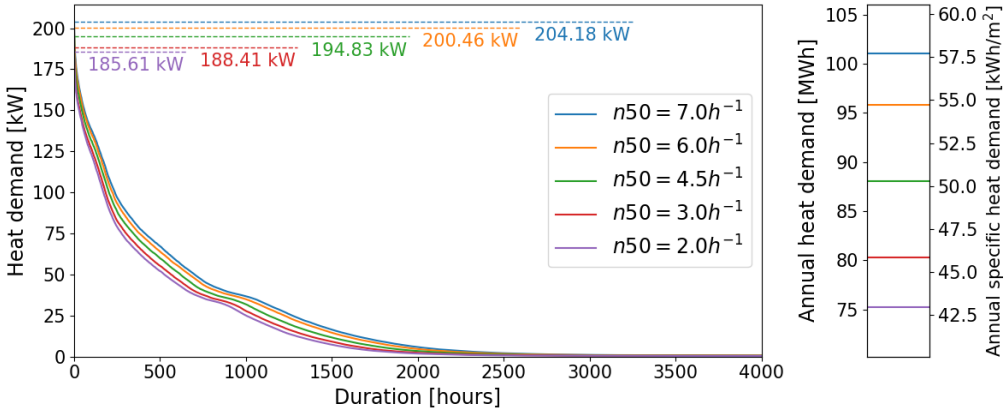

FIGURE 6.3: HLDCs for different values of $n50$.

Figure 6.3 shows what is expected: the greatest annual heat demand and the highest peak heat demand occur when the infiltration rate is highest. A higher value of $n50$ means more infiltration losses. However, the impact of $n50$ is smaller than the impact of $\bar{U}_{env}$, as the amount of infiltration losses is lower than the amount of transmission losses.

$n50$ [h^{-1}]	7.0	6.0	4.5	3.0	2.0
E_{heat} [MWh/year]	101.0	95.7	88.0	80.3	75.2
$\dot{Q}_{peak}$ [kW]	187.6	181.8	180.8	175.1	171.3
P_{boi} [kW]	188	182	181	176	172
TD [(degree h)/year]	203.2	190.3	166.3	145.0	130.3
P_{hp} [kW]	24	24	20	20	20
P_{hp}/P_{boi} [%]	12.8%	13.2%	11.0%	11.4%	11.6%
$E_{heat,hp}/E_{heat}$ [%]	31.4%	31.1%	31.7%	31.5%	31.2%
$C_{an,tot}$ [€/year]	10 539	10 115	9 384	8 760	8 357
$\Delta C_{an,tot}$ [%]	+31.9%	+33.7%	+33.9%	+37.5%	+40.5%
CE [tCO_2/year]	21.0	20.0	18.3	16.7	15.7
ΔCE [%]	−25%	−25%	−25%	−25%	−25%
$C_{\Delta CE}$ [€/tCO_2]	364	383	390	428	461

TABLE 6.4: Results for various airtightness values.

Table 6.4 again shows that $C_{\Delta CE}$ decreases for increasing heat demand. Additionally, a similar observation can be made as in the investigation of the impact of $\bar{U}_{env}$. If the investigated building has more infiltration losses (higher $n50$), the ratio of average heat demand to peak heat demand becomes larger. The ratios of the average heat demand to the peak heat demand are, in order of increasing $n50$: 4.6%, 4.9%, 5.2, 5.5% and 5.6%. This explains why the capacity ratio P_{hp}/P_{boi} is higher for the two cases with the highest value of $n50$.

6.4 Building orientation

The final investigated building parameter is the building orientation, represented by the parameter γ_{front}, which is the orientation of the front façade of the school building. The dynamic simulation of the *Modelica* school building model is repeated for eight different building orientations. The resulting HLDCs and values of the total annual heat demand are shown in Figure 6.4. Again, the resulting annual heat demand profiles are used as input for the *nPro* tool, which conducts a hybrid heating system optimisation for each case. All relevant results are shown in Table 6.5.

The floor plan of the modelled school building was shown in Figure 4.1. The building is rectangular, the front façade being one of the long sides of the building. The windows are not evenly distributed over the entire building envelope: when $WWR = 30\%$, the front façade has 46.0% of the total window area, the back façade 40.8%, the left façade 8.8% and the right façade 4.4%.

Building orientation can have an impact on two things: on the solar gains because of the sun's path throughout the day, and on the infiltration losses if there is a prevalent wind direction. However, in the *Modelica* school building model, infiltration losses are assumed to be constant and not affected by wind conditions.

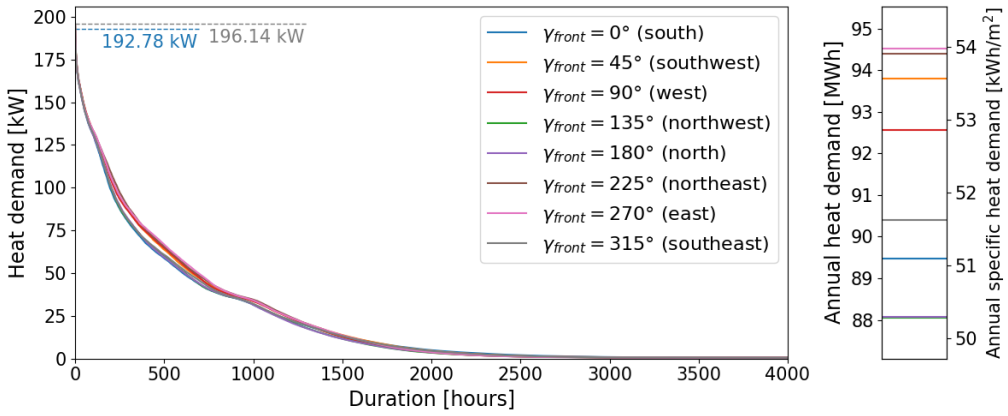

Figure 6.4: HLDCs for different values of γ_{front}.

Figure 6.4 illustrates that building orientation has a minimal impact on the peak heat demand. This can be attributed to the fact that the peak heat demand typically occurs on a winter morning, when sunrise has not occurred yet. The impact of building orientation on total heat demand is also rather limited, but not negligible.

Total heat demand is highest for the east, northeast, southwest and west cases. These cases have in common that one of the short façades of the building is pointed to the southeast or the south, which means that the amount of solar gains before and during noon is lower than if the long façade would be pointed to the southeast or south. This aspect becomes more clear in Figure 6.5, where the HLDCs are plotted relative to the average HLDC of the eight cases.

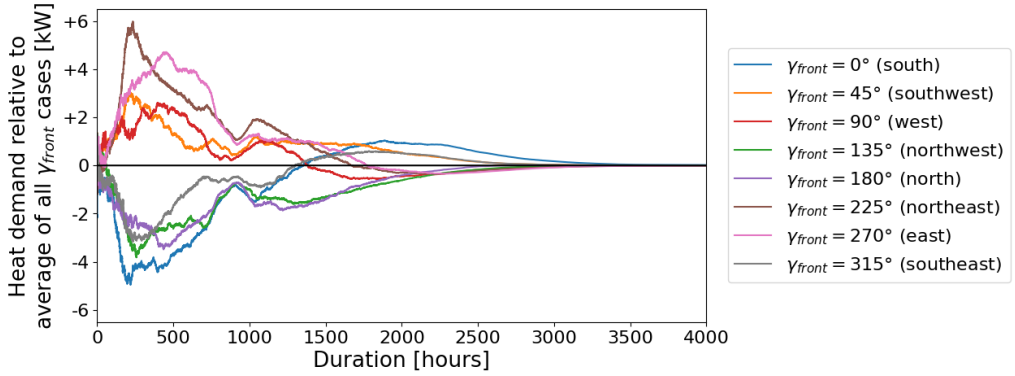

FIGURE 6.5: HLDCs for different values of γ_{front}, relative to the average HLDC of the eight cases.

Figure 6.5 illustrates that the average heat demand is higher for the east, northeast, southwest and west cases, although the peak demands of the eight cases do not differ much. The fact that the heat demand for the southwest and northeast case (and for the north and south case, and for the east and west case, etc.) are not equal is caused by the asymmetry of the modelled school building and its windows.

The previous observation is also reflected in Table 6.5. For the east, northeast, southwest and west cases, a heat pump of 24 kW is needed to achieve an emission reduction of 25%, while for the other cases a heat pump of 20 kW suffices. Again this can be explained by the average heat demand being higher relative to the peak heat demand for these cases. This higher heat pump capacity leads to higher values of $C_{an,tot}$ and $\Delta C_{an,tot}$. The varying values of TD in Table 6.5 can be explained by the fact that solar gains are not taken into account when the nominal output of the heat emission system is calculated.

6.5 Conclusion

This chapter covered the second part of SQ3 (see Section 1.2). The impact of different building parameters on heat demand and optimal hybrid heating system size was investigated, which mainly revealed that an increase in heat demand leads to lower values of $\Delta C_{an,tot}$ and $C_{\Delta CE}$. Also, when the ratio of average heat demand to peak heat demand becomes larger, a higher capacity of heat pump will be required to achieve a certain coverage ratio. This was the case for low values of $\bar{U}_{env}$, for high values of $n50$ and for the cases in which one of the short façades of the building is pointed to the southeast or south.

γ_{front}	0°	45°	90°	135°	180°	225°	270°	315°
E_{heat} [$\frac{\text{MWh}}{\text{year}}$]	89.5	93.8	92.6	88.0	88.1	94.4	94.5	90.4
$\dot{Q}_{peak}$ [kW]	177.0	180.7	175.3	180.8	177.6	177.7	179.3	179.3
P_{boi} [kW]	177	181	176	181	178	178	180	180
TD [(degree h)/year]	298.5	276.1	208.1	166.3	163.7	233.0	282.7	305.6
P_{hp} [kW]	20	24	24	20	20	24	24	20
P_{hp}/P_{boi} [%]	11.3%	13.3%	13.6%	11.0%	11.2%	13.5%	13.3%	11.1%
$E_{heat,hp}/E_{heat}$ [%]	31.5%	31.5%	31.2%	31.7%	31.7%	31.2%	31.4%	31.4%
$C_{an,tot}$ [€/year]	9 391	9 974	9 950	9 384	9 342	10 062	10 083	9 523
$\Delta C_{an,tot}$ [%]	+32.8%	+34.3%	+35.3%	+33.9%	+33.4%	+34.3%	+34.5%	+33.3%
CE [tCO_2/year]	18.6	19.5	19.3	18.3	18.3	19.7	19.7	18.8
ΔCE [%]	−25%	−25%	−25%	−25%	−25%	−25%	−25%	−25%
$C_{\Delta CE}$ [€/tCO_2]	374	392	404	390	383	392	395	379

Table 6.5: Results for various building orientations.

Chapter 7

The impact of optimal control

In this chapter, an exploratory investigation of the impact of optimal control (OC) on heat demand and hybrid heating system size is conducted, which is the subject of SQ4. First, the optimisation model and the definition of the optimisation problem is presented in Section 7.1. Then, in Section 7.2, OC is applied to the heating system which is currently present in most school buildings: a gas-fired heating system consisting of a natural gas boiler. In Section 7.3, OC is applied to different hybrid heating system configurations.

7.1 Optimisation model and settings

As mentioned in Chapter 2, *TACO* [17] is used in this chapter. It is capable of translating an optimal control problem (i.e. the combination of a *Modelica* building and heating system model, an objective function and constraints) into an optimisation problem, which it then solves.

The *Modelica* school building model that is used is the same as the one described in Chapter 4 and used in Chapters 5 and 6. Four different heating system models are created: one model of the current gas-fired heating system, and three models of possible hybrid heating systems (series configuration, parallel configuration with a three-way valve and parallel configuration with two two-way valves).

The *Modelica* model for the gas-fired heating system is shown in Figure C.1, which can be found in Section C.1 of Appendix C. It is a slight adaptation of the heating system described in Section 4.5: the TRVs are changed into controllable valves, the heating curve is removed because supply temperature also becomes a control variable, and the 18 different pumps (one for each zone) are changed into one circulation pump, as using these different pumps led to flow reversal issues in the optimisation. In total, there are 19 optimisation variables: the opening degrees of each of the 18 radiator valves, and the water supply temperature at the outlet of the boiler. The nominal capacity of the boiler is set to 160 kW, the sum of the design heat loads of each zone. For all *TACO* optimisations, the time step is set to one hour.

The *Modelica* models for the different hybrid heating systems are shown in Figures C.2, C.3 and C.4, in Section C.1 of Appendix C. The model equations for the *TACO* heat pump model are explained in Section C.2 of Appendix C. For the series configuration, a heat pump with a nominal capacity of 20 kW is placed at the inlet of the gas boiler. A capacity of 20 kW corresponds to a capacity ratio of 12.5%, which was approximately the average value of this parameter in the results of the *nPro* optimisations of Chapters 5 and 6. There are 20 optimisation variables: the 18 valves, the supply temperature of the gas boiler, and the modulation of the heat pump. For the parallel configuration, two variations are modelled: one where the inlets of the 20 kW heat pump and the gas boiler are connected using a controllable three-way valve, and one where the inlets are connected using two separate, controllable two-way valves. With the three-way valve, this gives one extra optimisation variable, with the two-way valves this gives two extra optimisation variables.

The optimal control problem that *TACO* translates into an optimisation problem is similar to the one described by Jansen et al. [78]:

$$\begin{aligned} \min_{\boldsymbol{o}(t)} \quad & \int_0^{\Delta t_p} \left(\boldsymbol{J_{ene}}(t) + \sum_{k=1}^{18} w_k s_k(t)^2 \right) dt \\ \text{s.t.} \quad & \text{model equations,} \\ & T_{in,k}^{set} - s_k(t) \leq T_{in,k}(t), \quad k = 1 \ldots 18, \\ & s_k(t) \geq 0, \qquad\qquad\qquad\quad k = 1 \ldots 18, \end{aligned} \tag{7.1}$$

where $\boldsymbol{o}(t)$ are the continuous optimisation variables of the system and Δt_p is the prediction horizon. This prediction horizon is chosen to be one year. The first term of the objective integrand, $\boldsymbol{J_{ene}}(t)$, represents the energy cost objective, which differs between the gas-fired heating system case (Equation 7.2) and the hybrid heating system case (Equation 7.3).

$$\boldsymbol{J_{ene}}(t) = \frac{\dot{Q}_{boi}(t)}{\eta_{boi}(t)} \cdot 0.07 \ \frac{€}{\text{kWh}_{\text{gas}}} + \dot{P}_{pump}(t) \cdot 0.20 \ \frac{€}{\text{kWh}_{\text{ele}}} \tag{7.2}$$

$$\boldsymbol{J_{ene}}(t) = \frac{\dot{Q}_{boi}(t)}{\eta_{boi}(t)} \cdot 0.07 \ \frac{€}{\text{kWh}_{\text{gas}}} + \left(\dot{P}_{pump}(t) + \frac{\dot{Q}_{hp}(t)}{COP(t)} \right) \cdot 0.20 \ \frac{€}{\text{kWh}_{\text{ele}}} \tag{7.3}$$

The energy objective represents the cost per hour (in 10^{-3} $\frac{€}{\text{h}}$) of electricity and gas usage. A time step of one hour is considered, so the integration yields a value in 10^{-3} €. Again, a constant electricity cost of 0.20 $\frac{€}{\text{kWh}}$ and a constant natural gas cost of 0.07 $\frac{€}{\text{kWh}}$ are assumed. The second term of the objective integrand is the thermal comfort objective for each of the 18 zones. In this term, w_k is a weighting factor for the soft constraint, and s_k is the slack variable, which is penalised quadratically. The weighting factor w_k is set to either 100 $\frac{W}{K^2}$, 500 $\frac{W}{K^2}$ or 1 000 $\frac{W}{K^2}$ based on the heat demand of each zone k, in order to ensure that the optimisation is well-conditioned

and to achieve a similar level of thermal comfort as in the rule-based control (RBC) model. The optimisation tolerance is set to 10^{-3}. The efficiency of the gas boiler η_{boi} depends on the supply and return temperature, its definition is based on the efficiency curves found in [79]. The COP of the heat pump component depends on the ambient temperature and the supply temperature, it is calculated based on the COP curves that were also used in the *nPro* calculations (Figure A.8).

7.2 Optimal control of gas-fired heating system

Figure 7.1 illustrates two HLDCs for the case of a gas-fired heating system, which is the typical configuration in Flemish schools. One HLDC is for the case of the RBC strategy, as described in Section 4.5.5. The other HLDC is for the case of OC. In the case of RBC, the total annual heat demand is 88.26 MWh, while in the case of OC it is 72.21 MWh, a reduction of 18%. The peak heat demands are 185.32 kW (hourly averaged 171.90 kW) and 155.90 kW, respectively. The annual thermal discomfort, as defined in Section 4.5.6, is 157.0 degree h for the RBC case and 209.9 degree h for the OC case. However, in the OC case, thermal discomfort is more evenly distributed over time, with the zone temperature for example remaining 0.2°C below the setpoint throughout the entire day. In contrast, in the RBC case, this thermal discomfort is concentrated in the mornings, where the zone temperature can for example still be 2°C below the setpoint temperature when the occupants arrive. It is also important to recall that the setpoint temperature is increased one and a half hour before the school building is occupied, while the calculation of thermal discomfort only considers the occupied periods of each zone. It can thus be assumed that the thermal discomfort experienced by occupants is comparable in both cases, or perhaps even worse in the case of RBC.

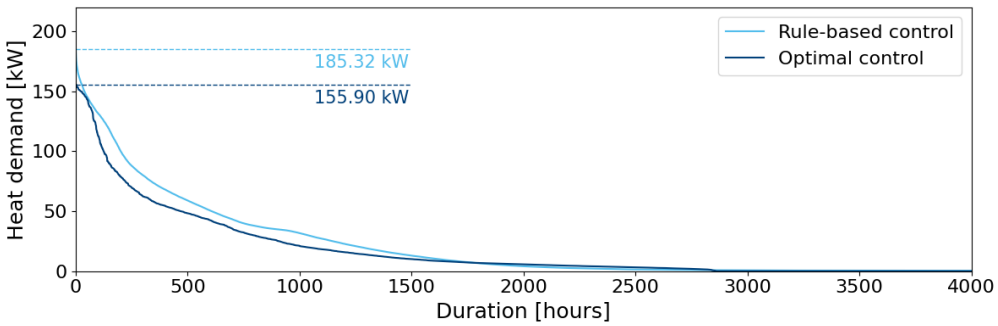

FIGURE 7.1: HLDCs for two different control strategies of a gas-fired heating system.

Reasons for the reduction in total annual heat demand and peak heat demand can be observed in Figures 7.2 and 7.3. The former shows the total heat demand for an eight-day period in February. It should first be noted that the results of the dynamic simulation in *Modelica* (i.e. the RBC case) have a resolution of five minutes. The results of *TACO* (i.e. the OC case) have a resolution of one hour. This provides a partial explanation for the more smooth demand profile and the lower peak demand

of the *TACO* results. Another reason for the smooth demand profile of days 47 and 48 is the fact that with RBC, the pumps are controlled using an on/off-strategy with a certain hysteresis. With OC, there is no hysteresis. It should also be noted that in the RBC model of the gas-fired heating system, described in Section 4.5, the model for the natural gas boiler has an unlimited capacity. In the OC model, the gas boiler capacity is set to the sum of the design heat loads of each heated zone, which is 160 kW. A second explanation for the lower peak demand in the case of OC is the fact that the boiler already starts working before the temperature setpoint increases. This can be seen in the heat demand profile of Figure 7.2, but even better in the profile of the temperature and heat demand of zone 13, shown in Figure 7.3.

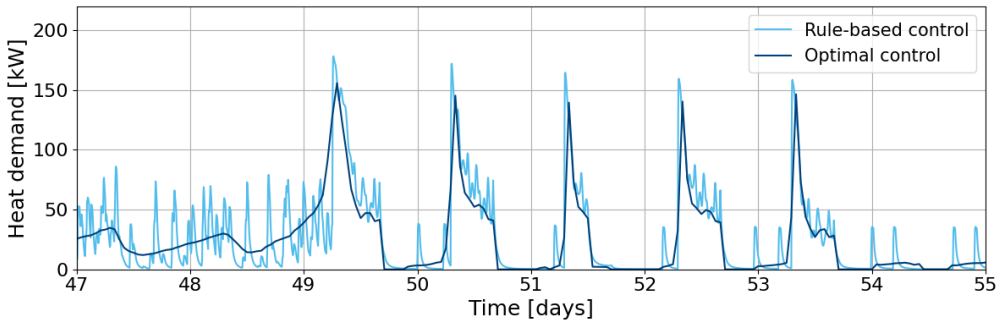

Figure 7.2: Comparison of the total heat demand, for an eight-day period, using RBC and OC.

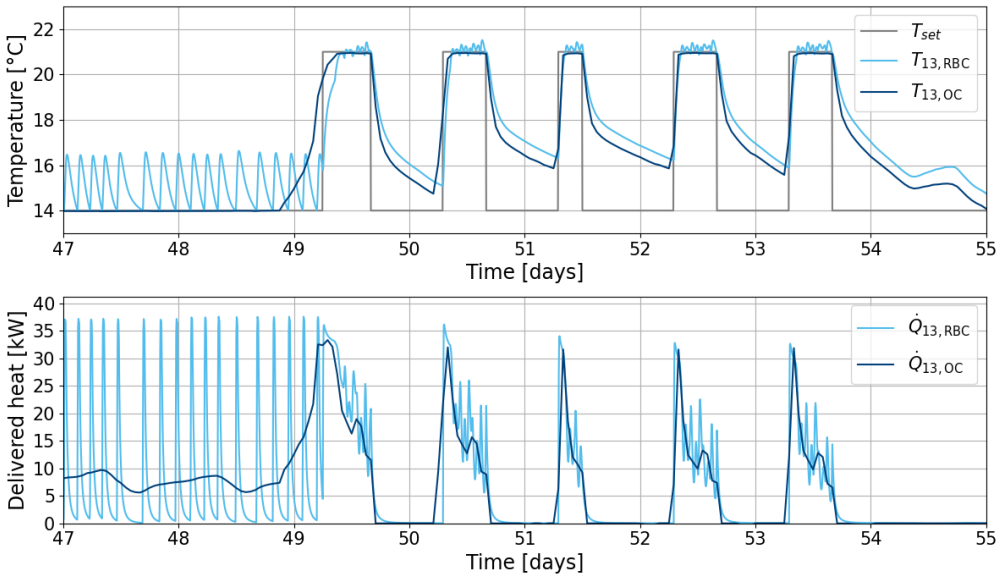

Figure 7.3: Comparison of the temperature of zone 13 and the delivered heat in zone 13, for an eight-day period, using RBC and OC.

In summary, the implementation of an OC strategy in a gas-fired heating system

can result in a reduction of the total annual heat demand, consequently leading to a decline in the total annual energy cost and the annual amount of CO_2 emissions, while maintaining or increasing thermal comfort. It is also possible to (slightly) reduce the peak heat demand by starting the heating of the building at an earlier point in time.

7.3 Optimal control of hybrid heating system

7.3.1 Series configuration

Figure 7.4 shows the annual heat demand profile and HLDC for the optimal control of a 160 kW natural gas boiler and a 20 kW heat pump in series. It should be noted that the nominal thermal capacity of a heat pump in *TACO* is defined in a different manner than it was in *nPro* (see Section 5.4). In *nPro*, the nominal thermal capacity of this heat pump would be 27.4 kW, resulting in a heat pump capacity ratio of 17.0%. With optimal control, this leads to a coverage ratio of 66.6%, whereas in Chapters 5 and 6, the coverage ratio was consistently around 30% for a heat pump capacity ratio between 10% and 15%. In the case of optimal control of the gas-fired heating system, the annual heat demand was 72.2 MWh. Now, annual heat demand equals 89.75 MWh. The red curve in Figure 7.4 shows that the 'base' heat demand has significantly increased compared to the case of the gas-fired heating system. However, because the cost of electricity per kWh is lower than the cost of natural gas, the annual energy cost decreases from €5 622 to €4 977. When assuming an electricity cost of 0.20 $\frac{€}{\text{kWh}}$, a natural gas cost of 0.07 $\frac{€}{\text{kWh}}$, and a constant boiler efficiency of 90%, heating using the heat pump is cheaper than heating using the boiler if $\frac{0.20}{COP}\ \frac{€}{\text{kWh}_{\text{thermal}}} < \frac{0.07}{90\%}\ \frac{€}{\text{kWh}_{\text{thermal}}}$, so if $COP > \frac{0.20}{0.7/90\%} = 2.6$. Annual CO_2 emissions decrease from 20.01 tonnes for the gas-fired heating system case to 10.33 tonnes for the series hybrid heating system case.

Figure 7.5 shows the change in heat demand profile between the case of the gas-fired heating system and the case of the series hybrid heating system. The heat pump is employed to its full capacity throughout the nights between weekdays, thus preventing the school building from cooling down to the same extent as in the previous case. Consequently, the peak in heat demand in the morning is reduced. When Friday is over, the heat pump does lower its output, but it increases again the more the weekend progresses, starting to heat up the building for Monday.

Annual thermal discomfort is 109.3 degree h, so better than the 209.9 degree h for the case of the gas-fired heating system.

7.3.2 Parallel configuration

Parallel configuration with two two-way valves

For the parallel configuration, results are very similar. In the case of two two-way valves, the annual heat demand is 91.26 MWh. The coverage ratio is 65.6%, so slightly lower than in the case of the series configuration. The annual energy cost is

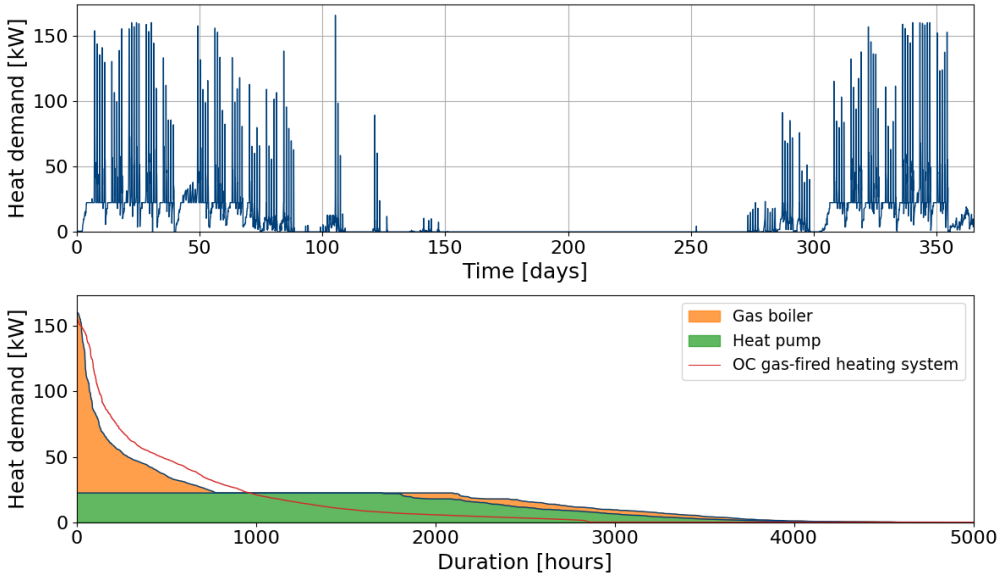

Figure 7.4: Results for optimal control of a series hybrid heating system consisting of a natural gas boiler of 160 kW and a heat pump of 20 kW.

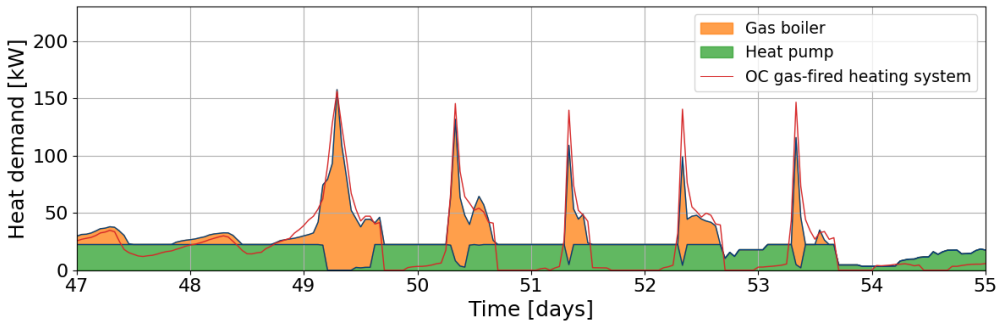

Figure 7.5: Heat demand profile, for an eight-day period, of optimal control of gas-fired heating system and optimal control of series hybrid heating system.

€5 073 and the annual amount of CO_2 emissions is 10.67 tonnes. Annual thermal discomfort is 98.8 degree h. Figure C.5 shows the annual heat demand profile and HLDC, and Figure C.6 shows the heat demand profile for an eight-day period. Both figures can be found in Section C.3 of Appendix C.

Parallel configuration with one three-way valve

In the case of one three-way valve, the annual heat demand is 90.15 MWh. The coverage ratio is 66.0%, so also slightly lower than in the case of the series configuration. The annual energy cost is €5 013 and the annual amount of CO_2 emissions is 10.55 tonnes. Annual thermal discomfort is 111.0 degree h. The slightly lower energy cost is thus compensated by a slightly higher thermal discomfort. Again,

in Section C.3 of Appendix C, Figures C.7 and C.8 show the same plots as for the previous configurations.

It can thus be concluded that, when optimally controlled, there is little difference between the three investigated configurations of hybrid heating systems.

7.4 Conclusion

This chapter investigated the impact of optimal control on heat demand and optimal hybrid heating system size, which was the subject of SQ4 (see Section 1.2). The findings of this chapter demonstrated that optimising the control strategy of a gas-fired heating system can have a significant impact on total annual heat demand, which in turn affects the annual energy cost and annual CO_2 emissions. Furthermore, optimising the control of a hybrid heating system can result in a significant increase in the coverage ratio of the heat pump, while maintaining thermal comfort. This implies that, when a hybrid heating system is being considered, the heat pump can be sized smaller if optimal control will be implemented, for instance in the form of MPC, while still achieving the desired CO_2 emission reduction. The results for the different investigated configurations of hybrid heating systems were found to be highly comparable.

Chapter 8

Recommendations for schools

Based on the findings and conclusions of the research conducted in the previous chapters, it is now possible to formulate some general recommendations for schools seeking to reduce their carbon footprint through the implementation of a hybrid heating system.

The first finding is the fact that schools can achieve the 2030 emission target for non-residential buildings (emission reduction of approximately 25% compared to 2021, see Table 1.1) through the implementation of a heat pump with a relatively small capacity compared to the peak heat demand, and operating it alongside the existing natural gas boiler, thereby creating a hybrid heating system. This emission reduction is thus achieved without the necessity for immediate additional measures such as improving insulation levels or installing underfloor heating, which would be required if the new heating system consisted solely of a heat pump.

An air-source heat pump is a suitable option in this context given its lower initial investment cost and minimal locational and infrastructural requirements in comparison to a ground-source heat pump. Especially the aspect of cost is important as schools often have only limited budgets available. The installation of a heat pump reduces the annual energy cost, but an initial investment is always required. Schools do have the possibility to apply for a subsidy in the case of the installation of a hybrid (air-source) heat pump[†].

It should however be noted that, if practically feasible and if the available budget is high enough, a ground-source heat pump is also worth considering if a significant CO_2 emission reduction is desired, for example more than 50%. This type of heat pump can achieve higher average COP values, particularly during the coldest periods of the year, when heat demand is highest. Especially when a school is large and has a high heat demand, the initial investment will be paid back at a relatively faster rate, as the annual energy cost is reduced more.

If historical annual heat demand profiles are available, for example because of the presence of a digital natural gas meter, a planning tool such as *nPro* can be used

[†]This subsidy can range from €1 500 to €31 250, depending on heat pump capacity and date of request. For more information, see: https://www.vlaanderen.be/premies-voor-renovatie/mijn-verbouwpremie/mijn-verbouwpremie-voor-warmtepomp.

to estimate the impact of installing a heat pump of a given capacity on energy costs and CO_2 emissions. A design decision can then be made based on the criteria most important to the school, such as minimum investment cost or minimum total annual cost.

If annual heat demand profiles are not available, which is the case in most schools, peak heat demand is a good indicator for the sizing of the heat pump component in a hybrid heating system. Selecting an air-source heat pump with a nominal capacity between 10% and 20% of this peak demand is likely to result in achieving a reduction of CO_2 emissions of 25%. If the school building has a well-insulated building envelope (low $\bar{U}_{env}$), or if it has average insulation levels but high infiltration rates, or if due to building orientation the amount of solar gains is limited, it would be advisable to select the capacity of the heat pump slightly higher. If no information is available regarding the peak heat demand, sizing is more difficult. Tools like *nPro* might underestimate peak demands or would require input data that are not available to achieve accurate results. Peak heat demand can be calculated by conducting a dynamic building simulation, but this can be very complex and costly. However, an estimation of peak heat demand can always happen based on the currently installed heating capacity.

When an optimised control strategy is adopted in the new hybrid heating system, the achieved CO_2 emission reduction for a given heat pump capacity can increase significantly, or a smaller heat pump can be installed to achieve the same emission reduction. By optimising the control of the heating system, the annual energy cost can also be significantly reduced. The impact of the configuration of the hybrid heating system on its overall performance is minimal when optimal control is implemented.

In particular when the currently installed natural gas boiler is in good condition and for example minor improvements can extend its lifetime, the adoption of an air-source heat pump can be the ideal transition towards further low-carbon or even carbon neutral heating in the future. The installation of a relatively small heat pump now allows for the implementation of different energy-saving measures, which always come with a certain cost, to be spread out in time. This is advantageous given the limited budgets that are typical of schools.

If the currently installed heating system still uses heating oil, which emits more CO_2 than natural gas, and requires replacement, or if the current natural gas boiler has reached the end of its lifetime, opting for a hybrid heating system will be relatively cheaper compared to the baseline scenario than when the currently installed heating system can continue to be used. So, if the current heating system needs to be replaced, a hybrid heating system is even more worth considering. The new natural gas boiler can be sized smaller than the previous one, but not significantly so, as the peak heat demand typically occurs during the coldest period of the year, when the COP of the heat pump is low.

It was mentioned before that different energy-saving measures can be implemented in the years following the installation of the hybrid heating system. These measures can for example be the improvement of insulation levels or the reduction of unwanted air infiltration. Especially the first one has a significant impact on overall heat demand. Another option would be the implementation of optimal control, which can

significantly impact heat demand and make that all technologies are used at their optimal efficiency. The implementation of these energy-saving measures results in a reduction of the demand for heat and thus in a reduction of CO_2 emissions and energy cost. Additionally, these measures increase the coverage ratio of the installed heat pump.

Chapter 9

Conclusion

The main goal of this thesis was to investigate how heat pumps can be integrated into the fossil-fuel based heating system of typical Flemish school buildings to achieve a cost-effective CO_2 reduction, while maintaining thermal comfort. The introductory chapter outlined the significant potential for increasing the share of renewable energy in Flemish school buildings. However, it also highlighted the challenges faced by schools due to budget constraints and aging infrastructure. The implementation of a hybrid heating system, which combines a heat pump with a fossil fuel-based heating system, is proposed as a cost-effective and feasible solution. However, an important aspect of hybrid heating systems is the sizing of the heat pump component.

First, the parameters that influence the heat demand of typical Flemish school buildings were identified. These parameters were then taken into account in the analysis of this heat demand and its impact on optimal hybrid heating system size. The most important parameters were the U-values of the building envelope, the window-to-wall ratio, the building's airtightness and the building's orientation. The findings of the literature research also indicated that an air-source heat pump may be the optimal choice for schools considering a hybrid heating system, due to the fact that it has a lower investment cost and less stringent locational requirements.

Next, *nPro* was presented, which is a web-based planning tool allowing to design energy systems for buildings and evaluate them from a techno-economic perspective. This tool was tested on a real-life case of a school building: building D of the Campus Proximus site of UCLL. The application of *nPro* to this case led to several findings regarding the limitations and assumptions of the tool. These aspects were then taken into account in the further investigation, where *nPro* was used to conduct different hybrid heating system optimisations.

These hybrid heating system optimisations were conducted using annual heat demand profiles that resulted from dynamic simulations of a *Modelica* building model of a representative Flemish school building. The optimisations showed that, for the modelled school building, achieving a certain CO_2 emission reduction by means of a hybrid heating system always entails a certain cost compared to the baseline scenario. Because of this, the *nPro* optimisation will always lead to the hybrid heating system capable of reaching the imposed minimum CO_2 emission reduction, but not exceeding

it. It also became clear that achieving a 25% emission reduction is feasible with a relatively small heat pump. The investigation of the impact of the relevant building parameters showed that an increase in heat demand leads to lower values of the increase in total annual cost compared to the baseline scenario and cost per tonne of CO_2 emission. It was also found that a higher capacity of heat pump relative to the peak heat demand is needed to achieve a certain coverage ratio, for low values of $\bar{U}_{env}$, for high values of $n50$ and for the cases in which one of the short façades of the school building is pointed to the southeast or south.

The last part of the investigation focused on the aspect of optimal control. Optimisations conducted by means of *TACO* demonstrated that optimising the control strategy of a heating system can have a significant positive impact on total annual heat demand, which in turn affects annual energy cost and annual CO_2 emissions positively. For hybrid heating systems specifically, optimal control leads to a higher coverage ratio, while maintaining thermal comfort. It also became clear that in terms of performance, there is little variation between the different configurations of hybrid heating systems when an optimal control strategy is employed.

Finally, general recommendations for schools seeking to reduce their carbon footprint through the implementation of a hybrid heating system were formulated. Schools can achieve the 2030 emission targets by implementing a hybrid heating system with an air-source heat pump sized between 10% and 20% of peak heat demand, alongside the existing natural gas boiler. This approach significantly reduces CO_2 emissions without the need of immediate costly insulation upgrades. The system is cost-effective for schools with limited budgets, and subsidies are available to offset initial investments. This allows schools to spread energy-saving measures in time, paving the way for carbon neutrality in space heating by 2050.

Suggestions for future research

A topic not fully explored in this thesis is the impact of two accessible technologies that might be beneficial for the operation of the hybrid heating system: thermal energy storage and solar panels. The installation of a thermal energy storage system in the form of a hot water tank may result in a larger reduction of annual energy costs or an even larger decrease in CO_2 emissions due to a higher coverage ratio. Similarly, solar panels may be beneficial in certain cases because they provide free and green electricity after installation.

However, the aspect dealt with in this thesis having the most possibilities regarding further research, is optimal control. While constant energy prices were assumed in this thesis, in reality, energy prices fluctuate. By employing optimal control, it is possible to adapt the control strategy based on these variable energy prices, thereby reducing the annual energy cost. Furthermore, the practicalities of implementing an optimal control strategy in a school's hybrid heating system require further investigation. One of the conclusions of the investigation into optimal control was that it allows the heat pump in a hybrid heating system to be sized smaller, while still achieving the same CO_2 emission reduction. However, the exact reduction in

heat pump capacity that leads to the same emission reduction was not determined. This can be investigated by conducting more optimisations using *TACO*, for different heat pump sizes.

This thesis also showed how schools can pave the way to carbon neutrality in space heating by 2050. However, the most cost-effective system design to achieve this goal of carbon neutrality in 2050 was not addressed, leaving room for further investigation.

Appendices

Appendix A

nPro [16]

A.1 Screenshots

A.1.1 Literature research

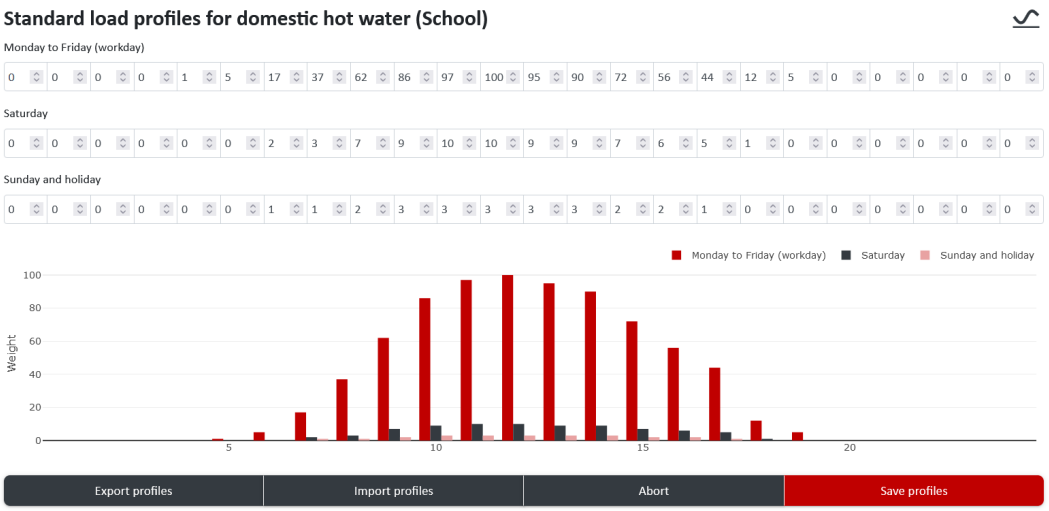

FIGURE A.1: Adapting standard daily load profiles.

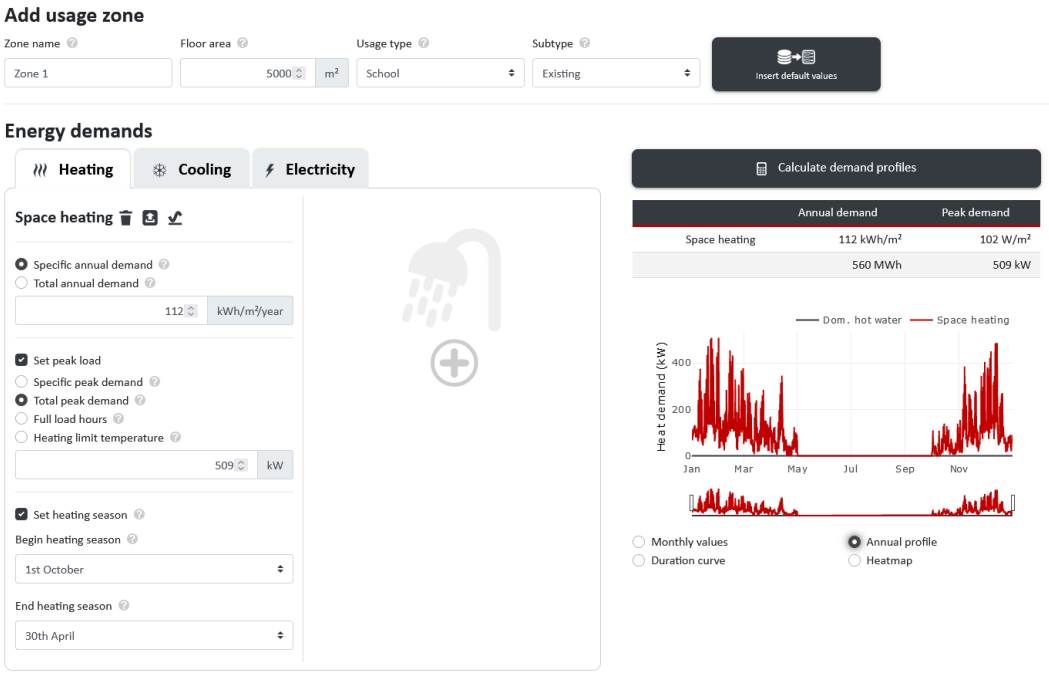

FIGURE A.2: Example of space heating load generation.

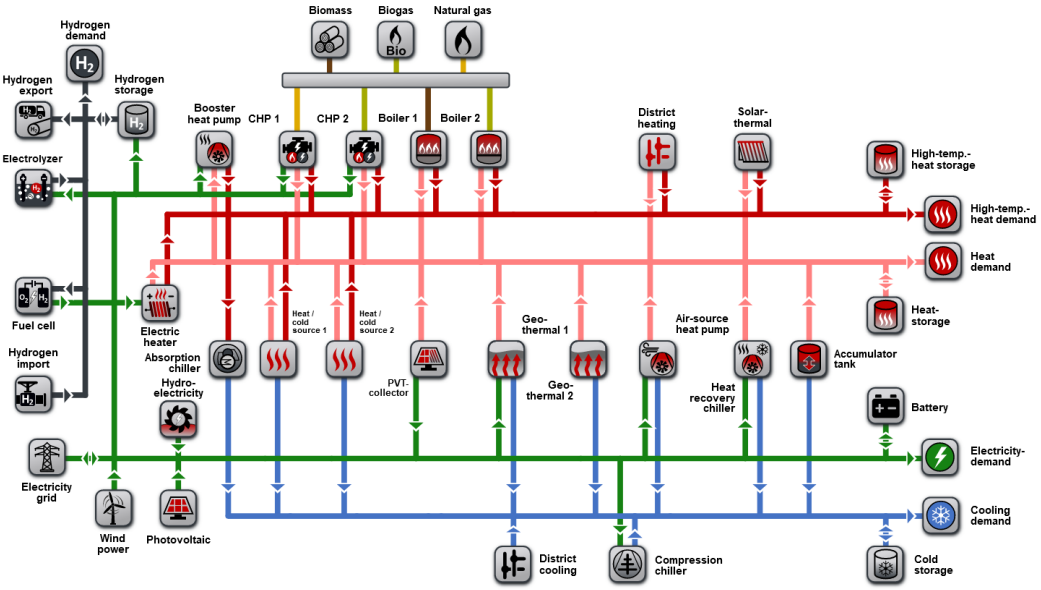

FIGURE A.3: All possible technologies.

System design

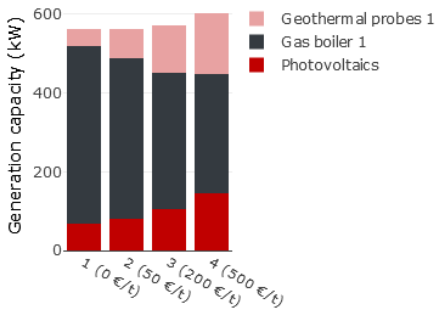

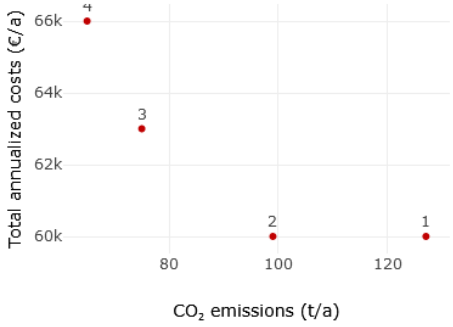

	System 1	System 2	System 3	System 4
CO_2 price	0 €/t	50 €/t	200 €/t	500 €/t
Total annualized costs	ca. 60.000 €/a	ca. 60.000 €/a	ca. 63.000 €/a	ca. 66.000 €/a
Comparison to system 1		+ 0 %	+ 5 %	+ 10 %
CO_2 emissions	ca. 127 t/a	ca. 99 t/a	ca. 75 t/a	ca. 65 t/a
Comparison to system 1		– 22 %	– 41 %	– 49 %
Photovoltaics	67 kW_p / 394 m^2	80 kW_p / 471 m^2	104 kW_p / 612 m^2	145 kW_p / 853 m^2
Gas boiler 1	453 kW_{th}	407 kW_{th}	347 kW_{th}	303 kW_{th}
Geothermal probes 1	42 kW_{th}	76 kW_{th}	121 kW_{th}	154 kW_{th}
Electricity import	ca. 102 MWh/a	ca. 130 MWh/a	ca. 150 MWh/a	ca. 151 MWh/a
Electricity feed-in	ca. 27 MWh/a	ca. 35,2 MWh/a	ca. 53 MWh/a	ca. 86 MWh/a
Natural gas import	ca. 364 MWh/a	ca. 213 MWh/a	ca. 89 MWh/a	ca. 46,9 MWh/a
System selection	○	○	○	○

FIGURE A.4: Example of multi-objective optimisation.

A.1.2 Testing the *nPro* tool

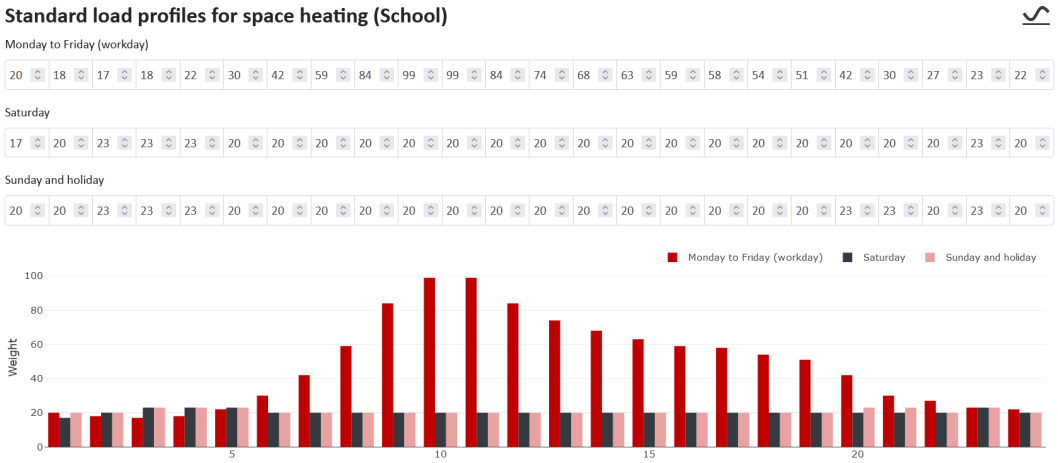

FIGURE A.5: Original (default) normalised day profile of heat demand in school buildings.

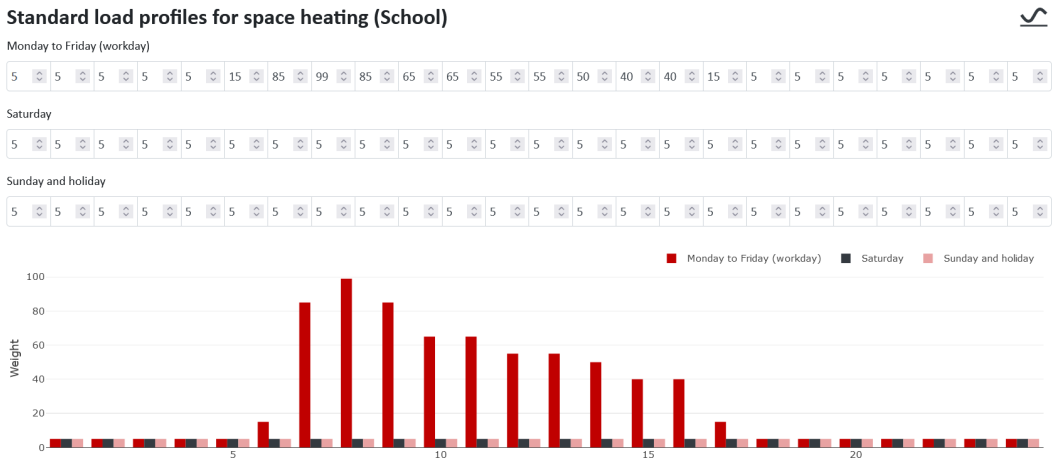

FIGURE A.6: Newly defined normalised day profile of heat demand in school buildings.

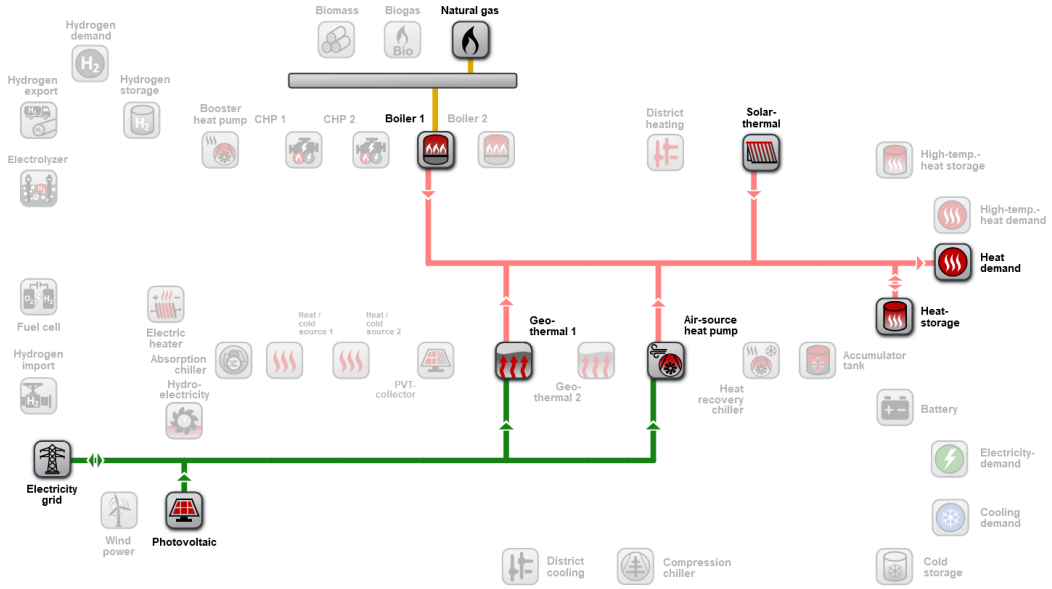

FIGURE A.7: All enabled technologies for the case of building D of UCLL Campus Proximus.

A.2 Input parameters

A.2.1 Gas boiler

For the thermal efficiency, a typical value of 90% is assumed [80]. Only a constant efficiency can be modelled in *nPro*. The fuel type is set to natural gas.

A.2.2 Air-source heat pump

The COP of the air-source heat pump is calculated based on the COP curves of the 'Carrier 30 AW (ASHP)' heat pump type in *nPro*, shown in Figure A.8.

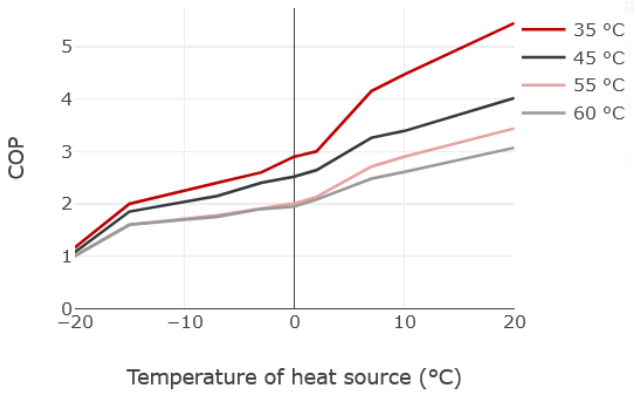

FIGURE A.8: COP curves for 'Carrier 30 AW (ASHP)' as defined in *nPro* [16].

A.2.3 Ground-source heat pump

The COP of the ground-source heat pump is calculated based on the COP curves of the 'Carrier 30 WG (water/brine)' heat pump type in *nPro*, shown in Figure A.9. The extraction temperature is assumed to be 10°C [81].

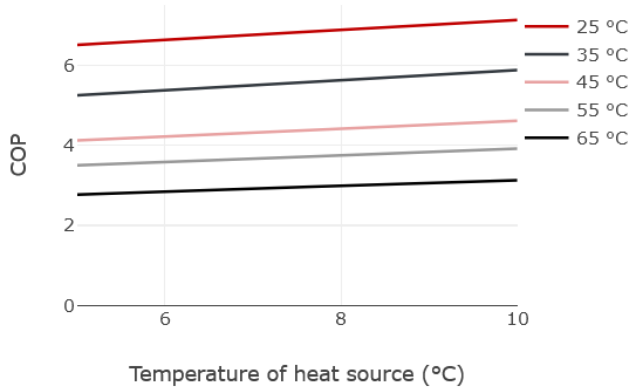

FIGURE A.9: COP curves for 'Carrier 30 WG (water/brine)' as defined in *nPro* [16].

A.2.4 Solar panels

The tilt angle is set to 30°, which is the default value of *nPro*. As the peak heat demand typically happens before noon, having southeast-facing solar panels will maximise self-sufficiency. Therefore, the azimuth is set to −45°. The module type is set to 'Monocrystalline', which makes that the module efficiency equals 21% and the temperature coefficient 0.36 $\frac{\%}{°C}$. The default values of *nPro* for inverter efficiency and system losses are 97% and 14% respectively.

A.2.5 Heat storage

Standby heat losses are assumed to be 20% per five days. The temperature difference between a fully charged and a fully discharged storage is 20 K. Both are default values of *nPro*.

A.2.6 Solar thermal collectors

Tilt angle and azimuth are set to 30° and −45° respectively, as for the solar panels. The collector type is set to 'Flat-plate collector'. The mean collector temperature is assumed to be 70°C, which is the default value of *nPro*.

Appendix B

The school building model

B.1 Model validation

As the school building model used in this thesis is based on the building simulation model described in [37], this paper can assist in validating the model. It is mainly useful for checking orders of magnitude, given that the models are obviously not identical. The heat demand for the baseline scenario defined in this paper has a 95% confidence interval of 49.2 ± 6.9 $\frac{\text{kWh}}{\text{m}^2 \text{ year}}$. The baseline scenario defined in this thesis resulted in a total annual heat demand of 88.3 MWh, which equates to a specific heat demand of 50.44 $\frac{\text{kWh}}{\text{m}^2 \text{ year}}$. This value thus is comparable to the value found in [37]. It should be noted that their baseline scenario assumed an average U-value of the building envelope lower than the 1.00 $\frac{\text{W}}{\text{m}^2 \text{ K}}$ used in the baseline scenario of this thesis. This, of course, results in a reduction in heat demand. However, this effect may be compensated for by their assumption of a simple extraction ventilation system, which leads to an increase in heat demand. Additionally, the authors of [37] assumed the presence of solar shading, blocking 70% of the solar radiation when it exceeds 250 $\frac{\text{W}}{\text{m}^2}$. This can also lead to a significant increase in heat demand, particularly on sunny winter days. It is possible that other minor differences exist between both building models, but it can be concluded that the order of magnitude of the total heat demand is accurate.

In the case study by Stocker et al. [82], eight primary schools in the Alps were investigated. The floor area of these schools ranged from 787 m^2 to 6 090 m^2, the window-to-wall ratio from 18% to 42% and the construction period from 1919 to 1990. The specific annual heat demand varied from 68.5 $\frac{\text{kWh}}{\text{m}^2 \text{ year}}$ for one of the most recently constructed buildings to 133.2 $\frac{\text{kWh}}{\text{m}^2 \text{ year}}$ for one of the oldest buildings. These values are more than the 50.44 $\frac{\text{kWh}}{\text{m}^2 \text{ year}}$ of the baseline scenario of the modelled school building in this thesis. The difference can be attributed to the colder climate in the Alps, where the amount of heating degree-days typically is between 4 000 and 5 500, while between between 2 500 and 4 000 in Belgium [83].

Figure B.1 illustrates the typical heat demand profile of a week in winter for the modelled school building. The morning peak in heat demand is clearly visible, as the setpoint temperature suddenly increases. Furthermore, the heat demand on

Wednesday is lower than on the other weekdays, due to the imposed temperature setpoint profile. The shape of the daily heat demand profiles is comparable to those found in [43] and [44]. The small peaks observed during the different nights are the result of the on/off-strategy employed during unoccupied periods. These peaks specifically are due to the heating of zone 12 (gym), which is the zone with the largest external wall area and the only zone whose temperature falls below 14°C in this specific period.

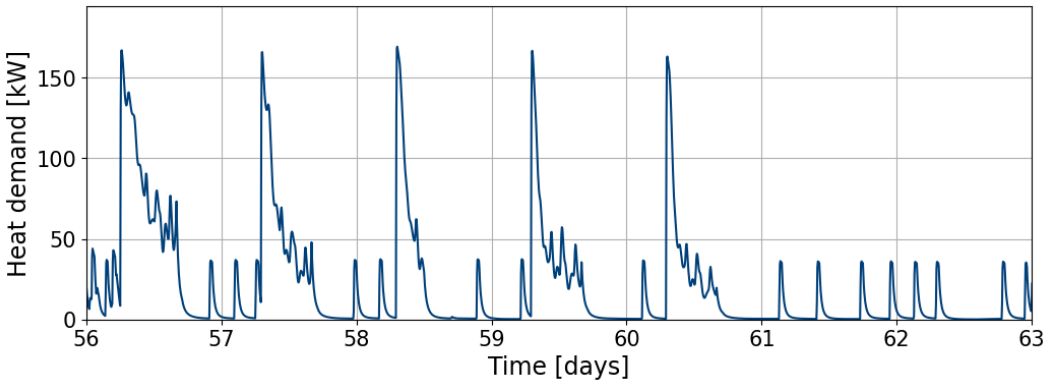

Figure B.1: Typical heat demand during a week in winter.

Figure B.2 shows the average daily heat demand profile. The times of day when most zones are occupied are shaded. During these times, the heat demand decreases due to the internal gains from the occupants.

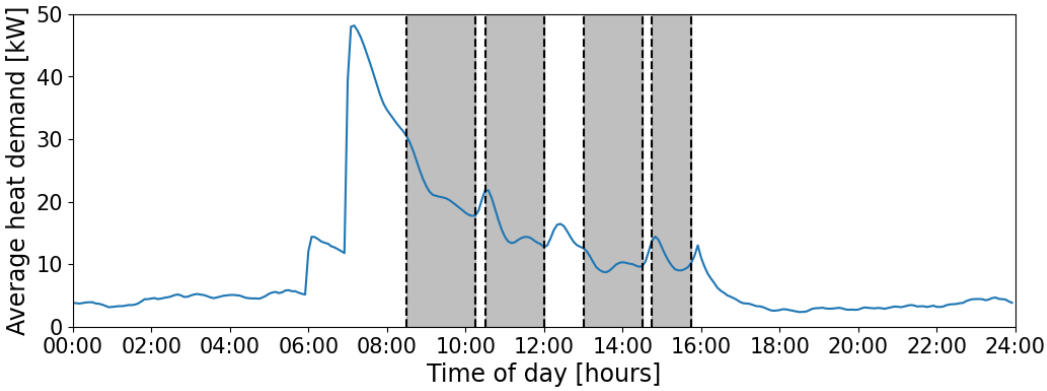

Figure B.2: Average daily heat demand and occupancy schedule.

Figure B.3 presents two two-week temperature profiles of zone 12 (gym), with the initial zone temperature set to 20°C. The profile of the global horizontal solar irradiance for the same period is also shown. The school building is oriented so that the short external wall of zone 12 faces south. In the 'With windows' case, the zone has one window on each external wall. Each window has a height of 1.55 m and a width equal to 68% of the width of the external wall in which it is located. In the

'Without windows' case, zone 12 has no windows. The number of occupants is set to zero in both cases. Initially, the temperature in zone 12 decreases more rapidly in the 'With windows' case, due to the higher U-value of the windows in comparison to the wall itself. However, during the day, the temperature in zone 12 rises due to the solar gains. In the 'Without windows' case, no solar gains occur.

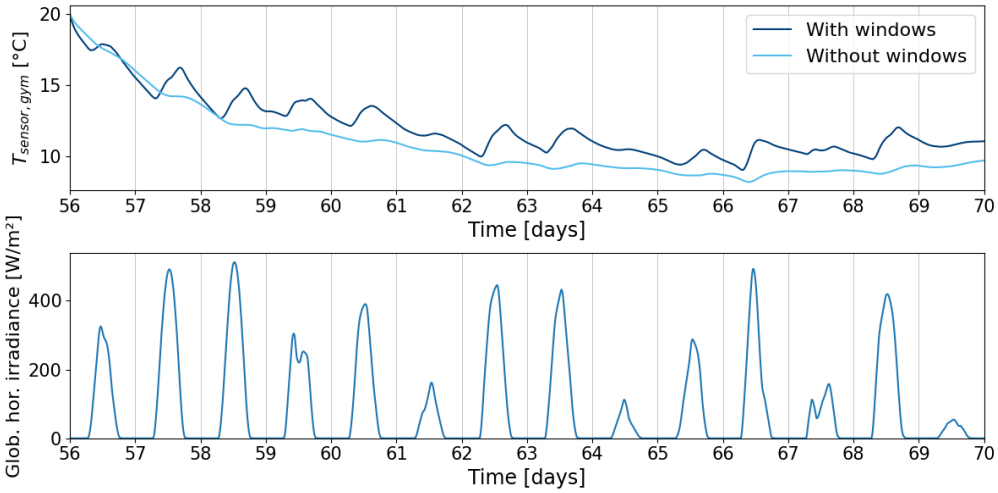

FIGURE B.3: Temperature profile of zone 12 and global horizontal irradiance.

It can thus be assumed that the effects of internal gains due to occupancy and solar gains through windows have been modelled correctly.

B.2 Building architecture

General building data	
Front façade length	84.00 m
Side façade length	13.80 m
Zone height	2.80 m
Total floor area	2 052.06 m^2
Total heated area	1 751.28 m^2
Total building volume	6 491.52 m^3
Building envelope surface area	
Roof	1 159.20 m^2
Floor	1 159.20 m^2
External wall	1 095.36 m^2
Total	3 413.76 m^2
Surface area to volume ratio	0.53 m^{-1}

TABLE B.1: Architectural properties of the modelled school building.

B.3 *Modelica* representation of building model

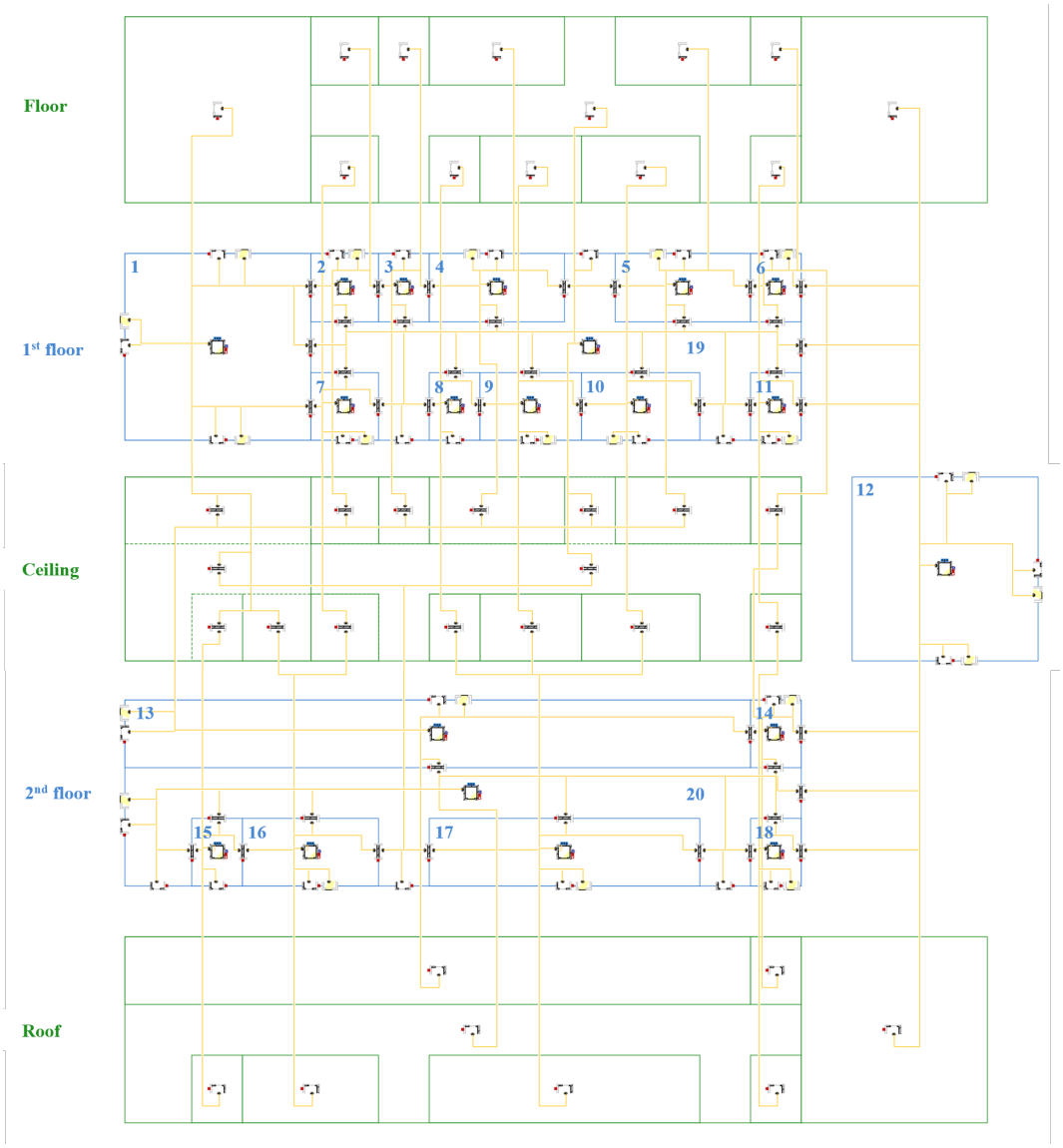

Figure B.4: Graphical *Modelica* representation of the school building model.

B.4 Building envelope

Construction	Material per layer	Thickness d [cm]
External wall	PUR	d_{PUR}
	Brickwork	14
	Plaster finish	1
Internal wall	Plaster finish	1
	Brickwork	14
	Plaster finish	1
Floor	Bitumen	0.2
	Heavy concrete	15
	PUR	d_{PUR}
	Light concrete	10
	Tiles	1
Ceiling	Hollow core concrete slab	12
	Heavy concrete	4
	PUR	3
	Chape	10
	Tiles	2
Roof	Bitumen	0.2
	PUR	d_{PUR}
	Light concrete	10
	Heavy concrete	15
	Plaster finish	1

TABLE B.2: Constructions used in school building model [37].

Material	Density ρ [kg/m^3]	Thermal conductivity k [W/(m K)]	Specific heat capacity c [J/(kg K)]
PUR	30	0.03	1400
Brickwork	1550	0.54	1000
Plaster finish	1300	0.52	1000
Bitumen	1100	0.23	1000
Heavy concrete	2400	1.70	1000
Light concrete	1050	0.32	1000
Tiles	2300	1.20	840
Hollow core concrete slab	1500	0.92	840
Chape	1000	1.35	840

TABLE B.3: Thermodynamic properties of used materials [37].

B.5 Occupancy data

B.5.1 Occupancy schedules

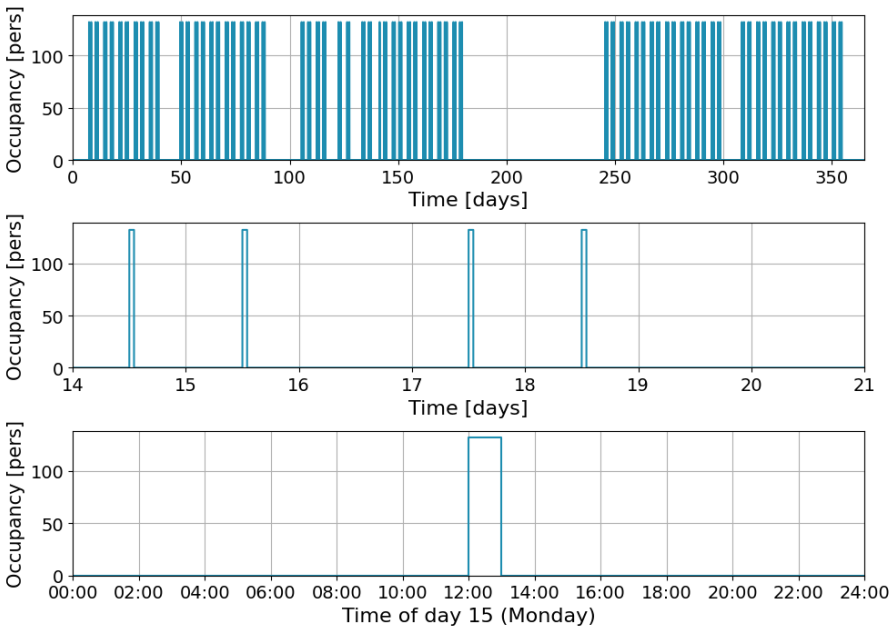

Figure B.5: Year, week and day occupancy schedule of zone 1 (canteen).

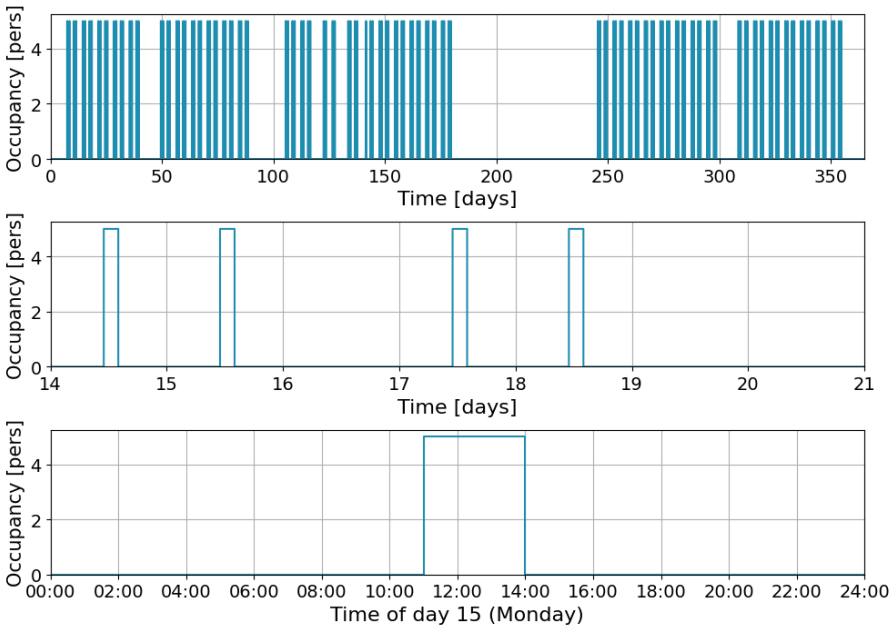

Figure B.6: Year, week and day occupancy schedule of zone 2 (kitchen).

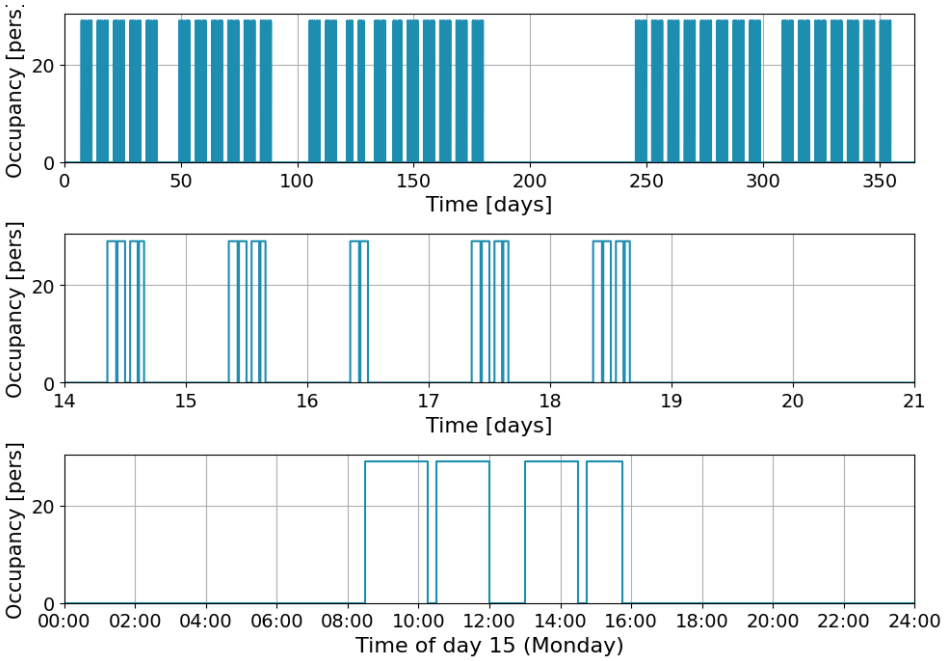

FIGURE B.7: Year, week and day occupancy schedule of zone 4 (classroom).

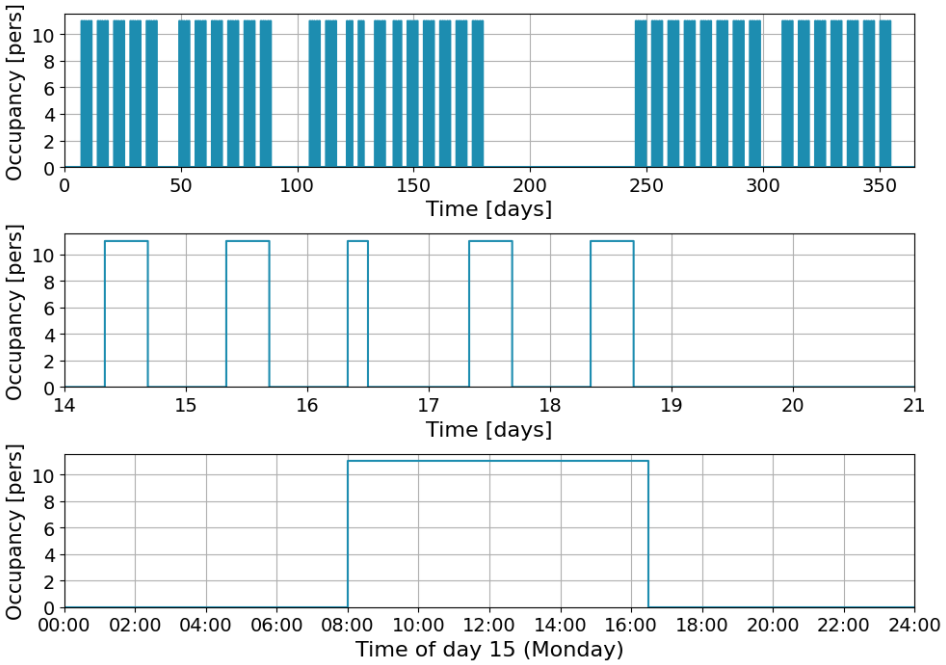

FIGURE B.8: Year, week and day occupancy schedule of zone 9 (teachers' room).

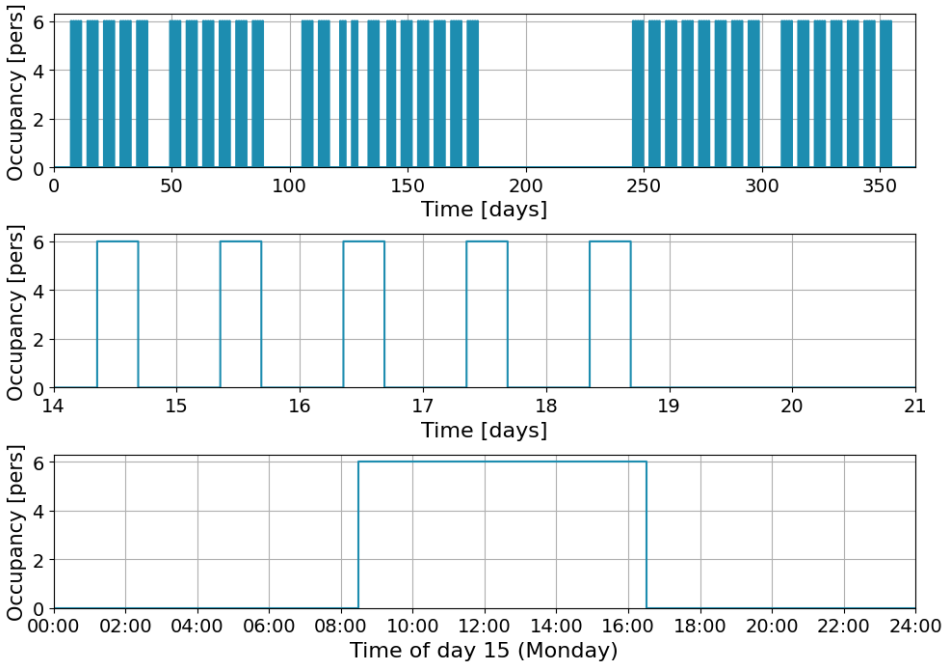

Figure B.9: Year, week and day occupancy schedule of zone 10 (office).

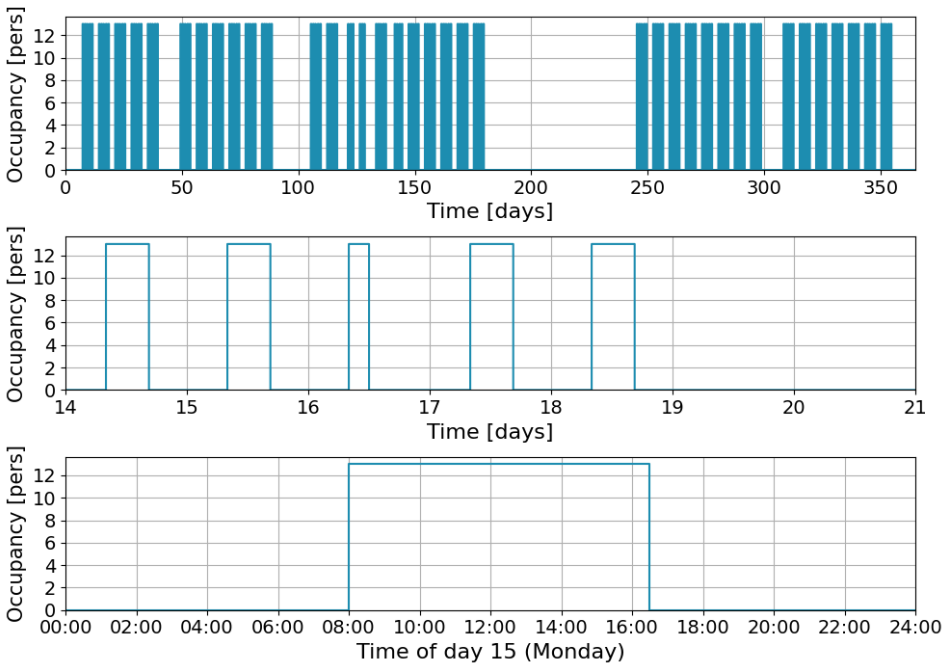

Figure B.10: Year, week and day occupancy schedule of zones 19 and 20 (hallways).

B.5.2 Temperature setpoint schedules

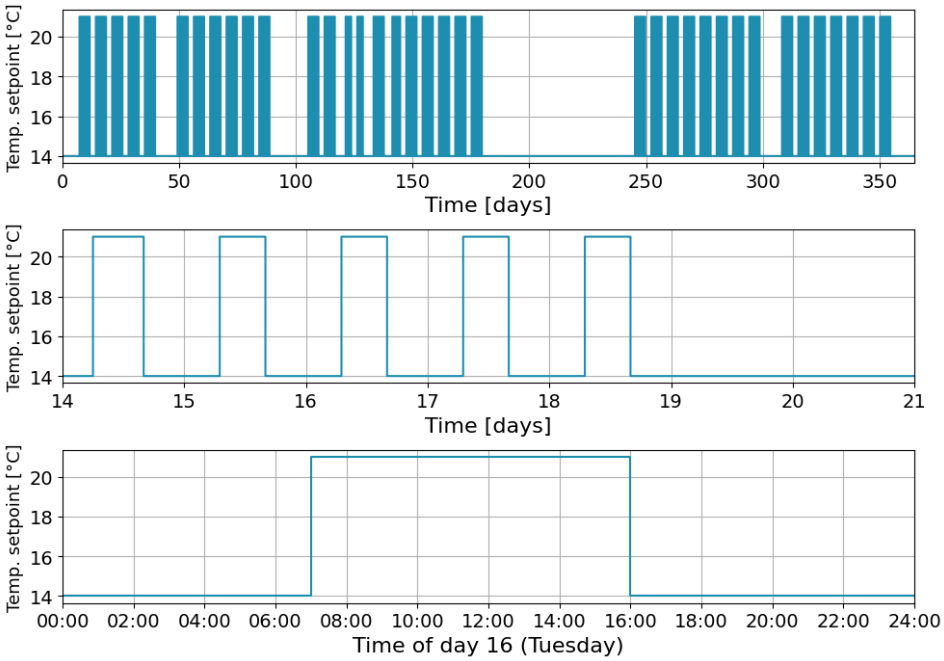

FIGURE B.11: Year, week and day setpoint schedule of zone 10 (office).

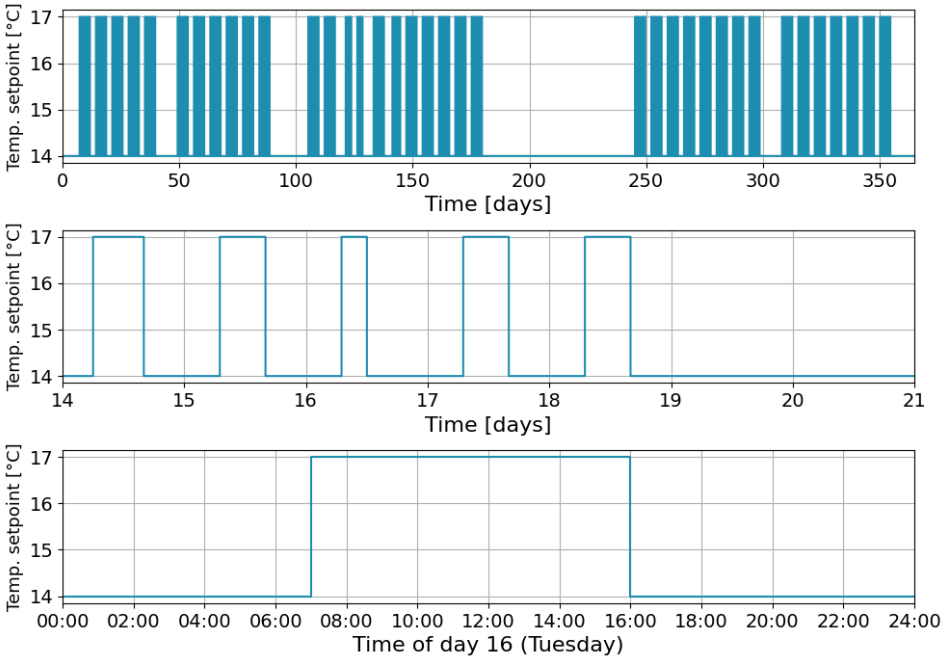

FIGURE B.12: Year, week and day setpoint schedule of zone 12 (gym).

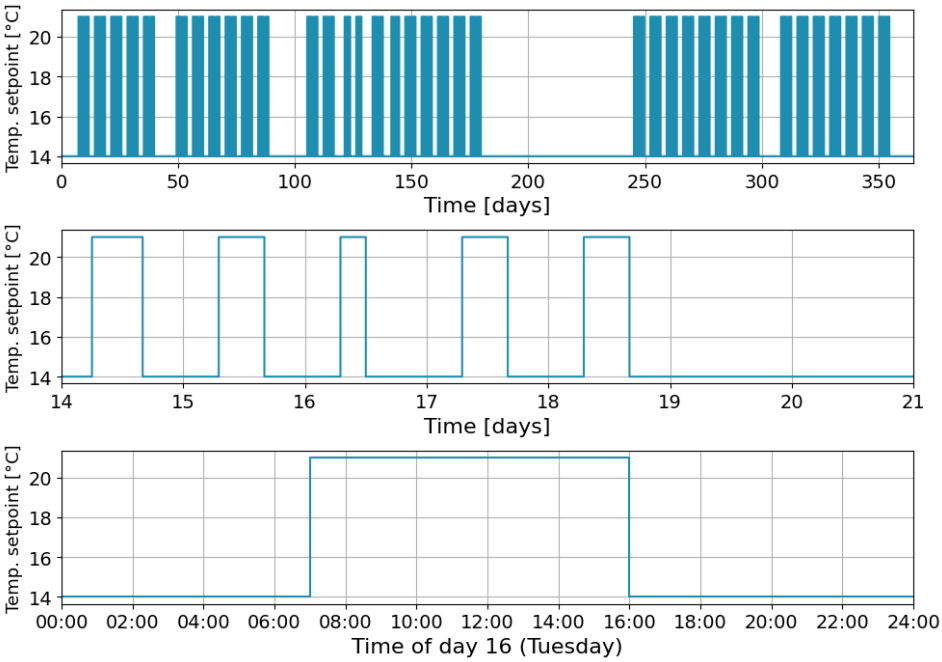

Figure B.13: Year, week and day setpoint schedule of all other zones.

B.6 Nominal pressure rise of pumps

The calculation of the nominal pressure rise of each pump is shown in Table B.4. The last column shows the value to which `dp_nominal` of the pump component in *Modelica* is set. It is the sum of a share of the nominal pressure rise of the heater ($\Delta P_{hea,nom}$) and the nominal pressure rise of the corresponding TRV and radiator(s) ($\Delta P_{TRV,nom}$ and $\Delta P_{rad,nom}$).

The total nominal pressure difference over the heater is assumed to be 40 kPa, which is the typical order of magnitude for larger boilers[†]. One tenth of this value (so 4 kPa) is attributed to the nominal pressure rise of each pump, because there will always be multiple pumps working at the same time.

The nominal pressure drop of each TRV (when fully open) is chosen to be 10 kPa, also a typical value[‡].

The nominal pressure drop of one radiator is chosen to be 1.5 kPa, as explained in [84]. The amount of radiators in each zone is chosen based on the size of the zone.

The parameter `dpValve_nominal` parameter of each `TwoWayTRV` component is set equal to $\Delta P_{TRV,nom}$. The `dpFixed_nominal` parameter is set equal to the sum of $\Delta P_{hea,nom}$ and $\Delta P_{rad,nom}$. These pressure drops are not defined in the `Heater_T` and `RadiatorEN442_2` components because this could lead to flow reversal issues.

Zone	$\Delta P_{hea,nom}$ [Pa]	$\Delta P_{TRV,nom}$ [Pa]	$\Delta P_{rad,nom}$ [Pa]	$\Delta P_{pum,nom}$ [Pa]
1	4 000	10 000	$3 \cdot 1\,500$	18 500
2	4 000	10 000	$1 \cdot 1\,500$	15 500
3	4 000	10 000	$1 \cdot 1\,500$	15 500
4	4 000	10 000	$2 \cdot 1\,500$	17 000
5	4 000	10 000	$2 \cdot 1\,500$	17 000
6	4 000	10 000	$1 \cdot 1\,500$	15 500
7	4 000	10 000	$1 \cdot 1\,500$	15 500
8	4 000	10 000	$1 \cdot 1\,500$	15 500
9	4 000	10 000	$1 \cdot 1\,500$	15 500
10	4 000	10 000	$2 \cdot 1\,500$	17 000
11	4 000	10 000	$1 \cdot 1\,500$	15 500
12	4 000	10 000	$4 \cdot 1\,500$	20 000
13	4 000	10 000	$4 \cdot 1\,500$	20 000
14	4 000	10 000	$1 \cdot 1\,500$	15 500
15	4 000	10 000	$1 \cdot 1\,500$	15 500
16	4 000	10 000	$2 \cdot 1\,500$	17 000
17	4 000	10 000	$3 \cdot 1\,500$	18 500
18	4 000	10 000	$1 \cdot 1\,500$	15 500

TABLE B.4: Calculation of nominal pressure rise of each pump.

[†]This is for example the case for the *Evomod* boilers of *Ideal Heating Commercial*, see: https://idealcommercialboilers.com/products/evomod.

[‡]For example, see: http://brunata.gr/fileadmin/datasheets/UK/UK-QB101162.pdf.

Appendix C

The impact of optimal control

C.1 Heating system models

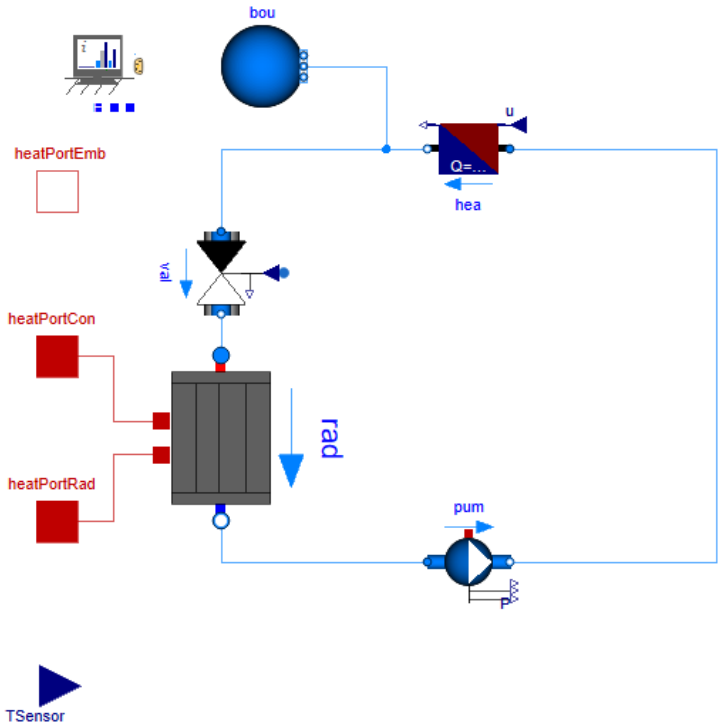

FIGURE C.1: *Modelica* heating system model in the case of optimal control of a gas-fired heating system.

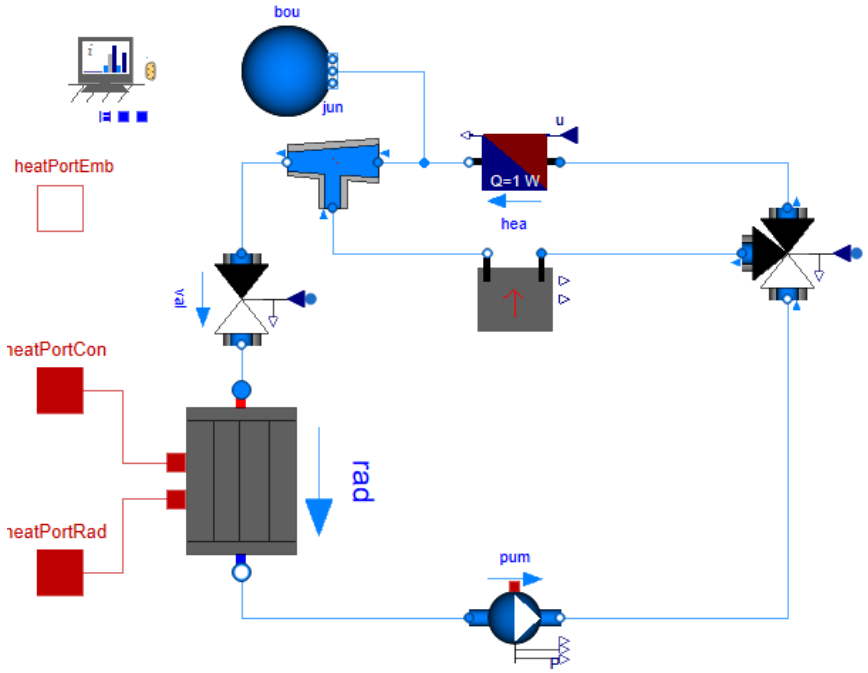

Figure C.2: *Modelica* heating system model in the case of optimal control of a series hybrid heating system.

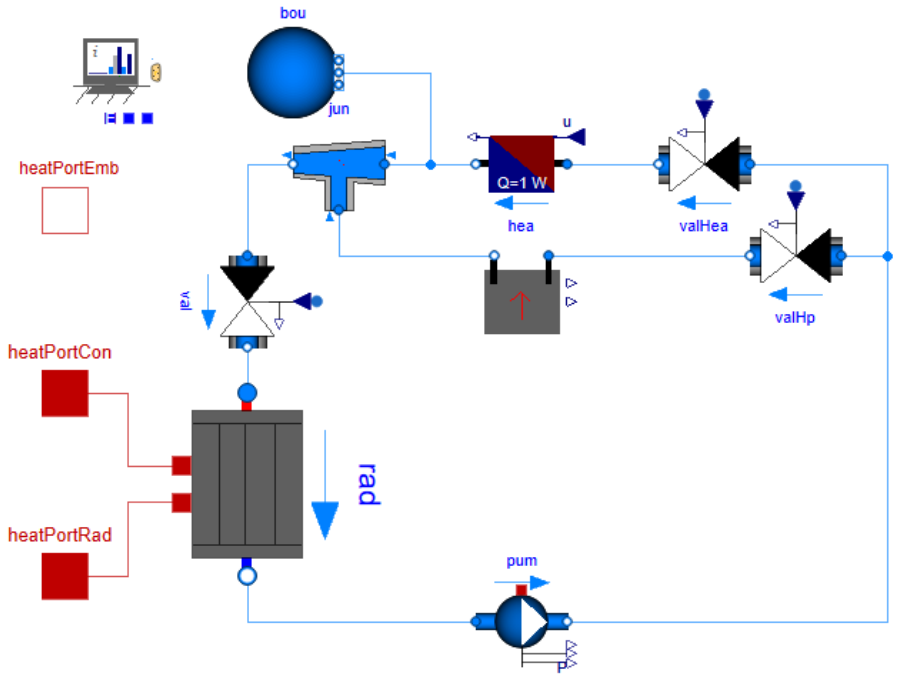

Figure C.3: *Modelica* heating system model in the case of optimal control of a parallel hybrid heating system with two two-way valves.

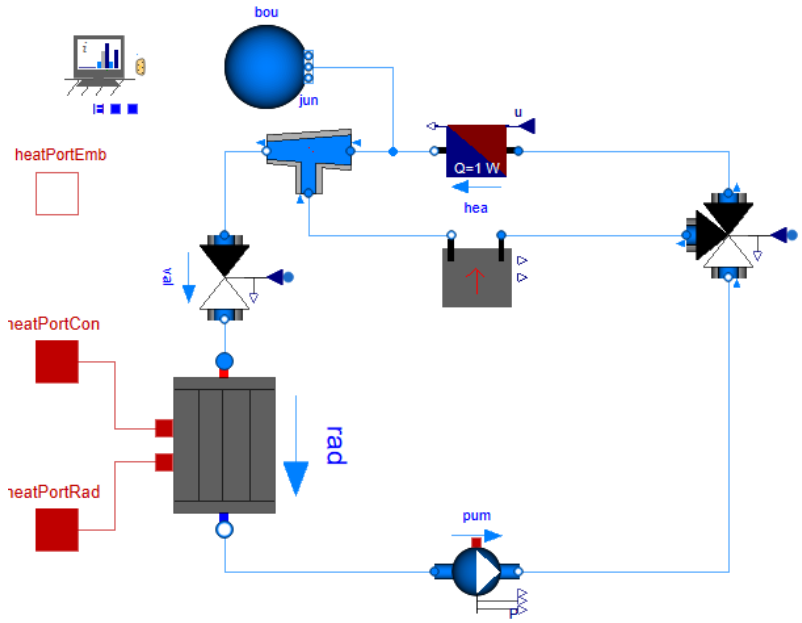

FIGURE C.4: *Modelica* heating system model in the case of optimal control of a parallel hybrid heating system with a three-way valve.

C.2 Heat pump model equations

The equations found in this section are based on the PhD thesis of Filip Jorissen [85].

Based on the COP curves of Figure A.8, the COP of the heat pump is assumed to be:

$$\begin{aligned} COP(t) &= c_1 + c_2 \cdot (T_{con,out}(t) - c_3) + c_4 \cdot (T_{eva,out}(t) - c_5) \\ &= 4 - 0.08 \, \frac{1}{^\circ\text{C}} \cdot (T_{con,out}(t) - 35^\circ\text{C}) - 0.08 \, \frac{1}{^\circ\text{C}} \cdot (T_{eva,out}(t) - 2^\circ\text{C}) \,, \end{aligned} \tag{C.1}$$

where $T_{con,out}(t)$ is the temperature at the outlet of the condenser, and $T_{eva,out}(t)$ is the temperature at the outlet of the evaporator, which is assumed to be 5°C more than the temperature of the inlet of the evaporator. This COP is used to calculate the electrical power consumption $P_{el}(t)$ of the heat pump as:

$$P_{el}(t) = \frac{\dot{Q}_{con}(t)}{COP(t)}, \tag{C.2}$$

where $\dot{Q}_{con}(t)$ is the heat flow rate at the condenser, so the output of the heat pump. This heat flow rate depends on different parameters:

$$\dot{Q}_{con}(t) = \dot{m}_{con}(t) \cdot c_p \cdot mod(t) \cdot \Delta T_{con,max}, \tag{C.3}$$

where $\dot{m}_{con}(t)$ is the mass flow rate through the condenser, c_p is the specific heat capacity of water and $mod(t)$ is the modulation of the heat pump (which always has a value between zero and one). $\Delta T_{con,max}$ is a parameter depending on the nominal conditions:

$$\begin{aligned} \Delta T_{con,max} &= \frac{\dot{Q}_{con,nom}}{\dot{m}_{con} \cdot c_p} \\ &= T_{sup,nom} - T_{ret,nom} \\ &= T_{con,out,nom} - T_{con,in,nom}. \end{aligned} \tag{C.4}$$

The nominal mass flow rate through the condenser is set equal to the sum of the nominal mass flow rates of all radiators in the modelled school building heating system. In the analysis of Chapter 7, $\dot{Q}_{con,nom}$ is always assumed to be 20 kW.

C.3 Optimal control of hybrid heating system

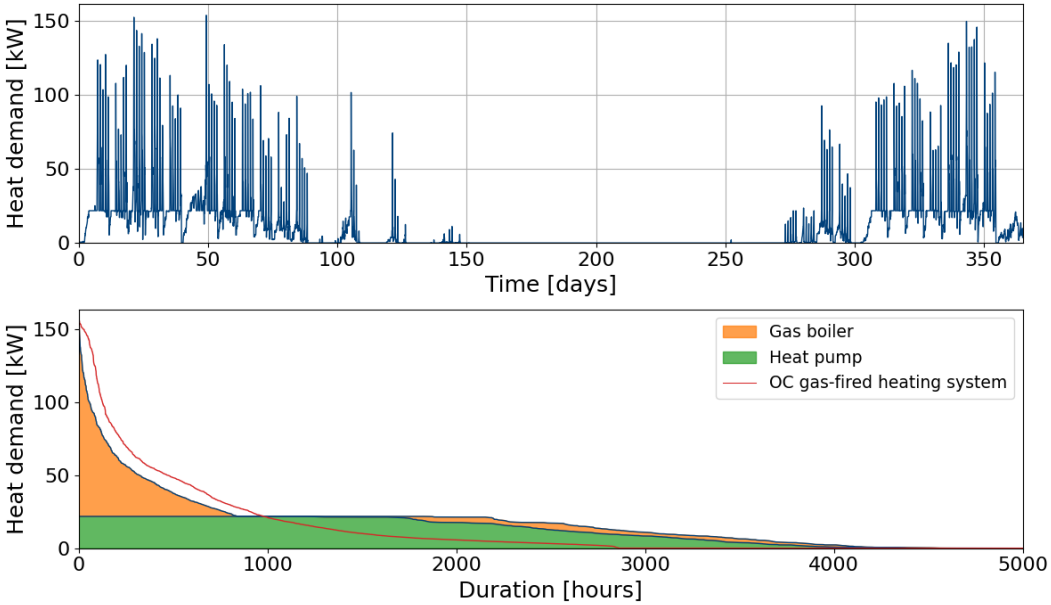

Figure C.5: Results for optimal control of a parallel hybrid heating system (with two two-way valves) consisting of a natural gas boiler of 160 kW and a heat pump of 20 kW.

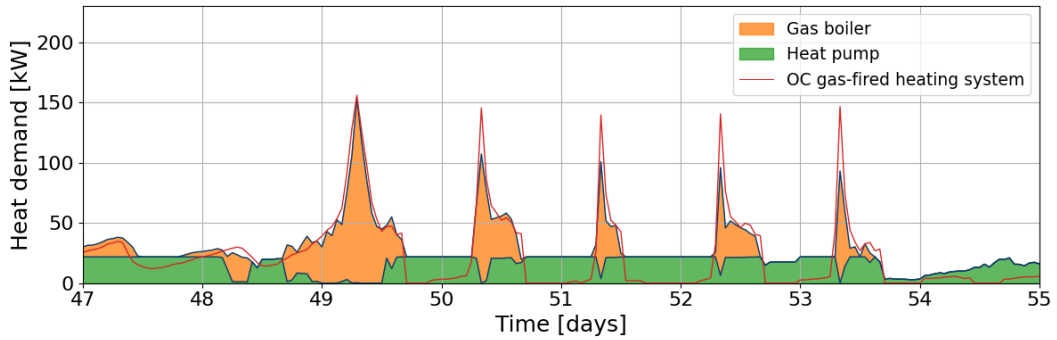

FIGURE C.6: Heat demand profile, for an eight-day period, of optimal control of gas-fired heating system and optimal control of parallel hybrid heating system (with two two-way valves).

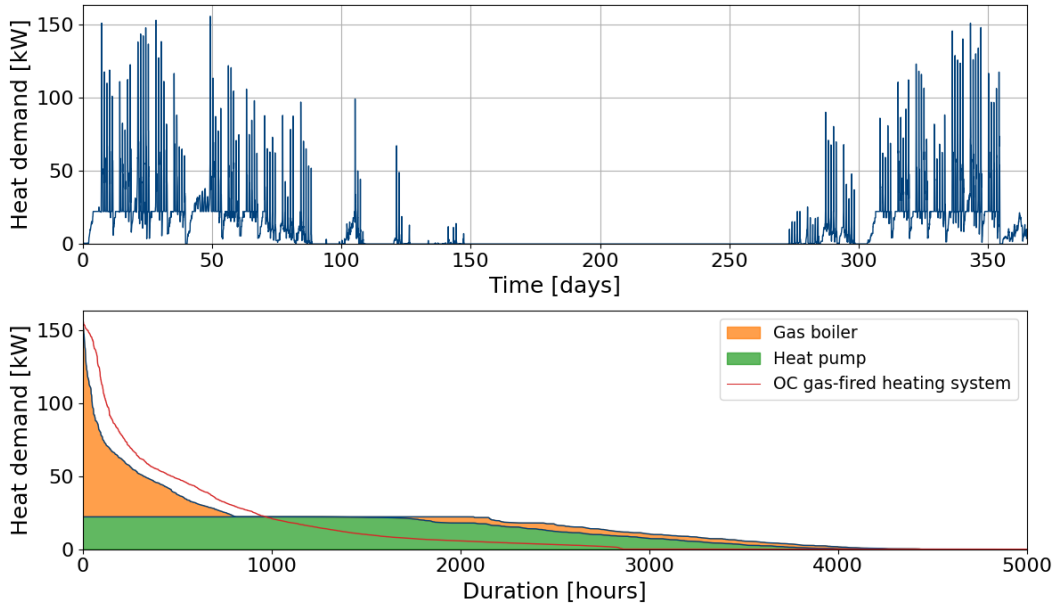

FIGURE C.7: Results for optimal control of a parallel hybrid heating system (with one three-way valve) consisting of a natural gas boiler of 160 kW and a heat pump of 20 kW.

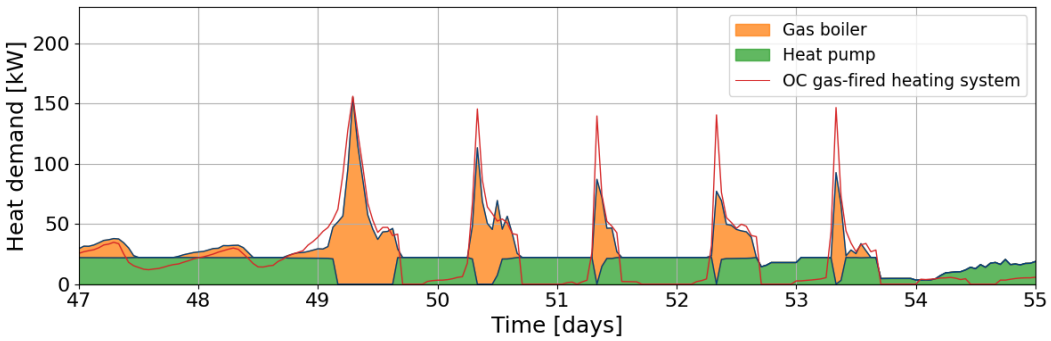

Figure C.8: Heat demand profile, for an eight-day period, of optimal control of gas-fired heating system and optimal control of parallel hybrid heating system (with one three-way valve).

Bibliography

[1] United Nations Framework Convention on Climate Change (UN FCCC), "Report of the Conference of the Parties on its twenty-first session, held in Paris from 30 November to 13 December 2015," United Nations, Tech. Rep., 2016.

[2] J. Rogelj, D. Shindell, K. Jiang, S. Fifita, P. Forster, V. Ginzburg, C. Handa, H. Kheshgi, S. Kobayashi, E. Kriegler, L. Mundaca, R. Seferian, and M. Vilarino, *Mitigation Pathways Compatible with 1.5°C in the Context of Sustainable Development*. Cambridge University Press, 2018, pp. 93–174, DOI: 10.1017/9781009157940.004.

[3] Vlaamse Milieumaatschappij, "Totale broeikasgasuitstoot per gas (ETS en ESR)," 8 2023. [Online]. Available: https://www.vmm.be/klimaat/totale-broeikasgasuitstoot-ETS-ESR

[4] Vlaams Energie- & Klimaatagentschap, "Vlaams Energie- en Klimaatplan (VEKP) 2021-2030," 2023. [Online]. Available: https://www.vlaanderen.be/veka/energie-en-klimaatbeleid/vlaams-energie-en-klimaatplan-vekp-2021-2030#publicaties

[5] Vlaamse Regering, "Vlaamse klimaatstrategie 2050," 12 2019. [Online]. Available: https://www.vlaanderen.be/publicaties/vlaamse-klimaatstrategie-2050

[6] European Environment Agency, "Greenhouse gas emissions from energy use in buildings in Europe," 10 2023. [Online]. Available: https://www.eea.europa.eu/en/analysis/indicators/greenhouse-gas-emissions-from-energy

[7] Eurostat, "Heating and cooling from renewables gradually increasing," 2 2023. [Online]. Available: https://ec.europa.eu/eurostat/web/products-eurostat-news/w/DDN-20230203-1

[8] Agentschap voor Infrastructuur in het Onderwijs (AGION), "Schoolgebouwenmonitor 2018-2019: Indicatoren voor de kwaliteit van de schoolgebouwen in Vlaanderen," Tech. Rep., 2020.

[9] J. Packroff, "New EU scheme could hike petrol, gas prices higher than expected key lawmakers admit," May 2024, last accessed on 17.05.2024. [Online]. Available: https://www.euractiv.com/section/emissions-trading-scheme/ne

ws/new-eu-scheme-could-hike-petrol-gas-prices-higher-than-expected-key-lawmakers-admit/

[10] M. Beccali, M. Bonomolo, F. Martorana, P. Catrini, and A. Buscemi, "Electrical hybrid heat pumps assisted by natural gas boilers: A review," *Applied Energy*, vol. 322, 2022, DOI: 10.1016/j.apenergy.2022.119466.

[11] Heat Pump Centre, "Final Report for HPT TCP Annex 45 - Hybrid Heat Pumps," 10 2019. [Online]. Available: https://heatpumpingtechnologies.org/publications/hybrid-heat-pumps-final-report/

[12] F. Decock, "Zomercomfort in Schoolgebouwen," Aug 2022, last accessed on 06.03.2024. [Online]. Available: https://www.nav.be/artikel/2384/zomercomfort-in-schoolgebouwen/

[13] A. Poulin, M. Dostie, M. Fournier, and S. Sansregret, "Load duration curve: A tool for technico-economic analysis of energy solutions," *Energy and buildings*, vol. 40, no. 1, pp. 29–35, 2008, DOI: 10.1016/j.enbuild.2007.01.020.

[14] M. Sun, P. Djapic, M. Aunedi, D. Pudjianto, and G. Strbac, "Benefits of smart control of hybrid heat pumps: An analysis of field trial data," *Applied energy*, vol. 247, pp. 525–536, 2019, DOI: 10.1016/j.apenergy.2019.04.068.

[15] T. Berthou, P. Stabat, R. Salvazet, and D. Marchio, "Optimal control for building heating: An elementary school case study," in *Proceedings of BS2013: 13th Conference of International Building Performance Simulation Association, Chambéry, France*, 2013, pp. 1944–1951.

[16] "nPro - District Energy Planning Tool," last accessed on 02.06.2024. [Online]. Available: https://www.npro.energy

[17] F. Jorissen, W. Boydens, and L. Helsen, "TACO, an automated toolchain for model predictive control of building systems: implementation and verification," *Journal of building performance simulation*, vol. 12, no. 2, pp. 180–192, 2019, DOI: 10.1080/19401493.2018.1498537.

[18] Element Energy Limited, "Hybrid Heat Pumps, Final report for Department for Business, Energy & Industrial Strategy," Suite 1, Bishop Bateman Court, Thompson's Lane, Cambridge, Tech. Rep., 12 2017. [Online]. Available: https://www.gov.uk/government/publications/hybrid-heat-pumps-study

[19] C. O. Suong and A. Asanakham, "Evaluation of a single stage heat pump performance by figure of merit (FOM)," *Energy Reports*, vol. 6, pp. 2735–2742, 2020, DOI: 10.1016/j.egyr.2020.09.038.

[20] I. Staffell, D. Brett, N. Brandon, and A. Hawkes, "A review of domestic heat pumps," *Energy & Environmental Science*, vol. 5, no. 11, pp. 9291–9306, 2012, DOI: 10.1039/c2ee22653g.

[21] G. Bagarella, R. Lazzarin, and M. Noro, "Annual simulation, energy and economic analysis of hybrid heat pump systems for residential buildings," *Applied Thermal Engineering*, vol. 99, pp. 485–494, 2016, DOI: 10.1016/j.applthermaleng.2016.01.089.

[22] A. S. Gaur, D. Z. Fitiwi, and J. Curtis, "Heat pumps and our low-carbon future: A comprehensive review," *Energy Research & Social Science*, vol. 71, 2021, DOI: 10.1016/j.erss.2020.101764.

[23] K. Klein, K. Huchtemann, and D. Müller, "Numerical study on hybrid heat pump systems in existing buildings," *Energy and buildings*, vol. 69, pp. 193–201, 2014, DOI: 10.1016/j.enbuild.2013.10.032.

[24] E. Roccatello, A. Prada, P. Baggio, and M. Baratieri, "Analysis of the influence of control strategy and heating loads on the performance of hybrid heat pump systems for residential buildings," *Energies*, vol. 15, no. 3, 2022, DOI: 10.3390/en15030732.

[25] M. Lee, D. Cha, S. Yun, S.-M. Yoon, and Y. Kim, "Comparative heating performance evaluation of hybrid ground-source heat pumps using serial and parallel configurations with the application of ground heat exchanger," *Energy conversion and management*, vol. 229, 2021, DOI: 10.1016/j.enconman.2020.113743.

[26] H. Park, J. S. Lee, W. Kim, and Y. Kim, "The cooling seasonal performance factor of a hybrid ground-source heat pump with parallel and serial configurations," *Applied energy*, vol. 102, pp. 877–884, 2013, DOI: 10.1016/j.apenergy.2012.09.035.

[27] J. Jansen, F. Jorissen, and L. Helsen, "Optimal control of a fourth generation district heating network using an integrated non-linear model predictive controller," *Applied Thermal Engineering*, vol. 223, 2023, DOI: 10.1016/j.applthermaleng.2023.120030.

[28] R. De Coninck and L. Helsen, "Practical implementation and evaluation of model predictive control for an office building in Brussels," *Energy and Buildings*, vol. 111, pp. 290–298, 2016, DOI: 10.1016/j.enbuild.2015.11.014.

[29] K. Allaerts, J. Al Koussa, J. Desmedt, and R. Salenbien, "Improving the energy efficiency of ground-source heat pump systems in heating dominated school buildings: A case study in Belgium," *Energy and Buildings*, vol. 138, pp. 559–568, 2017.

[30] M. Dongellini, C. Naldi, and G. L. Morini, "Influence of sizing strategy and control rules on the energy saving potential of heat pump hybrid systems in a residential building," *Energy Conversion and Management*, vol. 235, 2021, DOI: 10.1016/j.enconman.2021.114022.

[31] A. Meessens, W. Peere, L. Verleyen, F. Maertens, L. Helsen, and W. Boydens, "Micro energy communities: collective residential heating system retrofits for carbon emission abatement," 2021, Master's thesis.

[32] J. Zimny, P. Michalak, and K. Szczotka, "The energy efficiency of a school building hybrid heating system with a heat pump. A case study," *Rynek Energii*, vol. 2012, pp. 144–152, 2012.

[33] M. N. Todorović, M. J. Banjac, T. S. Bajc, and M. R. Ristanović, "Achieving savings by implementation of efficient hybrid heating systems," *Thermal Science*, vol. 23, no. Suppl. 5, pp. 1683–1693, 2019, DOI: 10.2298/TSCI180726176T.

[34] D. Picard, "Modeling, optimal control and HVAC design of large buildings using ground source heat pump systems," 2017, PhD thesis.

[35] D. Etheridge, "Ventilation, air quality and airtightness in buildings," in *Materials for energy efficiency and thermal comfort in buildings*. Elsevier, 2010, pp. 77–100, DOI: 10.1533/9781845699277.1.77.

[36] A. V. Pasos, X. Zheng, L. Smith, and C. Wood, "Estimation of the infiltration rate of UK homes with the divide-by-20 rule and its comparison with site measurements," *Building and Environment*, vol. 185, 2020.

[37] B. Wauman, D. Saelens, and H. Breesch, "The definition of representative boundary conditions for Flemish schools for use in energy assessment methods," *Energy and Buildings*, vol. 87, pp. 1–13, 2015, DOI: 10.1016/j.enbuild.2014.10.033.

[38] D. Hawkins, S.-M. Hong, R. Raslan, D. Mumovic, and S. Hanna, "Determinants of energy use in UK higher education buildings using statistical and artificial neural network methods," *International Journal of Sustainable Built Environment*, vol. 1, no. 1, pp. 50–63, 2012, DOI: 10.1016/j.ijsbe.2012.05.002.

[39] S. Alghamdi, W. Tang, S. Kanjanabootra, and D. Alterman, "Effect of architectural building design parameters on thermal comfort and energy consumption in higher education buildings," *Buildings*, vol. 12, no. 3, 2022, DOI: 10.3390/buildings12030329.

[40] S. Mohamed, R. Smith, L. Rodrigues, S. Omer, and J. Calautit, "The correlation of energy performance and building age in UK schools," *Journal of Building Engineering*, vol. 43, 2021, DOI: 10.1016/j.jobe.2021.103141.

[41] A. Albatayneh, D. Alterman, A. Page, and B. Moghtaderi, "The significance of the orientation on the overall buildings thermal performance-case study in Australia," *Energy procedia*, vol. 152, pp. 372–377, 2018, DOI: 10.1016/j.egypro.2018.09.159.

[42] M. V. den Bosch, "Zonwering in scholen, nog heel wat ruimte voor verbetering," 2016, last accessed on 13.05.2024. [Online]. Available: https://www.architectura.be/nl/nieuws/zonwering-in-scholen-nog-heel-wat-ruimte-voor-verbetering/

[43] D. Ivanko, Y. Ding, and N. Nord, "Analysis of heat use profiles in Norwegian educational institutions in conditions of covid-lockdown," *Journal of Building Engineering*, vol. 43, 2021, DOI: 10.1016/j.jobe.2021.102576.

[44] K. B. Lindberg, S. J. Bakker, and I. Sartori, "Modelling electric and heat load profiles of non-residential buildings for use in long-term aggregate load forecasts," *Utilities Policy*, vol. 58, pp. 63–88, 2019, DOI: 10.1016/j.jup.2019.03.004.

[45] J. Guan, N. Nord, and S. Chen, "Energy planning of university campus building complex: Energy usage and coincidental analysis of individual buildings with a case study," *Energy and Buildings*, vol. 124, pp. 99–111, 2016, DOI: 10.1016/j.enbuild.2016.04.051.

[46] M. Wirtz, "nPro: A web-based planning tool for designing district energy systems and thermal networks," *Energy*, vol. 268, 2023, DOI: 10.1016/j.energy.2022.126575.

[47] H. Sha, P. Xu, C. Hu, Z. Li, Y. Chen, and Z. Chen, "A simplified HVAC energy prediction method based on degree-day," *Sustainable Cities and Society*, vol. 51, 2019, DOI: 10.1016/j.scs.2019.101698.

[48] Y. Wang and B. Li, "An optimized solar-air degree-day method to evaluate energy demand for poultry buildings in different climate zones," *Frontiers of Agricultural Science and Engineering*, vol. 7, no. 4, pp. 478–489, 2020, DOI: 10.15302/J-FASE-2019289.

[49] Dassault Systèmes, "Dymola - Multi-engineering modeling and simulation based on Modelica and FMI," last accessed on 26.03.2024. [Online]. Available: https://www.3ds.com/products/catia/dymola

[50] M. Wetter, W. Zuo, T. S. Nouidui, and X. Pang, "Modelica buildings library," *Journal of Building Performance Simulation*, vol. 7, no. 4, pp. 253–270, 2014.

[51] M. Wetter, M. Bonvini, T. S. Nouidui, and W. Zuo, "Modelica buildings library 2.0," in *Proc. of The 14th International Conference of the International Building Performance Simulation Association (Building Simulation 2015), Hyderabad, India*, 2015.

[52] Fluvius, "Lijst gemeenten overschakeling van laagcalorisch naar hoogcalorisch gas," last accessed on 19.05.2024. [Online]. Available: https://www.fluvius.be/sites/fluvius/files/2020-05/conversie-laag-naar-hoog-calorisch-gas.pdf

[53] K. Tránton, "Units of measurement and conversion factors," IEA Energy Statistics Division, last accessed on 19.05.2024. [Online]. Available: https://www.atrias.be/sector-data

[54] Atrias, "Sectorgegevens - gross calorific values," last accessed on 19.05.2024. [Online]. Available: https://www.atrias.be/sector-data

[55] A. Schmitt, "EU Energy Outlook 2050: How will the European electricity market develop over the next 30 years?" Energy Brainpool GmbH & Co. KG, 04 2022, last accessed on 22.05.2024. [Online]. Available:

https://blog.energybrainpool.com/en/eu-energy-outlook-2050-how-will-the-european-electricity-market-develop-over-the-next-30-years/

[56] Commissie voor de Regulering van de Elektriciteit en het Gas (CREG), "Hoe is de energieprijs opgebouwd?" last accessed on 22.05.2024. [Online]. Available: https://www.creg.be/nl/consumenten/prijzen-en-tarieven/hoe-de-energieprijs-opgebouwd

[57] European Environment Agency (EEA), "Greenhouse gas emission intensity of electricity generation in Europe," 10 2023, last accessed on 22.05.2024. [Online]. Available: https://www.eea.europa.eu/en/analysis/indicators/greenhouse-gas-emission-intensity-of-1

[58] Enerdata EnerOutlook, "CO2 intensity of electricity generation," 2024, last accessed on 22.05.2024. [Online]. Available: https://eneroutlook.enerdata.net/forecast-world-co2-intensity-of-electricity-generation.html

[59] B. Lorentz, F. Matthes, T. Johannes, R. Mendelevitch, E. Bovari, I. Österle, A. Guillon, A. Ailleret, and S. Sternberg, "Natural gas demand outlook to 2050," Deloitte, 09 2023. [Online]. Available: https://www2.deloitte.com/de/de/pages/sustainability-climate-dsc/studies/natural-gas-demand-outlook-to-2050.html

[60] J. E. Kang, K. U. Ahn, C. S. Park, and T. Schuetze, "Assessment of passive vs. active strategies for a school building design," *Sustainability*, vol. 7, no. 11, pp. 15 136–15 151, 2015, DOI: 10.3390/su71115136.

[61] W. Tian and R. Choudhary, "A probabilistic energy model for non-domestic building sectors applied to analysis of school buildings in greater London," *Energy and Buildings*, vol. 54, pp. 1–11, 2012, DOI: 10.1016/j.enbuild.2012.06.031.

[62] Chartered Institution of Building Services Engineers (CIBSE), "Climate change and the indoor environment: impacts and adaptation," 2005.

[63] D. Jenkins, P. Banfill, and G. Pellegrini-Masini, "Non-domestic conclusions of the Tarbase project - Reducing CO2 emissions of existing buildings," *Heriot-Watt University, Edinburgh, UK*, 2011.

[64] C. Demanuele, T. Tweddell, and M. Davies, "Bridging the gap between predicted and actual energy performance in schools," in *World renewable energy congress XI*. UAE Abu Dhabi, 2010, pp. 25–30.

[65] Department for Communities and Local Governemnt (DCLG), "Implementation stage impact assessment of revisions to parts F and L of the building regulations from 2010," Tech. Rep., 2010.

[66] D. Katić, H. Krstić, and S. Marenjak, "U-values of school building envelopes in the south region of the Federation of Bosnia and Herzegovina," *e-Zbornik, elektronički zbornik radova Građevinskog fakulteta*, vol. 10, no. 20, pp. 55–67, 2020, DOI: 10.47960/2232-9080.2020.20.10.57.

[67] F. R. Cecconi, N. Moretti, and L. C. Tagliabue, "Application of artificial neutral network and geographic information system to evaluate retrofit potential in public school buildings," *Renewable and Sustainable Energy Reviews*, vol. 110, pp. 266–277, 2019, DOI: 10.1016/j.rser.2019.04.073.

[68] Infrastrutture Lombarde, "Certificazione ENergetica degli EDifici (CENED)," last accessed by Cecconi et al. on 05.03.2018. [Online]. Available: http://www.cened.it/focus_ceer

[69] D. Johnston and A. Stafford, "Estimating the background ventilation rates in new-build UK dwellings - is n50/20 appropriate?" *Indoor and Built Environment*, vol. 26, no. 4, pp. 502–513, 2017, DOI: 10.1177/1420326X15626234.

[70] B. Jones, P. Das, Z. Chalabi, M. Davies, I. Hamilton, R. Lowe, A. Mavrogianni, D. Robinson, and J. Taylor, "Assessing uncertainty in housing stock infiltration rates and associated heat loss: English and UK case studies," *Building and environment*, vol. 92, pp. 644–656, 2015, DOI: 10.1016/j.buildenv.2015.05.033.

[71] M. Papaglastra, I. Leivada, K. Sfakianaki, F. R. Carrié, and M. Santamouris, "International comparison of envelope airtightness measurements," in *Proceedings of the 3rd European Blower Door Symposium, Kassel, Germany*, 2008, pp. 30–31.

[72] J. Fernández-Agüera, M. Á. Campano, S. Domínguez-Amarillo, I. Acosta, and J. J. Sendra, "CO2 concentration and occupants' symptoms in naturally ventilated schools in Mediterranean climate," *Buildings*, vol. 9, no. 9, 2019, DOI: 10.3390/buildings9090197.

[73] American Society of Heating, Refrigerating and Air Conditioning Engineers, *2009 ASHRAE Handbook - Fundamentals*. ASHRAE, 2009, ch. 18.

[74] F. E. Vignola, A. C. McMahan, and C. N. Grover, "Chapter 5 - Bankable solar-radiation datasets," in *Solar Energy Forecasting and Resource Assessment*, J. Kleissl, Ed. Boston: Academic Press, 2013, pp. 97–131, DOI: 10.1016/B978-0-12-397177-7.00005-X.

[75] K. Simic, I. T'Jollyn, W. Faes, J. B. Bastero, J. Laverge, and M. De Paepe, "Modelling of a gas-fired heating boiler unit for residential buildings based on publicly available test data," *Energy and Buildings*, vol. 253, 2021, DOI: 10.1016/j.enbuild.2021.111451.

[76] N. Terry and R. Galvin, "How do heat demand and energy consumption change when households transition from gas boilers to heat pumps in the UK," *Energy and Buildings*, vol. 292, 2023, DOI: 10.1016/j.enbuild.2023.113183.

[77] R. M. Lazzarin, "Condensing boilers in buildings and plants refurbishment," *Energy and Buildings*, vol. 47, pp. 61–67, 2012, DOI: 10.1016/j.enbuild.2011.11.029.

[78] J. Jansen, F. Jorissen, and L. Helsen, "Mixed-integer non-linear model predictive control of district heating networks," *Applied Energy*, vol. 361, 2024.

[79] M. Crane, "Energy efficient district heating in practice - the importance of achieving low return temperatures," in *CIBSE Technical Symposium Edinburgh, UK 14-15 April 2016*.

[80] HVAC HESS, "Factsheet boiler effiency." [Online]. Available: https://www.energy.gov.au/sites/default/files/hvac-factsheet-boiler-efficiency.pdf

[81] Brugeo, "Shallow geothermics," last accessed on 22.05.2024. [Online]. Available: https://geothermie.brussels/en/the-principles-of-geothermics/shallow-geothermics

[82] E. Stocker, M. Tschurtschenthaler, and L. Schrott, "Cost-optimal renovation and energy performance: Evidence from existing school buildings in the Alps," *Energy and Buildings*, vol. 100, pp. 20–26, 2015, DOI: 10.1016/j.enbuild.2015.04.005.

[83] Eurostat, "Heating and cooling degree days - statistics," EU, 02 2023, last accessed on 01.06.2024. [Online]. Available: https://ec.europa.eu/eurostat/statistics-explained/index.php?title=Heating_and_cooling_degree_days_-_statistics

[84] DAB Water Technology, *Quick guide for pump selection*, 2017. [Online]. Available: https://www.dabpumps.com/sites/default/files/2017-10/60118741_QUICK%20GUIDE%20FOR%20PUMP%20SELECTION_ENG.pdf

[85] F. Jorissen, "Toolchain for Optimal Control and Design of Energy Systems in Buildings," 2018, PhD thesis.